DLC-2, A CDC42 GAP INVOLVED IN ATTACHMENT OF MICROTUBULES AT THE CELL CORTEX AND AT THE KINETOCHORES

ELISA VITIELLO

This thesis is submitted for the degree of
Doctor of Philosophy
University College London
September 2013

Department of Cell Biology
UCL Institute of Ophthalmology
11-43 Bath Street
London
EC1V9EL

PhD Supervisor: Karl Matter

DECLARATION

I, Elisa Vitiello, confirm that the work presented in this thesis is my own. Where information has been derived from other sources, I confirmed that this has been indicated in the thesis.

London, September, 2013

This thesis is dedicated to my family and my friends, believing in my dreams.

Logic will get you from A to B. Imagination will take you everywhere.

Albert Einstein

TABLE OF CONTENTS

TABLE OF FIGURES

TABLE OF TABLES

ABSTRACT

Maintenance of epithelial tissue integrity requires correct organization of the polarity plane. This is promoted by assembly of cell-cell junctions, defining distinctive apical and basolateral domains. The establishment of polarity is a key point in tissue organization since it controls the plane in which cells divide. When a cell replicates, it duplicates DNA and aligns them before partitioning them evenly between the two daughter cells. Although results from different laboratories indicate a role of cell-cell junctions in the orientation of the mitotic spindle, it is poorly understood if there is a cross-talk between the mitotic checkpoint and the attachment status of the microtubules at the cell cortex.

Previous works suggest that the small Rho GTPase Cdc42 regulates spindle orientation and chromosome capture. Cdc42 is also a crucial regulator of cell-cell junction assembly and dynamics. Cell junctions need to remodel during cell division to adapt to the changing cell shape, and allow the condensed chromosomes to be properly aligned. Therefore, we hypothesized that specific regulators of Cdc42 guide the interplay between cell junctions and the mitotic machinery.

Using a siRNA approach, we identified a GAP for Cdc42, DLC2, that associates with cell-cell contacts and mitotic spindles, and regulates junctional integrity and chromosome attachment during mitosis. Upon depletion of DLC2 in epithelial cells, the normally continuous immunofluorescence staining of junctional markers was disrupted in mitotic cells, and chromosomes are misaligned.

Following DLC2 depleted cells on live, it results clear that these cells are arrested in metaphase for longer timing, with some chromosomes unattached. The orientation of mitotic spindles relative to the substrate was not affected, suggesting that the defect was not due to a loss of polarity. Depletion of DLC2 led to increased levels of GTP-bound Cdc42, indicating that deregulation of Cdc42 contributed to the observed phenotypes. Indeed, partial depletion of Cdc42 by RNA interference rescued the phenotype induced by depletion of DLC2. We also found that DLC2 associates with the plus-end motor Kif1B, a kinesin-3 family member, and that depletion of Kif1B resulted in a similar phenotype as depletion of DLC2. Based on our observations, we speculate that DLC2 regulates Cdc42 to guide association of microtubules with the cell cortex and the kinetochores in metaphase and to regulate forces they exert at these sites.

LIST OF ABBREVIATIONS

AJs	Adherens junctions
APC	Anaphase promoting complex
APC	Adenomatous polyposis coli protein
aPKC	Atypical protein kinase C
Arg	Arginine
Arp 2/3	Actin-related protein 2/3
ATP	Adenosine triphosphate
ATPase	Adenosine triphosphate hydrolysing protein
BCL9-2	B-cell lymphoma 9-like protein
Caco-2	Colonic adenocarcinoma-2
CAR	Coxsackievirus-adenovirus receptor
CD2AP	CD2-associated Protein
Crb-3	Crumbs homolog 3
Cdc42	Cell division cycle 42
Cdk	Cyclin dependent kinase
CREST	Calcinosis, Raynaud's Syndrome, Esophageal Dysmotility, Sclerodactyly, Telangiectasia Syndrome
CTD	Carboxy terminal domain
cv-c	Crossveinless-c
Dbl	Diffuse B cell Lymphoma
DH	Dbl-homology domain
DLC	Deleted in Liver cancer
DMEM	Dulbecco's Modified Eagle Medium
DMSO	Dimethyl sulfoxide
DNA	Deoxyribonucleic acid
dNTP	Deoxynucleotide Triphosphate
DSG	desmosomal glycoprotein
DSC	desmocollin
DSP	desmoplakin
E-Cadherin	Epithelial Cadherin
EB	end-binding protein
ECL	Enhanced chemiluminescence
Ect2	epithelial cell-transforming sequence 2 oncogene

EDTA	Ethylenediaminetetraacetic acid
EF1A	elongation factor 1-alpha
ERK	Extracellular Signal-Regulated Kinase
FBS	Fetal bovine serum
FRET	Fluorescence energy resonance transfer
GAP	GTPase Activating Protein
GDI	Guanine nucleotide dissociation inhibitor
GDP	Guanosine diphosphatase
GEF	Guanine nucleotide exchange factor
GEF-H1	guanine nucleotide exchange factor H1
GFP	Green fluorescent protein
GLISA	G-protein linked immunosorbent assay
Gln	glutamine
GSK3	Glycogen synthase kinase 3
GST	Glutathione S-transferase
GTP	Guanosine triphosphate
GTPase	Guanosine triphosphatase
HCE	Human corneal epithelial cells
HCC	Hepatocellular carcinoma
HCL	Hydrochloric acid
HepG2	human hepatocellular carcinoma
IgG	Immunoglobulin G
JACOP	Junction-associated coiled-coil protein
JAM	Junction adhesion molecule
LB	Luria-Bertani
LGL	lethal giant larva
Kif	Kinesin family member
KO	Knock-out
M	mitosis
MAGI	membrane associated guanylate kinase
MDCK	Madin-Darby Canine Kidney
mDia	Mammalian diaphanous
MeOH	methanol
MLC	Myosin II regulatory light chain
MRCK	Myotonic dystrophy related kinase
MUPP1	Multi-PDZ-domain protein 1

MYPT	Myosin phosphatase target subunit
NF-kB	Nuclear factor kappa-light-chain-enhancer of activated B-cells
NTD	Amino Terminal domain
PAGE	Polyacrylamide gel electrophoresis
Pals-1	Protein associated with lin seven-1
PAK	p21-activated kinase
PAR	Partitioning defective protein
PATJ	Pals 1 associated tight junction protein
PBS	Phosphate buffered saline
PCNA	Proliferating cell nuclear antigen
PCR	Polymerase Chain Reaction
PDZ	Post synaptic density protein (PSD95), Drosophila disc large tumour suppressor (DlgA), and zonula occludens-1
PFA	Paraformaldehyde
PG	Plakoglobin
PH	Pleckstrin Homology
PI(3,4,5)P3	Phosphatidylinositol 3,4,5-trisphosphate
PI(3,5)P2	Phosphatidylinositol 3,4-bisphosphate
PI(3)P	Phosphatidylinositol 3-phosphate
PI(4,5)P2	Phosphatidylinositol 4,5-bisphosphate
PI(4)P	Phosphatidylinositol 4-phosphate
PI3K	Phosphatidylinositol 4,5-bisphosphate 3-kinase
PKP	plakophilin
PKC	Protein Kinase C
PMSF	Phenylmethylsulfonyl fluoride
Rac1	Ras-related C3 botulinum toxin substrate 1
Rho	Ras homolog
RNA	Ribonucleic acid
RNAi	Ribonucleic acid interference
ROCK	Rho-associated protein kinase
SAC	Spindle assembly checkpoint
SAM	sterile [alpha]-motif
SDS	Sodium dodecyl sulphate
SH3	Src Homology 3
SH3BP1	SH3 domain binding protein 1

shRNA	Short Hairpin ribonucleic acid
siRNA	Short interfering ribonucleic acid
StAR	steroidogenic acute regulatory protein
START	StAR-related lipid transfer (START)
TEM	Transmission electron microscopy
TER	Transepithelial electrical resistance
Tiam-1	T-cell lymphoma invasion and metastasis-inducing protein
TJ	Tight Junction
WASP	Wiscott-Aldrich Syndrome Protein
Wnt	Wingless and Int
ZO-1	Zonula Occludens 1
ZONAB	(ZO-1)–associated nucleic acid binding protein
WB	Western-blot
WT	Wild-type

CHAPTER 1:
INTRODUCTION

CHAPTER 1: INTRODUCTION

1.1 Maintaining epithelial integrity has its rules

Epithelia are tissues that cover external surfaces of the human body and line inner cavities of organs. Although each epithelium is peculiar and has a specific function, among the common main roles epithelia act to protect the organism against pathogens and injuries, and to select carefully what crosses the epithelium and enters in the body (nutrients, ions, salts and water).

Despite the fact that the structure of an epithelium can be more or less complex ("simple epithelium" with only one layer of cells or "stratified epithelium" formed by two or more cellular layers), all of them are composed by specialized cells tidily and compactly arranged in the tissue. The correct organization of these cells is crucial for maintaining the integrity of the barrier[1].

Damaging the epithelial integrity can be dangerous in several ways. It might favour exposure to pathogens and microorganisms, which can freely invade the organism and injure other tissues (Figure 1.1). Nevertheless, the danger does not only have to come from outside, but it might hide behind an uncontrolled homeostasis of the epithelial tissue itself. Many epithelial tissues can regenerate by proliferation and replacing the damaged cells. This is an advantage on one hand because it ensures that the integrity of the barrier will be restored after an injury, but, on the other hand, it represents a factor of risk. Indeed, if the proliferative potential of an epithelium is not wisely controlled, it can trigger cancer formation. Nowadays, it has been estimated that about 90% of all human cancers have an epithelial origin[2].

Hence, proper regulation of tissue homeostasis is of paramount importance. The correct organization of an epithelium is dependent on three features: first, the capability of these cells of establishing intercellular adhesion structures; second, the formation of apical and basal surfaces that align with the tissue barrier; third, proper controlled and specifically orientated cell division[3].

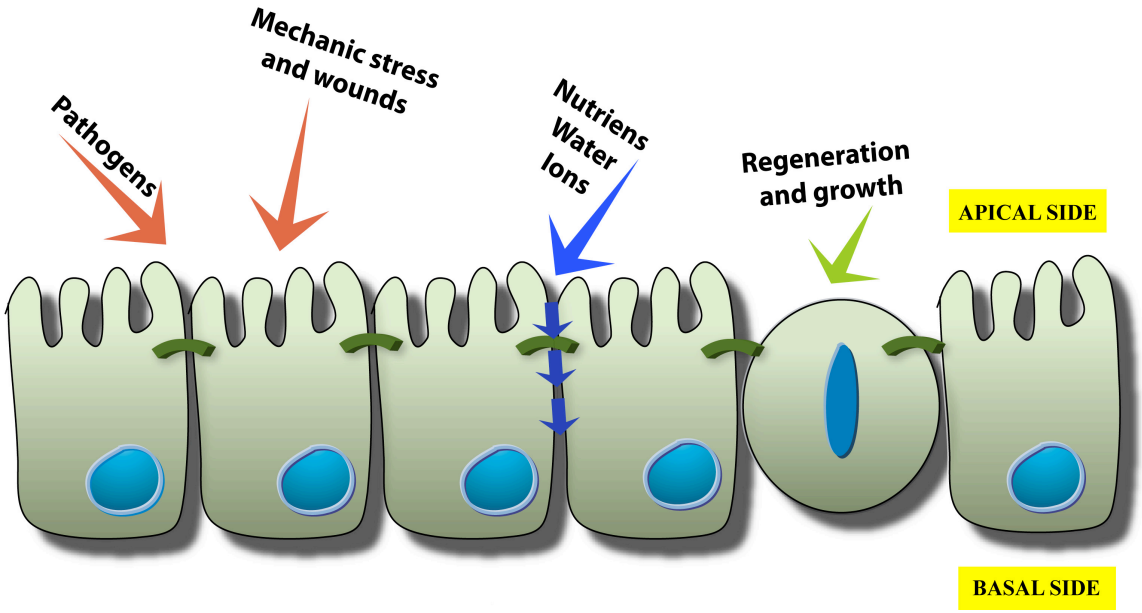

Figure 1.1 The epithelial barrier

A schematic representation of a simple columnar epithelial layer. These tissues are exposed continuously to the external environment. Hence, pathogens and other types of dangers such as mechanic stress or wounds (red arrows) can compromise its integrity. To maintain the barrier integrity, epithelial cells exhibit specific and peculiar physical and biochemical features, such as the complex of epithelial junctions (little green bridge across two neighbouring cells). This complex is located in the apical position and defines the border between apical and basal domain (yellow boxes). The correct functionality of junctions is required for the paracellular transportation (blue arrows through the junctions) of waters and selected nutrients molecules and ions. Moreover, the epithelial barrier is able to regenerate, by duplicating within the layer, to replace damaged cells (green arrows).

1.2 The "epithelial junctional complex"

Epithelial cells assemble specific structures to bridge the space between neighbouring cells that are known as junctions. Junctions allow cells on one hand to adhere to each other and on the other hand to regulate the flux of molecules through the space between cells (paracellular transport). In mammals, adhesion is generally mediated by three types of junctions: Tight Junctions (TJs), Adherens Junctions (AJs) and Desmosomes. The complex of these three is also referred as the "epithelial junctional complex"[4] (Figure 1.2).

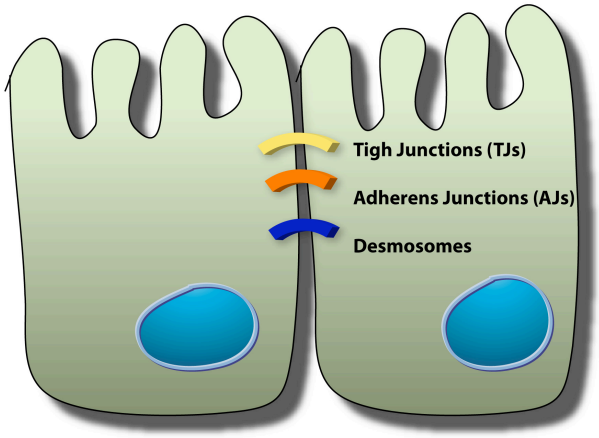

Epithelial Junctional Complex

Tigh Junctions
Transmembrane: Occludin, claudin
Plaque: ZO, cingulin
Function: sealing of the barrear, fence for nutriens and ions, connection to actin cytoskeleton

Adherens Junctions
Transmembrane: E- and P-Cadherin, nectin/AF6
Plaque: α- and β-catenin
Function: connection to actin cytoskeleton

Desmosomes
Transmembrane: desmocollins, desmoclein
Plaque: desmoplakins, plakoglobin
Function: connection to intermediate cytoskeleton

Figure 1.2 The Epithelial junctional complex
Components of the vertebrate *epithelial* junctional complexes found in polarized epithelia cells. This complex is formed by TJ, tight junction; AJ, adherens junction; Des, desmosome. Components of each type of junctions are listed in the yellow table on the right.

1.2.1 Tight Junctions

Tight Junctions are the most apical component of the epithelial junctional complex. They were visualized for the first time in utlrathin section by electron microscopy and appear to be contacts site, bringing opposite membranes next to each other, like gates for the regulations of molecules in the space between the cells[5,6].

Epithelial TJs group several transmembrane proteins: the tetraspans occludin, claudins, tricellulin, MarvelD3, the single transmembrane proteins JAMs (junctional adhesion molecules) and Crb-3, and Bves with three transmembrane domains. These proteins are involved in the adhesive contacts and regulate paracellular permeability. The role of the junctional membrane proteins in paracellular permeability is supported by the observations that overexpression of C-terminally truncated occludin causes paracellular leakage of small tracers in MDCK cells[7] and knock-out of some claudin genes in mice results in permeability defects, such as deletion of the claudin-1 gene, which led to death after birth because of water loss across the skin[8].

Many of the transmembrane proteins contain PDZ-binding domains. This is thought to be important for the recruitment of proteins containing the PDZ (PSD95/DlgA/ZO-1 homology) motif, which has been found in many proteins forming the junctional "plaque", such as ZO-1, ZO-2 and ZO-3 (Zonula Occludens 1-2-3), PAR3 (partitioning defective 3) and PAR6 (partioning defective 6), Pals1 (protein associated with lin seven 1) and PATJ (PALS1-associated tight junction protein), the MAGIs (membrane-associated guanylate kinase inverted) and MUPP1 (multi-PDZ domain protein 1).

Proteins of the plaque are involved in many signalling cascades: some can connect the TJs to the actin fibre network (such as ZO-1, ZO-2, ZO-3), some work as transcription factors (e.g. ZONAB), and others regulate assembly and permeability of TJs (PAR3 and PAR6, Pals1 and PATJ)[9]. These classes are not exclusive though, and most of these proteins play a role in more than one pathway. ZO-2, for instance, has been seen to localize in the nucleus, where it participates in the regulation of transcription of genes[10]. Regulation of ZONAB nuclear localization is controlled by cell density. In proliferating cells, ZO-1 is expressed at low levels, whereas ZONAB at high levels. ZONAB forms a complex with the cell division kinase CDK4. During proliferation, the ZONAB/CDK4 complex dissociates from ZO-1 and goes to the nucleus whereas ZO-1 stays in the cytoplasm. This defines a role for ZONAB in the regulation of entry into S-phase[11]. On the contrary, in high-density cells, ZO-1 is expressed at high and ZONAB at low levels, with consequent cytoplasmic sequestration of ZONAB as well as the interacting cell-cycle regulator CDK4.

It has been reported that the expression of several TJ components is affected in various carcinomas, although, it is not entirely understood how alteration of tight junction components leads to carcinogenesis. Claudins expression is particularly confusing as, depending on the type of tumour and the type of claudin, expression can be upregulated or reduced. For example, despite Claudins expression varies from tissues to tissue, Claudin-1 depletion had been shown to inhibit cell migration and metastatic behaviour in colon cancer, which may reflect a role of claudins in cell-matrix adeshion[12]. Similarly, OSP/claudin-11 and and β1 integrin complex downregulation inhibits proliferation and migration of oligodendrocytes, a process essential for normal myelination and tissue repair[13]. ZO-1 expression is decreased in breast cancer, which is considered to be a marker of poor prognosis[14]. By contrast, ZONAB is upregulated in hepatocellular carcinoma[15].

1.2.2 Adherens Junctions

Adherens junctions initiate and stabilise the cell-cell contacts. Intracellularly, they bind and regulate the actin cytoskeleton and the microtubule network, originate signalling cascades and direct transcriptional regulation, similarly to tight junctions. Adherens junctions are composed of transmembrane members of the cadherin superfamily and of intercellular adhesion proteins belonging to the catenin family. The transmembrane glycoprotein E-cadherin interacts with the cadherins on neighbouring cells. Interestingly, binding of Ca^{2+} to each E-cadherin molecule switches the weak initial interaction to strong adhesive sites: the presence of Ca^{2+} leads to the correct extracellular domain cadherin conformation and stabilisation of the interaction[16,17].

Cadherins can associate intracellularly with proteins of the catenin family. In particular, α–catenin can either act as a monomer or homodimer. It was shown that that monomer or a homodimer forms of α-catenin have different binding properties[18]. The homo-dimers of α-catenin bundle actin fibres and compete for Arp2/3 bining on the actin fibres, preventing the formation of branching networks of actin filaments[19]. On the contrary, the monomeric α-catenin binds more strongly to E-cadherin-β-catenin via the intracellular tail of E-cadherin. β-catenin binds also the C-terminal cytoplasmic domain of E-cadherin but in a phospho-regulated manner. It has been proposed that phosphorylation of Y142 on β-catenin favours BCL9-2, a transcription factor involved in epithelial-mesenchymal transition, and induces a relocalization of β-catenin in the nucleus where it acts as transcription factors[20].

Another member of the cytoplasmic core of the adherens junctions is p120catenin. This catenin is able to bind to the cytoplasmic tail of cadherins and it has been suggested that it increases the retention of cadherins at the plasma membrane. Loss of p120catenin destabilizes E-cadherin contacts and leads to tumour progression and invasion[21]. Moreover, p120catenin regulates microtubules dynamics via EB1 binding and by stabilizing the plus ends. p120catenin depletion results in an increase of catastrophe events and promotes cell migration[22].

Among the transmembrane proteins of AJs we also need to mention nectin proteins. There are four nectin family members (nectin 1-4), which are Ca^{2+}-independent immunoglobulin-like adhesion molecules[23]. In contrast to cadherins, nectins are able to trans-interact both homophilically and heterophilically (interactions between the same and different nectin members), and their

heterophilic trans-interactions are much stronger than their homophilic trans-interactions. Alongside cell adhesion, nectins regulate various cellular functions, such as cell movement, proliferation, polarization, survival and differentiation.

1.2.3 Desmosomes

Desmosomes are intercellular junctions anchoring intermediate filaments at the cell cortex. They do play an adhesive role, and also participate in cell signalling during development, tissue morphogenesis and wound healing.

Desmosomes are composed of the desmosomal cadherins desmoglein (DSG) and desmocollin (DSC), and desmosomal plaque proteins that include desmoplakin (DP), and the arm (armadillo) proteins plakoglobin (PG) and plakophilin (PKP). DP connects the desmosomal plaque to the intermediate filaments, and PG and PKP are adaptor proteins that link the desmosomal cadherins and DP[24].

Desmosomal adhesion molecules contain five repeats of a calcium binding domain. Upon calcium binding, a conformational change occurs and leads to a strongly adhesive state known as hyperadhesion. When hyperadhesion is established, this state becomes insensitive to calcium chelation[25]. Only under some conditions of wound repair and neoplasia can desmosomes switch back to a Ca^{2+}-dependent state[26].

The importance of desmosomes in normal tissue function has become more evident with the start of genetic loss-of-function studies. It was reported that constitutive deletion of Dsc3, Dsg2 or Dsp causes early embryonic lethality probably because of defective adhesion in processes related to implantation. In contrast, mice with constitutive knockout of Dsc1 or Dsg3 or with conditional deletion of Dsp or Dsc3 in the skin survive, but they show epidermal integrity defects. Moreover several human diseases have desmosome components inactivated by mutation, or targeted by autoantibodies or proteolysed by bacterial toxins. Loss or reduction of any of DSG1-3, DSC2, DSC3, PG, PKP1-3 and DSP has been reported frequently in several human epithelial cancers (skin, head and neck, gastric, colorectal, bladder, breast, prostate, cervical and endometrial cancers)[27].

1.3 Establishment of cell-cell contact sites

Although the establishment of cell polarity can vary between model organisms and different mammalian epithelial cells, in a simple epithelium this is driven by the assembly of cell-cell contacts. Behind this complicated and not entirely understood mechanism lays a delicate equilibrium of interplay between TJs, AJs and cell polarity complexes. The cell polarity complexes are largely conserved among flies, worms, yeast and higher organisms. Three major polarity complexes have been identified: the PAR polarity complex, including PAR3, PAR6, atypical protein kinase C (aPKC) and cell division control protein 42 (CDC42), responsible for the establishment of the apical-basal membrane border; the crumbs (CRB) complex, formed by CRB and PALS1 and PATJ, required to establish the apical membrane; and the scribble homologue (SCRIB)–lethal giant larvae homologue (LGL) complex, which defines the basolateral plasma domain[28].

At the initial stages of the process, epithelial cells adhere to the substrate via their intergin receptors, they extend filopodia to look for other cells around and contact them. Once they found each other, the nectin–afadin complex associates with PAR3, and is thought to trigger the recruitment of E-cadherin and JAM-A to the cell cortex (Figure 1.3). These primordial adhesion sites are known as puncta and are composed by a mixture of AJs and TJs components. Under the fine regulation of Rho-GTPase activity, the primordial junctions anchor the actin cytoskeleton and progressively extend the interface of adhesion along the basolateral domain[29]. The process involves both, the active GTP-bound Rac, which stimulates the activity of phosphatidylinositol 3-kinase (leading to the formation of PIP2), and the activation of Cdc42 with the following Arp2/3- mediated actin nucleation as well as the recruitment of cortactin, Mena, PAK-4, and formin-1. Several studies showed that cell–cell junction formation is modulated in a force-dependent manner[30]. When E-cadherin-expressing cells contact each other, MLC phosphorylation increases, and myosin II is recruited to the peripheral zone of the contact where it aids in expanding the contact area and strengthening[31–33]. Next, adherens junctions are separated from tight junctions and the complex matures to the typical belt-like structures with distinct adherens and tight junctions. This happens when PAR3 is excluded from apical sites. Even at this stage active Cdc42 and active Rac1 play an important role: via Par6, they lead to the activation of atypical PKC (aPKC). aPKC (PKCι and PKCζ in humans) phosphorylates Par3, leading to its dissociation from PAR6/aPKC and exclusion from the apical

domain, allowing tight junction formation and separation of the apical and subapical domains[29] (Figure 1.3).

At the beginning of cell-cell contacts establishment, also RhoA activity plays an important role. In epithelial cells, the RhoGTPase family member RhoA is in fact activated at cell junctions on adhesion sites and, concomitantly, deactivated in other parts of the cells, contributing to reduced cell spreading and stress-fibre formation, and inhibition of proliferation. Regulation of RhoA at the cell-cell junctions is essential for the correct control of the junction-associated actinomyosin cytoskeleton, which drives apical constriction and tissue remodelling.

Although the model of apical constriction involves constriction of actin filaments at the cell–cell AJs, recent work in the fly mesoderm and amnioserosa has revealed that constriction can also be triggered by an apical actomyosin network covering the surface of each cell[34–38].

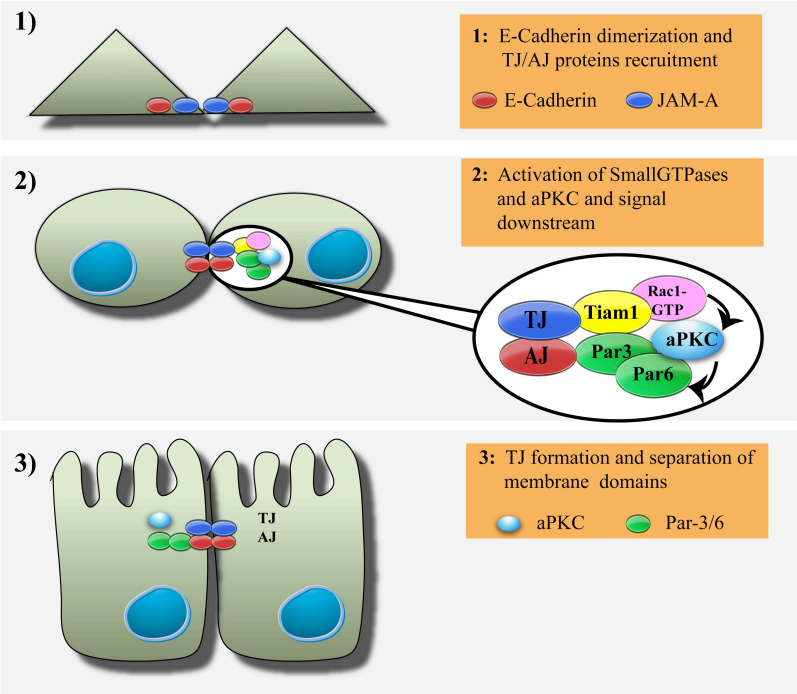

Figure 1.3 Cell-cell contact maturation

Formation of cell-cell contacts, establishment of the epithelial junctional comlex and determination of apical–basal polarity in mammalian epithelial cells. Initially, cells start contacting the neighbouring cells, by sensing them through filopodia and lamellipodia. At the contact site, E-cadherins clusters together and recruit JAM-A (panel1). This triggers the activation of smallGTPases, in particular Cdc42 and Rac. Local activation of Par-3/Par-6/aPKC downstream Rac1 leads to maturation of junctions (panel2), with the separation of TJs and AJs components. While more proteins are recruited at cell junctions, RhoA regulates the zipper sealing. The process ends when the epithelial junctional complex is properly formed and the apical and the basal domains are spatially separated (panel3).

1.4 Small GTPases in the maintenance and regulations of Junctions

I mentioned above that the assembly of cell-cell junctions is regulated by the activity of Rho GTPases. Rho GTPases are present in all eukaryotic cells, and they form a distinct family within the superfamily of Ras-related smallGTPases[39,40]. Whereas yeast Saccharomyces cerevisiae has 5 Rho proteins (Rho 1, 2, 3, and 4 and Cdc42), Caenorhabditis elegans and Drosophila melanogaster are predicted to have 10 and 11, respectively. In mammals, this subgroup comprises 22 genes. Among all the members of the mammalian gene family, the most studied and better characterised are the three Rho isoforms A, B, and C, the three Rac isoforms 1, 2, and 3; and Cdc42[41].

As other Ras-like proteins, Rho small GTPases act as molecular switches. They cycle between an inactive GDP-bound and an active GTP-bound form. The transition between the GDP- and the GTP-bound state is regulated by a variety of positive and negative regulators called GEFs, GAPs and GDI. GEFs are guanine nucleotide exchange factors and they facilitate the exchange of GDP for GTP[42]. On the contrary GAPs are GTPase activating proteins. They interact via specific residues of arginines ("arginine fingers") directly with the Rho small GTPases and trigger hydrolysis of GTP to GDP[43]. GDIs are guanine nucleotide dissociation inhibitors (GDI), which, by binding the Rho GTPases in their GDP bound state, prevent the exchange of GDP with GTP and therefore the activation of the Rho GTPases (Figure 1.4).

In their GTP bound state, Rho GTPases can bind effectors and signal to control pathways downstream. Over 50 effectors have been identified so far for Rho, Rac, and Cdc42 and they include serine/threonine kinases, tyrosine kinases, lipid kinases, lipases, oxidases, and scaffold proteins[44]. Via their own effectors, Rho GTPases are capable to trigger many more cellular responses, spanning from cell adhesion, migration, proliferation, cell survival, death and morphogenesis[45].

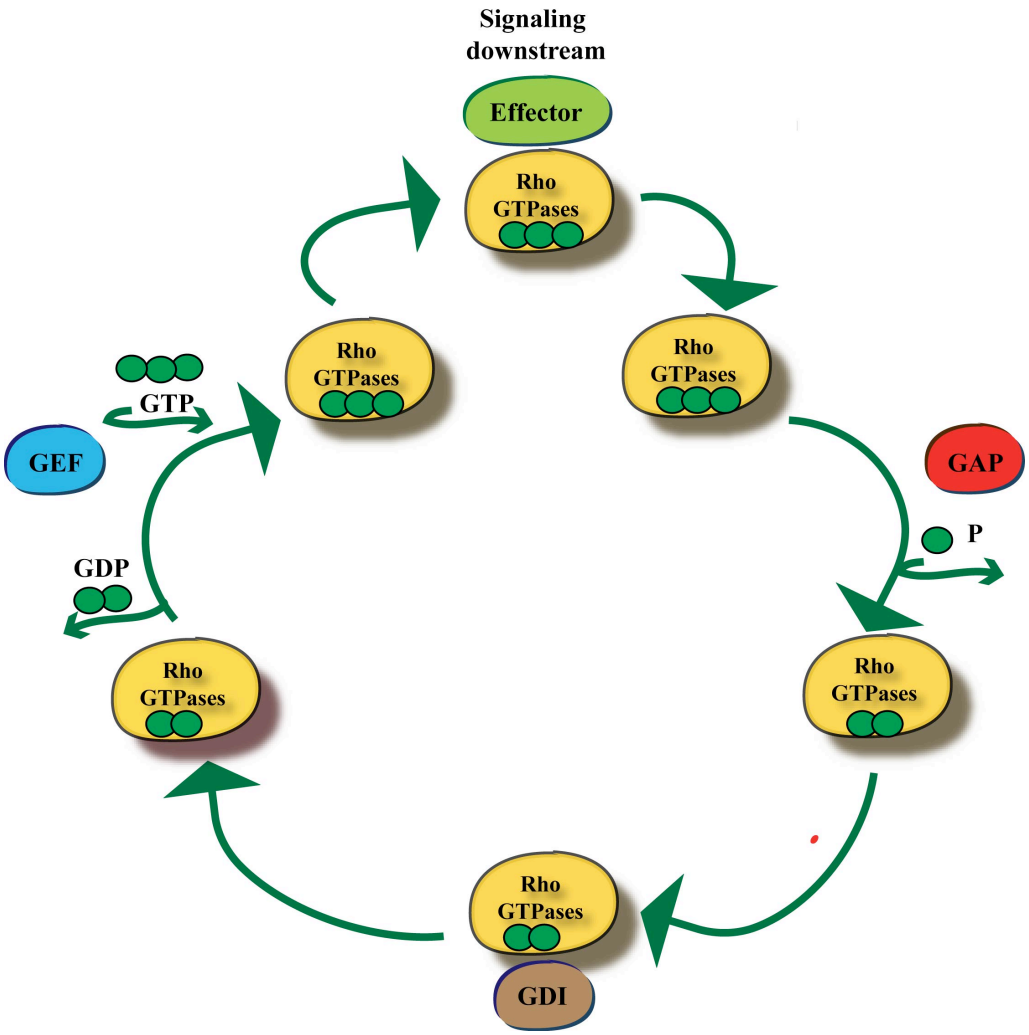

Figure 1.4 Regulation of RhoGTPases

RhoGTPases act as molecular switches and cycle between an active (GTP-bound) state and an inactive (GDP-bound) state. Binding to GTP induces conformational changes that allow RhoGTPases interaction with several effectors, which will pass the signal downstream. The temporal and spatial regulation of GTPase activity is tightly control by three classes of regulators: guanine nucleotide-exchange factors (GEFs), which promotes the exchanging of GDP with GTP; the GTPase-activating proteins (GAPs), that prompts the GTP hydrolysis activity of Rho GTPases, and will turn off the signal; the guanine nucleotide-dissociation inhibitors (GDIs), which block the release of GDP and trap the RhoGTPase in an inactive state.

1.5 How do RhoGTPases control life of cell-cell junctions?

One of the first evidences the role of smallGTPases in junction assembly dates to 1991: In that year, Balda et al showed how correct activation and deactivation of G proteins is required for junction formation. The authors took advantage of a technique known as calcium-switch. This is an experiment that involves culturing cells in a low calcium medium, in order to prevent assembly of cell-cell junctions. To follow up the junction assembly, it is possible to switch to a calcium-rich medium, which will trigger initiation of cell-cell contacts. In this experiment, Balda et al demonstrated that treatment with a non-hydrolysable GTP analogue, GTPγS, which prevents the correct cycling of GTPases, inhibits junction formation[46].

Moreover, treatment with C3 transferase (toxin capable to inactivate RhoA-C, but not Rac or Cdc42) also results in inhibition of junction formation and affects junction permeability. Overall, these studies suggest that the fine balance of Rho GTPases activity is required for junction integrity.

Years later, it became evident that regulations of Rho GTPases is orchestrated in time and space by specific proteins (GEFs, GAPs and GDIs). In fact, some of these regulators associated with junctions were reported to be fundamental for the correct establishment or maintenance of the apical junctional complex. Three TJ-associated GEFs have been identified and functionally linked to TJs: Tuba, GEF-H1 and p114RhoGEF. Tuba, a Cdc42 activator is recruited to TJs in a ZO-1- dependent manner and regulates junction assembly in a Ca^{2+}-switch experiment[47]. GEF-H1 is a Rho GEF and it was shown to regulate paracellular permeability, as well as disassembly of junctions in response to calcium removal[48]. GEF-H1 is regulated by interactions with cingulin and JACOP/paracingulin, two homologous junctional adaptors. This interaction, by regulating GEF-H1 recruitment to the junction, inhibits its exchange factor activity and is though to regulate RhoA-stimulated cell cycle progression[49,50]. Moreover, GEF-H1 directly binds to microtubules and in this state it is unable to activate RhoA[51,52]. Expression of mutated GEF-H1 unable to bind microtubules results in morphological changes associated with RhoA activation such as increased contractility and stress fiber formation.

In contrast, p114RhoGEF is recruited to tight junctions by cingulin and activates RhoA restrictively at cell-cell junctions, leading ROCKII myosin II activation. Hence, depletion of p114RhoGEF inhibits junctions formation[53].

One GAP was identified as regulator of junction assembly: SH3BP1, a GTPase-activating protein for Cdc42 and Rac. SH3BP1, via interaction with JACOP/paracingulin, a junctional adaptor, and CD2AP, an anti-capping protein, regulates spatial activation of Cdc42, controlling filopodia and junction formation[54].

At AJ, the RhoGEF Trio is know to associate with different cadherins, and regulate Rac1 activity via interaction with Tara (Trio-associated repeat on actin). Inhibition of Tara expression results in an enhanced Trio-mediated Rac1 activity, which leads to enhanced p38 activity and decreased E-cadherin expression. Alternatively, pharmacological inhibition of either Trio or p38 activity abrogated E-cadherin repression, suggesting that Tara controls a Trio-induced Rac1 and p38 activation, controlling E-cadherin expression and adherens junction stability[55,56].

Tuba plays a role also on AJs. In fact, depletion of Tuba in Caco2 colon carcinoma cells causes fragmentation of E-cadherin and reduces actin filaments at the contact sites[47]. As downstream effectors of Cdc42, Wallace et al identified that Par6B and PAK4: the authors showed that with the establishments of contacts site, PAK4 and aPKC are recruited and they are essential for promotion of junction maturation[57].

Ect2 and p190 regulates RhoA activity to maintain junctional integrity in the latest stages of mitosis. In particular, centralspindlin, a cytokinetic regulator, localizes to the interphase zonula adherens by interacting with α-catenin. Centralspindlin recruits the RhoGEF, ECT2, to activate Rho. Centralspindlin also inhibits the junctional localization of p190B RhoGAP, and prevents inactivation Rho.

A Rac1 GTPase-specific GTP exchange factor, Tiam1 (T lymphoma invasion and metastasis) has been shown to regulate junction stability. Its deregulation promotes breast cancer metastasis. Its activity is controlled by Par3. Loss of Par3 results in higher Tiam1 activity and hence GTP-bound Rac level within the cell. This results in junction destabilization and invasive cell behaviour. Expression of dominant-negative Rac or downregulation of Tiam1 rescued the Par3 loss phenotype.

1.6 When the regulation of cell polarity is lost, cancer can evolve

Maintaining cell polarity is crucial for tissue integrity and homeostasis. I refer here to previous sections where I presented how several cases of loss in cell

polarity proteins correlates to tissue disorganization and initiation and cancer progression. On the other hand, more than a decade ago already, it was shown that overexpression of wild-type and constitute-active forms of Rho GTPases in murine fibroblasts induces tumorigenesis[58]. Abnormal activity of RhoGTPases was also reported to be able to enhance metastases[59,60] (Figure 1.5).

Considering the role that RhoGTPases play in the modulation of cell-cell junctions, it is not surprising that one of the models proposed for RhoGTPases to trigger cancer formation is via deregulation of cell polarity.

Interestingly, although for the three Ras isoforms, Ki-Ras, N-Ras and Ha-Ras, mutations were found in 15% of all human tumours, RhoGTPases are only rarely mutated in tumours. Instead, their activity is often misregulated in cancer.

RhoA is proposed to stimulate actomyosin-based cortical contractility via ROCKs and lead to disorganization of cell polarity and acquisiton of a more migratory phenotype. Abnormal activation of RhoA in cancer has been reported to be associated with the oncogenes Dbl, Ost, Ect-2, GEF-H1 and Vav-1, all RhoGEFs[61]. On the contrary, RhoGDI or RhoGAPs are usually decreased in expression or lost in the case of tumorigenesis. One famous case of RhoGAPs reported as tumour suppressors is the family of DLCs proteins, which were first found to be deleted in liver cancers and afterwards were found to be downregulated in many other cancers such as breast, colon and prostate carcinomas[62].

Similarly, Cdc42 expression is upregulated in some breast cancers[63], and liver-specific knock-out indicates that loss of Cdc42 enhances liver cancer development[64]. Cdc42 activity was shown to be modulated by the Par polarity complex Par3, Par6 and aPKC. Overexpression of Par6B was reported in breast cancer and results in loss of TJ assembly and membrane localization of atypical PKCζ (aPKC). Interestingly, Cdc42 depletion also resulted in broken TJs, confirming that for a stable TJ complex a complete PAR6-aPKC-CDC42 is required[65].

Moreover, multiple studies suggest that aPKC is involved in the progression of human cancer, and in human non-small cell lung cancer (NSCLC), aPKCz overexpression correlates with poor prognosis[66]. On the contrary, Par3 is lost in many varieties of cancer, such as pancreatic cancers, breast cancer melanomas, colorectal carcinomas, head and neck squamous cell carcinomas, leukaemias, hepatocellular carcinomas, ovarian cancers, neuroblastomas, prostate cancer, bladder cancer[67].

Regarding Rac, little is known about its role in cancer progression in vivo. It has been shown that Rac1 knock-out in mice is embryonic lethal[68], therefore, conditional knock-out mice have been studied extensively. Deletion of Rac 1 in lung seems to be required for K-Ras-induced tumorigenesis to take place[69]. Interestingly, mice lacking Tiam1, a Rac-specific GEF, are less susceptible to Ras-induced skin cancer and develop fewer tumors, although when tumors form they are more aggressive[70].

Moreover, destabilization of junctions is fundamental for triggering cell migration. Misregulation of junction stability is indeed linked to invasive behaviour and metastasis progression. It is important to underline here that, although I did not go in details in how smallGTPases and their regulators are involved in cell migration, many of the proteins I discussed above and in the previous sections can also promote cancer metastasization.

PROTEIN	FEATURES IN CANCER	REF
RhoGEFs: Dbl, Ost, Ect2,Vav1	Increase in expression	*49*
RhoGAPs DLCs	Decreased in expression	*50*
Cdc42	Reported upregulated in breast cancer	*51*
Cdc42 effectors		
Par6/aPKC	Overexpressed	*53,54*
Par3	Lost	*55*
Rac1GEF Tiam1	Mice laking of it are less susceptible to K-Ras-induced tumorigenesis	*58*

Figure 1.5 Table of some smallGTPases and their effectors/regulators altered in cancer
The table reports names of proteins (yellow box), evidences of their involvement in cancer tissues (orange box) and specific references (grey box).

1.7 Maintaining cell polarity in a dividing cell

Due to the position of most epithelia in the body and their role as a protective barrier, it is evident that epithelial tissues are constantly exposed to damages and injuries. In fact, they need often to replace damaged or dead cells to maintain the integrity of the tissue[71] or do so as part of the normal self-renewal of a tissue. The continuous cell replacement is called tissue homeostasis and it varies among different epithelia. The intestinal epithelium completely self-renews within 5 days, the interfollicular epidermis takes 4 weeks to renew; the lung epithelium can take as long as 6 months to be replaced. Some epithelia undergo renewal through out life continuously, such as the hair follicles.

The self-renewal is assured by the presence of multipotent or unipotent stem cells and amplifying cells within tissues. These cells are able to divide and give origin to new cells that will replace the old or damaged ones. The process of cell division is called mitosis. Mitosis can occur in three different ways: symmetrically, along the polarity axis, to self-renew; or asymmetrically, perpendicularly or with a tilted angle to the polarity axis, in order to create differentiated and specialized cells[72]. Symmetry of cell division is in fact an important factor that defines exactly the role and the fate of a new-born cell[28]. Either symmetrical or asymmetrical cell divisions aim to segregate chromosomes between two daughters in a directional manner.

A specific structure in the cell is responsible for the equal separation of chromosomes during cell division: the mitotic spindle. This machinery is composed of microtubule filaments, nucleated from two spindle poles (centrosomes).

Mitosis starts in interphase, with duplication of DNA and centrosomes, and synthesis of many proteins that will be involved in the mitotic process later on. During prophase, the chromatin fibers in the nucleus become tightly coiled, condensing into chromosomes. Meanwhile, microtubules nucleated by the centrosomes approach and contact the nuclear envelope. It is in prometaphase that the nuclear envelope collapses, torn apart from dynein directed-MTs, and actin fibres[73],[74]. At this stage, microtubules capture chromosomes, align them onto the metaphase plate. Metaphase is the moment the cell checks that all the chromosomes brought onto the metaphase plate are correctly attached to MTs. This would be fundamental for anaphase, when chromosomes will be split between the two daughter cells [75]. Mitosis ends up with segregation of cytoplasm.

This last phase is called citokinesis and relies on the efficiency of a structure known as the cleavage furrow. The cleavage furrow is responsible for contractile ring constriction, till the complete separation of cytoplasm and membranes.

Microtubules are not only taking part in chromosome capture, alignment and segregation, but in positioning of the mitotic spindle within the cell. A set of microtubules, called astral microtubules, is nucleated from the centrosomes and directed toward the cell cortex (an actin-rich layer on the inner face of the plasma membrane that supports the plasma membrane and it is an responsible for movements of the cell surface) where they are anchored at several components of cell-cell junctions. It is known that astral microtubules can dock at the AJs via p120catenin[22] and it was previously reported that depletion of E-cadherin, blocking of E-cadherin-E-cadherin complexes via blocking antibodies or deprivation of calcium alter spindle positioning and consequentially symmetry of cell division[76]. Several other components of the cell-polarity complex have been reported to, if altered, to affect the symmetry of cell division: Par6[77], Par3[78], aPCK[77,78], β-catenin[79] and APC[80]. This suggests that cell polarity establishment and maintenance is required for the cells to know which plane they have to divide in, in order to guarantee a perfect tissue order. Interestingly, Garrod's group showed already in 1993 by fluorescent microscopy that epithelial junctions (TJs, AJs and desmosomes) are retained during the entire process of cell division[81]. These results were further corroborated by electron microscopy confirming the importance of cell-cell junctions in the establishment of the polarity plane in dividing cells in conjunction with the need of the epithelium of not opening gaps within the layer, even while mitosis occurs. In fact, it is known that, during mitosis, mitotic cells round up, partially detaching from the substrate by remodelling focal adhesion sites interacting with the matrix components. This is thought to help to accommodate the shape changes supporting the mitotic spindle and chromosomes during separation[82]. Despite this big change, apical junctions are not disassembled, keeping cells close to each other and within the layer, and, thereby, the barrier intact[83–87].

1.8 Small GTPases regulate cell division

Since the discovery of their role as actin regulators, smallGTPases have been identified as regulators of many cellular processes, as well as cell division. As I described in the previous section, cell division is a complicated event that can be

split into many steps. Different smallGTPases have been associated with various stages of the cell cycle (Figure 1.6).

The first step of cell division that is regulated by Rho GTPases is entry into the cell cycle and G1/S phase progression. They have been demonstrated to regulate transcription of genes required for efficient progression of the cell cycle and cell division. Among these genes, are those encoding cyclin D1 and p21[88]. The first step of this process, it is the duplication of the centrosomes, in S phase, which are fundamental for the nucleation of microtubules during spindle assembly. Duplication of centrosomes was reported to be controlled by RhoA and RhoC, via ROCKII[89,90]

At the onset of mitosis, cells round up. At this level, many reports appeared showing the major role of Rho smallGTPases in the organization of cortical actin. Cytoskeleton rearranges lead to the changes in cell shape that will be necessary to accommodate the bulky structure of the mitotic spindle and chromosomes.

Increase in RhoA activity during mitosis has been proposed to occur via inhibition of p190RhoGAP-A, which is activated upon phosphorylation by Cdk1. Active RhoA mediates rounding up during mitosis through its effector ROCK (Rho-associated kinase), which activates myosin-II. Overexpression of RhoA leads to aberrant cell rounding during mitosis and their detachment from the epithelial sheet[91,92].

Later on in prometaphase and metaphase, RhoA or Cdc42 have been suggested to play a role in spindly assembly attachment of microtubules to kinetochores. RhoA, possibly activated by the RhoGEF Lfc/GEF-H1, binds its effector mDia1 and assures correct spindle formation. When Lfc is depleted, cells accumulate in prometaphase and mitotic spindles form in an aberrant way[93].

In parallel, Cdc42 signals via mDia3 to microtubules and promoting their attachment at kinetochores. It has later been shown that mDia3 binds microtubule tips. This process is controlled by Aurora B phosphorylation: when mDia3 is phosphorylated by Aurora B, its affinity for microtubules is reduced. Binding of mDia3 at the plus ends of microtubules seems to be important in regulating microubule dynamics. In fact, expression of a phosphomimetic mutant stabilize microtubules against cold-induced disassembly[94–96]. Considering that mDia3 is an effector of Cdc42, this underlines the possibility that Cdc42 controls microtubule dynamics via mDia3, in mitosis.

It is also important that Cdc42 is switched off at the right moment. Cdc42 activity might be turned off by the MgcRacGAP. During metaphase, MgcRacGAP binds the mitotic spindle-associated protein PRC1 and inhibits its GAP function

favouring Cdc42 activity. It has been suggested that phosphorylation of MgcRacGAP by Aurora B might disrupt the PRC1/MgcRacGAP complex and thus de-repress MgcRacGAP activity on Cdc42[97].

At the end of mitosis, chromosomes are segregated between the two daughter cells and the cleavage furrow contracts to separate the plasma membrane and cytoplasm of the two daughter cells. It is in this phase, called citokinesis, that the last membranous connection known as midbody is cleaved to release the two daughter cells[98,99]. It seems that Ect2 is recruited at the midzone in a Plk1-dependent manner, here it activates RhoA for the contraction of the actomyosin ring and the final cleavage of the midbody[100,101]. Ect2 activity is specifically limited at this stage by Cdk1 that phosphorylates Ect2 preventing the activation until after the onset of anaphase. In addition, Ect2 is regulated by association with MgcRacGAP. Once again it is Plk1 that phosphorylates MgcRacGAP to promote its interaction with Ect2 and Ect2 recruitment to the spindle midzone[102].

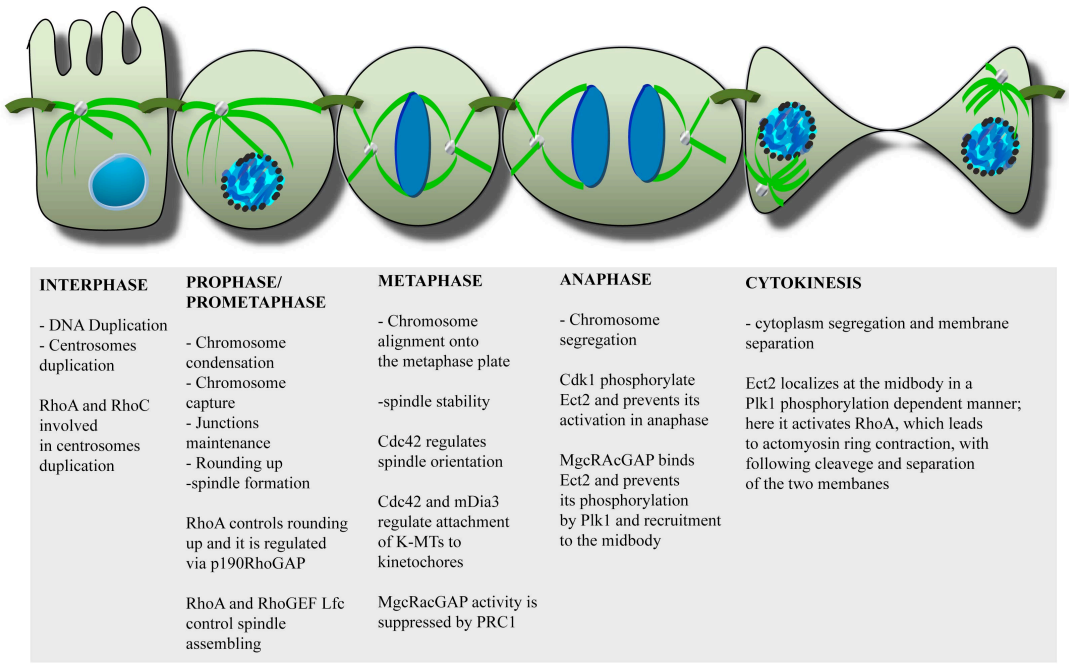

Figure 1.6 Role of smallGTPases in mitosis

Schematic cartoon of mitosis. Before entering mitosis, a cell duplicates DNA and centrosomes in interphase. Mitosis starts with the condensation of DNA in chromosomes and the nuclear envelop breaking-down. Chromosomes are captured in prometaphase, aligned onto the mitotic plate in metaphase and finally segregated in anaphase. The end of mitosis occurs with the separation of citoplasms between the two daughter cells in citokinesis.

Small GTPases play an important role throughout the different phases of mitosis. In the grey box are listed RhoGTPases that have been found involved in a particular mitotic phase and if regulators or effectors have been reported too.

1.9 Discovery of DLCs, GAPs for Cdc42 and RhoA

In, 1998, Yuan and colleagues indentified a segment of genomic DNA underrepresented in human hepatocellular carcinoma (HCC).[62] This frangment contains a gene frequently found lost in HCC samples and HCC cell lines. (HCC). For this reason the gene was called Deleted in Liver Cancer 1 (DLC1). Sequencing of DLC1 cDNA showed that it was the human orthologue of the rat p122RhoGAP protein, characterized by Homma and Emori as containing a 200 amino acids region responsible for RhoGAP activity[103]. The ArhGAP7/DLC1 gene is localized on chromosome 8p21-22 and encodes a 1091-amino acid protein with a predicted molecular mass of 122 kDa. There have been annotated different transcripts for DLC1: a long isoform, and a short one, lacking a portion of the N-terminus domain containing a protein-protein interaction domain (SAM). In mouse, there are two similar transcripts for DLC-1, suggesting that the biological relevance of the two isoforms is conserved.

DLC2 was identified in 2003 on chromosome 13q13 by analysis of genomic and cDNA sequences as a gene that encoded a RhoGAP domain protein related to DLC1, containing 1113-amino acid residues and encoding a protein with a molecular weight of 125 kDa. DLC2 is also expressed as different transcripts: as DLC1, there is a long isoform called DLC2α and a N-terminally truncated one called DLC2γ; in addiction, a quite different isoform has been reported, containing an alternatively spliced exon at its N-terminus (DLC2β). In mouse, there is a gene mapped to chromosome 5G3, which encodes a protein that is 90% identical to human DLC2[104].

Few years later, a gene on chromosome Xq13 was discovered in a screen of cDNA clones isolated from a human myeloid cell line library. From the analysis of this gene, it became evident that it encodes a protein of 1103 amino acids with a calculated molecular mass of 121 kDa. Due to its homology with DLC-1 and DLC-2, it was termed DLC3[105]. DLC3 exists in two isoforms: DLC3α, a long isoform, and DLC3β lacking the SAM domain at the N-terminus. The gene encoding DLC3 was mapped to the mouse chromosome X.

DLC1, DLC2 and DLC3 form the Deleted in Liver Cancer protein family. Despite of their original name, they have many times characterized as tumour

suppressors not only in liver cancer, but also in various other types of cancer such as breast, lung, ovary, kidney, colon, stomach, prostate and nasopharynx. All these reports highlighted the importance of investigating how DLCs alteration triggers cancer initiation. In fact, it is still poorly understood how DLCs act as tumour suppressors.

1.10 DLCs structure

Along the protein sequence of DLCs four distinct domains have been identified: the sterile α motif (SAM) at the N-terminus, a serin-rich region, a conserved RhoGAP (GAP) domain and the steroidogenic acute regulatory-related lipid transfer (START) domain at the C-terminus (Figure 1.7).

The N-terminus of the DLCs contains a SAM domain, a motif of about 70 amino acids discovered in more than 200 human proteins, including transcription factors and signalling proteins[106]. The main function of the SAM domain is thought to be mediating protein–protein interactions, but certain SAM modules have been reported to bind RNA and lipids. Some SAM domain proteins are able to interact with other SAM domains to form oligomers or multi-protein complexes, respectively. In 2007, the structure of the SAM domains of the DLC family proteins was published and described as having some unique features: in particular, the SAM domain of DLC-2 shows to form a four α–helical bundle, instead of the usual five helices typical of other SAM domains[107,108]. This domain exists in solution as a monomer and it may interact with a lipid ligand. The fact that in the case of all the three DLCs, one of the isoforms does not contain the SAM domain raises the possibility that biological properties might be different from the full length versions. An intriguing idea is that the SAM domain is an autoinhibitory domain for RhoGAP catalytic activity[109]. The four helixes of the DLC1 SAM domain are able to bind EF1A1, a factor increased in a wide variety of human cancers, including pancreas, lung, prostate, breast, colon and melanomas[110]. EF1A1 can regulate the actin network through its G-actin- binding and F-actin-bundling activity, and is able to stabilize microtubules, controlling cell migration and cell growth.

The region between the SAM and RhoGAP domains has the least sequence conservation among the DLCs, but alignment of this segment reveals short stretches of high similarity separated by gaps and insertions of variable length. This region is rich in serine residues that have been proposed as potential sites for

phosphorylation by serine-threonine protein kinases, possibly as a regulatory mechanism. An interesting site already characterized is Ser322 of rat p122RhoGAP (equivalent to Ser329 in human DLC1): this site is phosphorylated in rat adipocytes after insulin treatment. A cluster of 7 phosphorylation sites in rat DLC1 (equivalent to human Ser304, Ser305, Ser310, Thr312, Ser313, Ser 317 and Thr318) was found as phosphopeptides in vasopressin-treated rat kidney cells[111]. In a proteomic analysis of phosphorylated peptides in mouse liver Ser89 of DLC1 and an equivalent residue in DLC2 (Ser133 in the human sequence) were identified as phosphorylation sites[112]. An additional site was found in DLC2 (corresponding to Ser572 in the human protein), which seems identical to Ser572 in DLC1 and DLC3. Another interesting feature of this middle region is the presence of several proline-rich segments that could bind to proline recognition domains, such as the SH3 (src homology 3) domains present in many signalling proteins[113]. To support this hypothesis, the secondary structure of this region has been presented as a globular domain with flexibility and the ability to harbour multiple sites for interactions with other molecules.

The RhoGAP domain is the most highly conserved domain among the three DLC family members and has around 70% sequence identity. It is known that the intrinsic GTP hydrolysis rates of Rho proteins are low, and the role of GAP domains is to enhance the GTPase activity, by positioning the catalytic glutamine residue in the GTPases so that the nucleophilic water molecule would is aligned (and will attack the γ-phosphate of GTP[114,115]. Hence, GAPs promote GTPase activity via arginine residues that act like fingers that enter in the catalityc GTPase site, introducing a positive charge that stabilizes the transition state and, thereby, facilitating GTP hydrolysis. All of the DLC proteins have a conserved arginine residue corresponding to Arg677 of human DLC1[116]. Rat p122RhoGAP and human DLC1, DLC2 and DLC3 were found to have a specific preference for RhoA and Cdc42 over Rac-1.

At the C-terminus of DLCs is a domain of about 200 amino acids. This so-called START domain is a domain first identified in several proteins with a role in lipid transport or lipid metabolism (StAR and MLN64 bind cholesterol, and play a role in lipid transport into mitochondria)[117]. Up to today, the START domain has been found in 15 human proteins and for some of them the 3D structure was resolved. The STARD domain contains a hydrophobic tunnel formed by a curved 9-stranded β-sheet[118]. The role of the START domain within DLCs is not clear. It has been proposed that it may regulate subcellular localization and activity, as other lipid-binding found in other RhoGAP proteins, such as the Sec14 domain in

Cdc42GAP[119]. It has even been proposed that apart from lipids, START domains may bind corticosteroids, hence it may bind hormones and confer hormone-regulation. This is only a speculation, however, but it may be important for the biological functions of DLCs.

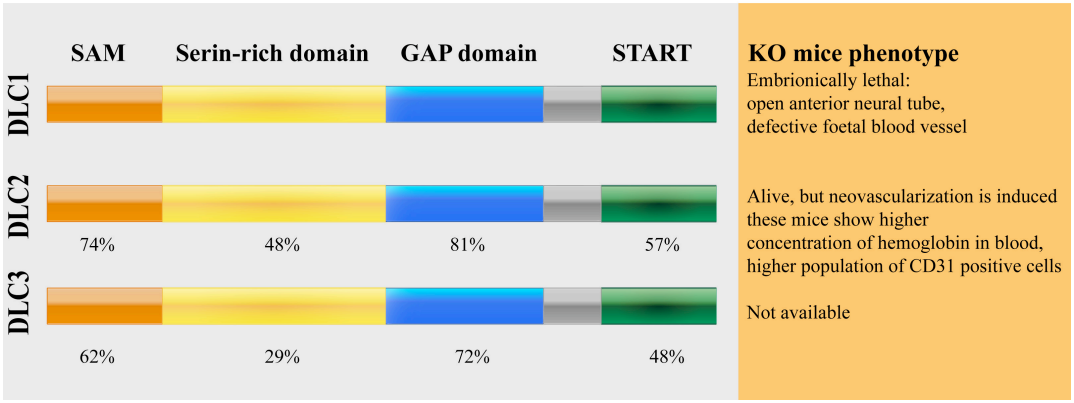

Figure 1.7 DLCs family, structure and KO mice phenotype
Shown is a schematic representation of the structure of human DLCs. Domains are indicated along with the percentage identity to the corresponding domains of human DLC1.

1.11 Tissue distribution and loss of function in mice and drosophila

DLC1 mRNA is widely expressed in various human and mouse tissues and at various stages of development, as shown by Northern blot hybridization [62,120]. The distribution of the DLC2 and DLC3 mRNAs appears to overlap with that of DLC- 1 in many adult tissues [104,105].

Since the distribution is so wide, a KO approach in mice seems very helpful to explore the biological function of DLCs. Up to today, there have been reported KO mice strains for DLC1 and DLC2, but not DLC-3 (Fig 1.7). Lack of DLC1 leads to embryonic lethality. DLC1 homozygous for the mutant allele do not survive beyond 10.5 days of gestation. Histological examination of 9.5-day DLC1 -/- embryos revealed that these mice have an open anterior neural tube, show abnormalities in the branchial arches, brain neuroepithelium and heart, and defective foetal blood vessels in the placental labyrinth[121]. Apparently, DLC2 and DLC3 gene products were unable to compensate for DLC1 deficiency during development. Analysis of fibroblasts from 9.5 day DLC1-/-embryos indicates that they were able to proliferate in culture and they show a reduction in actin stress fibres and vinculin-containing focal adhesions. On the contrary, over-expression of

DLC1 in cultured cells disrupts focal adhesions and actin stress fibres[122]. Despite it might seem a contraction, the fact that lack of DLC1 and its overexpression lead to similar response, could be due to the fact that immortalized cell lines are a very different system from an organism and some responses might have been altered by the immortalization process[123].

In contrast, DLC2 KO is not lethal and mice appeared normal and healthy, indicating that DLC2 is not required for embryonic development and mouse survival. Analyis for the microvascular density and morphology in stomach, skeletal muscle, brain did not reveal any difference between WT and KO mice[124]. Since DLC2 mRNA distribution shows that DLC2 is highly concentrated in endothelial cells, scientists investigated the role of DLC2 in angiogenesis. Subcutaneous injection of matrigel in WT and KO mice to induce neovascularization revealed that the formed matrigel plugs from the KO mice appeared bloodier and had a higher hemoglobin concentration than those of WT mice, and had also a higher population of CD31 positive cells in plugs. Experiments of DLC2 KO mouse aorta sections grown in a 3D matrigel culture showed an increase in sprouting in DLC2 KO samples, again indicating that DLC2 may modulate angiogenic responses of endothelial cells.

Interestingly, studies in Drosophila deficient for the homologue of DLCs show similar results to DLC1 KO mice phenotype: embryos develop multiple defects in various tissues during morphogenesis, including the Malpighian tubules, midgut, head, posterior spiracles and the epidermis during dorsal closure In the *Drosophila* genome, there is only one DLC-1-like protein, RhoGAP88 C, encoded by the gene *crossveinless*-c (cv-c)[125]. RhoGAP88 C protein has the SAM - GAP-START domain organization and has 40% identity with DLC-1 and DLC-2 and 36% identity with DLC3[126].

An RNA interference study specific for RhoGAP genes identified RhoGAP88C as essential for viability. When RhoGAP88C mutants were analysed in search of a phenotype, it was evident that cv-c is fundamental for actin cytoskeleton dynamics during morphogenesis, as the mutant strains revealed delayed dorsal closure of the epidermis and defects in head involution. This resulted in a loss of the posterior crossvein and detachment of the anterior crossvein in the wings of adult flies. By molecular characterization of embryonic lethal alleles two null alleles resulted from nonsense mutations, and a third (cv-c7) had a missense mutation (Arg601Gln) that, interestingly, targets the 'arginine finger' of the RhoGAP domain[127].

1.12 DLCs and cancer

After the discovery of DLC1 as a tumour suppressor gene in hepatocellular carcinoma[62], down- regulation of DLC1 was observed in a wide range of primary tumour tissues, including liver, breast, lung, ovarian, kidney, colon, stomach and prostate, or in cancer cell lines derived from breast cancer metastasis[121,128–131]. The under-expression of DLC1 has been shown to be due to either heterozygous deletions of the DLC1 gene or hypermethylation of its gene promoter[132–134]. Also DLC2 and DLC3 genes were shown to be involved in human neoplasm development. DLC2 was found to be downregulated in breast, lung, ovarian, renal, uterine, gastric, colon, rectal and liver tumors [105,135–137](figure 1.8).

Notably, from the individual DLCs mutation frequency of mutation in HCC cell lines it results that DLC2 is more frequently downregulated than DLC1[130].

How DLCs act as tumour suppressor genes is still poorly understood. Misregulation of DLC1 was shown to be associated with increased proliferation, cell migration and invasion, and induced apoptosis. There is evidence that this may be due to the RhoGAP activity. I mentioned above that DLC1 was shown to work as GAP for RhoA and Cdc42. DLC-1 was shown to negatively regulate the Rho/ROCK/MLC pathway in HCC cell lines in a RhoGAP-dependent manner, regulating actomyosin contractility. In fact, ectopic expression of DLC1 abrogates Rho/ROCK-mediated cytoskeletal stress fibres and focal adhesions by downregulating cortical phosphorylation of myosin light chain 2 (MLC2). RhoGAP- deficient mutants of DLC1 (DLC1 K714E) abolished these inhibitory events[122].

Another model of DLC-1 function proposed focuses on focal adhesions, where it has been shown to localize. Here, DLC-1 is thought to bind the tensin (mediator of actin fibres and focal adhesions plaques) SH2 domain. Disruption of this binding via a point mutation of a critical tyrosine residue (Y442F) in DLC1 does not alter the capability of DLC-1 to downregulate intracellular RhoA activity but compromises the integrity of focal adhesions with deleterious consequences for the cells. This results suggest that DLC1's biological activity might depend not only on the GAP functions, but also on the cooperation between DLC1 and its partners[131,138]

DLC2 was first reported as a gene encoding a RhoGAP protein that can inhibit transformation in Ras-transfected fibroblasts. Subsequently, it was shown

that ectopic transfection of DLC2 is able to inhibit growth in MCF-7 breast cancer cells[139]. Also transfection of DLC2γ can suppress growth in soft agar and RhoA activity in HepG2[136]. Inactivation of RhoA leads to cell morphological changes, from angular shapes to round ones, by deregulating focal adhesions. Another way by which DLC2 could act as a tumour suppressor was proposed by Leung et al in 2010: DLC2 may effect cell proliferation by controlling cell cycle progression. In fact, when DLC2γ is over expressed, an arrest in G1 cells is seen. This was shown to correlate with a misregulation of ribosomal kinase p7S6K phosphorylation. DLC2γ overexpression prevents p7S6K phosphorylation, a downstream target of ERK1/2 and resulted in a G1 phase arrest[135].

DLC-3 is the most recently discovered member of the DLCs and not much information is available about it. When it was identified for the first time in 2007, DLC3 was noted to be able to bind tensin, as well as DLC-1. A possible mechanism hence depicts DLC3 as acting as DLC-1 does in the regulation of focal adhesions, cell shape and morphology, but this has not been proven[138]. Recently, DLC3 has been proposed to localize at epithelial cell–cell contact sites, in particular adherens junctions[140]. I described before how stability of cell-cell junctions is regulated by a balanced and highly localized activity of Rho GTPases. Holeiter et al. have shown that DLC3 depletion leads to mislocalization of E-cadherin and catenins and results in impaired cell aggregation and increased migration. This could be explained by aberrant local Rho signalling because ROCK inhibition restored cell–cell contacts in DLC3 knockdown cells.

PROTEIN	REPORTED CANCERS	REF	MECHANISMS OF ACTION	REF
DLC1	hepatocellular carcinoma, liver, breast, lung, ovary, kidney, colon, stomach, prostate	50, 85, 101, 108-114	- negative regulation of Rho/ROCK/MLC patwhay - tensin binding and regulation of focal adhesion	102 111,118
DLC2	hepatocellular carcinoma, liver, breast, lung, ovarian, kidney, uterus, colon	85, 115-117	- inactivation of RhoA and regulation of focal adhesion via paxillin - control of G1/S checkpoint	116 115
DLC3	liver	118	- regulation of AJs - binding to tensin	120 118

Figure 1.8 Table of DLCs features in cancer

The table reports names of proteins (yellow box), a list of types of cancer tissues DLCs have been found mutated (orange box), with corresponding reference (grey box). In the green box, proposed mechanisms of action are listed for all the DLCs proteins, and the corresponding references are in the following grey box.

1.13 THE AIM OF THIS THESIS

The general goal of my thesis is to shed light on the mechanism by which DLC2 acts as tumour suppressor. As I discussed above, it is not entirely understood how DLC protein misregulation leads to cancer initiation and metastasis. In chapter three, I describe how DLC2 was identified with an siRNA screen designed to investigate small GTPase regulators and effectors involved in the regulation of cell-cell junctions in epithelial cells. I also describe how further analyses revealed that DLC2 not only regulates cell-cell contacts but also the mitotic spindle. Based on the data I obtained at the beginning of my thesis, I formulated the following specific aims.

.

1. To determine in which pathway DLC2 acts in and how it regulates Rho GTPase activity during mitosis

2. To identify forces altered in the mitotic spindle that could explain the DLC2 depletion phenotype observed. Taking advantage of knowledge available in literature, I have decided to investigate what is the role of Kif1B in DLC2 pathway and how this motor protein is affected by DLC2 depletion.

3. To understand how the mitotic spindle shape and functionality is altered upon DLC2 or Kif1B depletion.

4. To identity the Cdc42 effector that functions downstream of DLC2.

5. To determine how DLC2 regulates microtubule dynamics.

6. To test if DLC2 is required for faithful chromosome separation and maintenance of genome integrity.

CHAPTER 2:
MATERIALS AND METHODS

CHAPTER 2: MATERIALS AND METHODS

2.1 DNA PURIFICATION AND BACERIA CULTURE

2.1.1 Bacteria Transformation and DNA purification

$CaCl_2$ competent bacteria (*E.coli* strain DH5α) were thawed on ice. 1.7 μl of a 1.4M β-mercaptoethanol was added to 100 μl of bacteria and incubated for 10'. 10 ng of plasmid DNA was added to each 100 μl and mixed by pipetting up and down once. The bacteria were left to incubate on ice for 30 minutes, heat shocked for 45 seconds at 42°C and immediately put back on ice for 3 minutes. 900 μl of LB medium was added and the tube was incubated for 90 minutes at 37°C. 100 μl of the LB bacteria suspension were plated onto LB agar plates containing 100 μg/ml Ampicillin or 50 μg/ml Kanamycin, but in the case of ligation transformation cells were spun down for 1 minute at 13000 rpm and the pellet was resuspended in 100 μl of medium and plated. The plates were placed at 37°C and the bacteria left to grow overnight.

To purify plasmid from bacteria, a single bacterial colony transformed with the appropriate plasmid was picked using a sterile pipette tip and placed into 5ml of LB containing 100 μg/ml Ampicillin or 50 μg/ml Kanamycin for mini or 200 ml for midi preps. The cultures were left to grow overnight in an incubator at 37°C with shaking at 220 rpm. The following day the bacteria were centrifuged at 4000 rpm for 20 minutes and processed according to the standard Qiagen protocols. The plasmid DNA was resuspended in 10 mM Tris pH 8.5 0.1 mM EDTA (TE buffer). Concentrations and purity of plasmid DNA samples were determined with a spectrophotometer (Themo Scientific Helios β) to measure the absorbance of samples at wavelengths of 260 nm and 280 nm.

2.1.2 DNA agarose gel electrophoresis

1 % agarose gels were prepared by dissolving 1 g of Low Melt Clone Agarose (AGTC BioProducts) in 100 ml of TAE buffer (40 mM Tris-acetate, 1 mM EDTA pH 8.0), or 1 g of Agarose, Molecular Grade (BIOLINE) in TBE buffer (0.89 M Tris Borate pH 8.3 + 20 nM Na_2EDTA). SafeView (NBS Biologicals Ltd) was added prior to gel pouring. 6X DNA loading buffer (30% glycerol (v/v), 0.25% bromophenol blue (w/v), 0.25% xylene cyanol (w/v)) was added to DNA samples to achieve a final concentration of 1X DNA loading buffer. Samples were typically run at 70-90 V for approximately 1 hour and 30 minutes. DNA bands were visualized using a UV transilluminator.

2.1.3 Polymerase Chain Reaction (PCR)

Standard PCR to amplify fragments for sub-cloning was carried out using 100 ng of template plasmid DNA and 40 pmol of each primer (Eurofins/MWG see table) reactions were carried out in 50 µl total volume using 1 µl (2.5 Units) of Expand high fidelity polymerase (Roche Applied Science) and 200 μM of dNTP mix (Roche Applied Science). Where necessary 10% DMSO was added to the reaction mix. Reactions were carried out in a (PCR machine) using a typical program such as:

1 94°C for 2 minutes
2 94 °C for 30 seconds
3 67°C for 45 seconds
4 72°C for 1 minute / 1 kB
5 Step 2 for X25 cycles
6 72°C for 10 minutes

2.1.4 Restriction enzyme digests, DNA purification from gel and ligations

5μg plasmid DNA or PCR products were digested in a total volume of 30 μl, using 0.5 μl of the appropriate restriction enzymes (New England Biolabs) in the provided and recommended buffer solutions. Reactions were incubated at 37°C for 1 hour. Digested DNA fragments were purified by running on agarose gels, excising the appropriate bands under a long wave length UV transilluminator. To purify the DNA, 1ml of 6M solution of Sodium Iodide was added to the excised agarose bands and the agarose was melted at 70°C for 10 minutes. 50 μl silica beads (Sigma) were added to bind DNA. To help the binding, tubes were inverted every 5 minutes. Samples were then washed twice with silica wash buffer (50 mM NaCl, 10 mM Tris HCL pH 7.5 2.5 mM EDTA, 50% v/v Ethanol). DNA was eluted from the beads in 30 μl of 10 mM Tris pH 8.5 0.1 mM EDTA (TE buffer).

Ligations were carried out using a 1:3 molar ratio of Vector: Insert in a volume of 20 μl, using 1 μl (5 units) of T4 ligase (Roche) in the provided buffer.

Reactions were incubated overnight at 4°C, left at room temperature the day after for 2 hours. The whole volume was used to transform 100 μl DH5a *E.coli.*

2.1.5 Mini and midi: DNA extraction from bacteria

Mini and Midi protocols were performed in accord to the kits from NBS.

For the analysis of ligations, Mini preps were performed from 10-15 colonies for each construct to find the right clones. They were inoculated the night before in a 5ml LB solution and let to grow at 37ºC overnight with 200 rpm shaking. For Midi preps, single colonies were picked and grown overnight at 37ºC with 200rpm shaking.

2.2 CELL CULTURE AND CELL TREATMENT

2.2.1 Cell lines: culture, freezing and thawing

Human Cornel Epithelial cells (HCE), transformed with SV-40 large T-antigen were a gift from Chang M.S. (Vanderblit, University, Nashville, Tennessee). HeLa H2B-GFP/α-tubulin-mRFP and HeLa EB3–tdTomato eGFP–CENP-A cell lines were a gift from Patrick Meraldi (University of Geneva, Switzerland). HeLa Mad2-GFP cells line was a gift from Helder Maiato's lab, University of Porto, Portugal.

HeLa and HCE cells were cultured in DMEM medium containing 10% heat-inactivated FBS with 100ug/ml penicillin/Streptomycin (PAA cell culture), at 37°C and in 5% CO2 atmosphere.

For storage, cells in 6 wells-plates were frozen by trypsinizing for 15 minutes at 37ºC with 0.5 ml of 1X Trypsin. Cells were centrifuged at 1000 rpm for 5 minutes, and then re-suspended in freezing medium (DMEM containing 10% DMSO and 20% FBS).

For defrosting, cells were thawed, washed once with DMEM, every time centrifuging for 5 minutes at 1000 rpm. Then, the cells were plated in the appropriate medium.

2.2.2 Lipofectamine 2000 transfection of DNA

For transient transfection, Lipofectime 2000 (Invitrogen) was used. For 48-well plates, 1 ul of Lipofectime was mixed with 0.5 ug of DNA in a final volume of 50 ul of OptiMEM medium (Gibco/Invitrogen). Transfection tubes were left at room temperature for 30 minutes and then added to 80% confluent cells. After 4 hours, medium was changed with fresh DMEM. Cells were processed 16 hours later.

Construct	Name
Cdc42 CA	pRK5-Cdc42(L61)-Myc
Cdc42 DN	pRK5-Cdc42(N17)-Myc
RhoA CA	pRK5-myc-RhoA-Q63L
RhoA DN	pRK5-myc-RhoA-T19N
mDLC2	pCDNA/TO-HA-mDLC2
Tet-repressor	pCDNA6/Tr

Table 2.1 List of DNA construct used in this project

2.2.3 SiRNA transfection

4 siRNA specific for human DLC2 mRNA were initially purchased from Dharmacon (siGENOME), and tested by WB and IF, by comparing their effect to a non-specific control siRNA. The fourth was discarded on the basis of the efficiency and the α-tubulin levels since it was toxic.

For siRNA transfections, I used INTERFERin (Polyplus transfection). A single six well plate at 90% confluence was trypsinised and diluted 1/60 for WB and 1/90 for IF. 0.5 ml per well of 48-well plate was used. Transfection was carried on the same day for HCE cells, the day after for HeLa cells. Transfection mix was prepared with 1 µl INTERFERin (Polyplus transfection), 0.5 µl of 20 mM siRNA in 50 µl OptiMEM (Gibco/Invitrogen). The mix was left at RT for 30 minutes. 50 µl of transfection mix was added to each well of the 48-well plate. Medium was replaced the day after, and cells were left for a total of 96 hours before either fixation or protein extraction.

Target	Sirna	Brand
DLC2 1	5'-GAUGU GAACUUCCAAAGGA-3'	siGeNOME
DLC2 2	5'-CCAAGGCACUUUCUAUUGA-3'	siGeNOME
DLC2 3	5'-GGGCAACUUUCCACACUUA-3'	siGeNOME
Kif1B 1	5'-CGGAUAUCAACUACGAUGA-3'	SIGMA
Kif1B 2	5'-GGGUAAUUUGCGUGUGCGU-3'	SIGMA
Kif1B 3	5'-CACAUUAAAGAAGAGAGCAUU-3'	SIGMA
mDia3 1	5'-GAUCAGAGAUACUAAAUCA-3'	Dharmacon
mDia3 2	5'-GAAGAUACUCAACGAAUUA-3'	Dharmacon
mDia3 3	5'-CGAUUUAACUCAUCUGAUA-3'	Dharmacon
mDia3 4	5'-GAAUUACGAUCGGGUAUAU-3'	Dharmacon
Cdc42 1	5'-CGGAAUAUGUACCGACUGU-3'	SiGENOME
Cdc42 2	5'-GAUGACCCCUCUACUAUUG-3'	SiGENOME
RhoA 1	5'-AUGGAAAGCAGGUAGAGUU-3'	SiGENOME
RhoA 2	5'-GAACUAUGUGGCAGAUAUC-3'	SiGENOME
RhoA 3	5'-GAAAGACAUGCUUGCUCAU-3'	SiGENOME
RhoA 4	5'-GAGAUAUGGCAAACAGGAU-3'	SiGENOME
Control	non targeting	SIGMA

Table 2.2 List of siRNA used in this project

2.2.4 Cell Synchronization

Cells were incubated with Nocodazole 100μM (1:30000 from stock 3mM) for 6h as described in the reference[141].

To perform the wash off, cells were rinsed twice with normal DMEM and then incubated with fresh DMEM/FBS/P/S. Cells were harvested or fixed and stained at the following time points: 45' for the metaphase/anaphase peak, or 90' for the telophase/cytokinesis peak[141,142].

2.2.5 Microtubules stabilization assay

To stabilize microtubules, Taxol 0.5μM (1:20000 from a stock 10mM) was incubated with the cells ON at 37C. Cells were fixed and stained the day after as indicated in the microscopy section.

2.2.6 M Check-Point inhibition via MPS-1

To test the hypothesis that the delay in metaphase is check-point dependent, cells were treated with 200μM MPS-1 inhibitor. The inhibitor was added to the cells at 37°C, right before filming.

2.2.7 Monopolar spindle formation and wash-out

To induce formation of monopolar spindles, cells were treated with monastrol 100μM (Sigma-Aldrich) 2h at 37°C[143]. The last hour, MG132 was added. Cells were then washed 3X with fresh medium and let to rearrange bipolar spindles. Time points analyzed were 0′, 20′, 60′ and 90′. Over 60 cells were analyzed per conditions[144,145].

2.2.8 Aurora B inhibition

HCE cells were treated with ZM447439 (Tocris Bioscience) ON at 37°C at the final concentration of 3μM. Cells were afterwards fixed for further analyses[146,147].

2.2.9 K-fiber disassembling

The aim of this experiment is to test the stability of K-fibres. Treating cells with cold triggers the disassembly of these fibers. Cells were put on ice and were then fixed at the following time-points: 0', 10', 15', 20', 25' and 30'. To compare Control and DLC2 KD/ Kif1B KD/Cdc42 KD/mDia3 KD cells, cells were arranged in classes. For the experiment that regards control/DLC2 KD/Kif1B KD cells, the three classes for quantification purposes were: regular mitotic spindles, spindle with short K-fibres, long fibres and chromosome misalignment. On the contrary, for the experiment with control/Cdc42 KD/mDia3 KD cells, the four classes for quantification purposes were: regular mitotic spindle, spindle with short K-fibres, short fibres and chromosome misalignment[148].

2.2.10 Chromosome spread

Chromosome spreads were performed by treating HCE cells for 2 h with nocodazole (3.3mM diluted 1:1000) at 37ºC. and then incubated for 20 min in 75 mM KCl nocodazole (3.3mM diluted to 1:1000) at 37ºC to induce hypotonic shock. Cells were rinsed with 1X PBS and then fixed first with methanol -20ºC for 3' and then PFA 4% diluted in PBS for 20' at RT. Cells were blocked with PBS/0.01%Triton/10%FBS. To quantify the number of chromosomes present in chromosome spreads, CREST was used to stain the kinetochores. Kinetochore pairs through z-sections were counted in a minimum of 50 cells for each condition[143,149,150].

2.3 PROTEIN ANALYSIS

2.3.1 Western blotting

Protein lysates were prepared for SDS/PAGE analysis by washing cells twice with 1X PBS and then adding a buffer made of one part 3X sample buffer (6% SDS, 30% glycerol, 0.003% bromophenolblue, 0.3 M DTT, 0.1875 M Tris/pH 6.8) and 2 parts distilled water to give a final 1X concentration of sample buffer. 20 mM DTT and 6 M urea were used to help the denaturing of proteins. After three times homogenization with a 23 gauge micro-needle, samples were heated at 100°C for 10 minutes.

8% or 10% polyacrylamide gels were prepared few days in advance, using a MightySmall minigel electrophoresis system. The separating gel contained 5% Tris pH 8.8, 0.1% SDS, 0.1% APS, TEMED and distilled water. Stacking gel 50 ml was made with 5% Tris pH 6.8, 0.1% SDS, 0.1% APS, TEMED and distilled water.

Samples were loaded on the gels and run at 25 mA per gel, for 45 minutes.

Gels were transferred using a standard transfer apparatus (BioRad) using transfer buffer containing 25 mM Tris, 250 mM glycine pH 8.3 0.1% SDS, 20% MeOH. The nitrocellulose membrane (Santa-Cruz) was mounted with the gel in the apparatus, and the transfers were run for 2 hours and 30 minutes at 4°C at 100 V constant and 0.45 mA.

After the transfer, the membranes were stained with Amidoblack dye 0.1% for 30 seconds, then de-stained with (20% MeOH 7.5% acetic-acid) for 30 minutes, washed with PBS-0.2%Tween-20 for 30' and blocked in the blocking solution (5% Milk in PBS-0.2% Tween-20-0.1% NaN3) for 30 minutes with agitation. The membrane was then incubated overnight at 4°C on the shaker with the appropriate primary antibody, diluted in the blocking solution.

The day after the membranes were washed three times for 10 minutes with PBS 0.2% Tween-20 solution and then incubated with the appropriate horseradish peroxidase conjugated secondary antibodies diluted in PBS 0.1% Tween-20 for 1 hour. The membranes were washed three times for 10 minutes with PBS 0.1% Tween-20 solution and another three times with PBS for 5 minutes. Membranes were soaked in a solution of enhanced chemiluminescence detection system (reconstituted from individual products obtained from Sigma), and left in the dark with an x-ray film.

2.3.2 Immunoprecipitations

Cells were plated in a 14 cm plate and when they reached confluence, they were extracted at 4°C using 2 ml of Triton X100 0.5% PBS. A cocktail of protease inhibitors (10 μg/ml leupeptin, 10 μg/ml aprotinin, 10 μg/ml pepstatin A 50 μg/ml benzamide and 1 mM PMSF) and phosphatase inhibitors (10 mM sodium fluoride (NaF), 10 mM sodium pyrophosphate and 4 mM sodium orthovanadate) was added to the lysis buffer prior to extraction. The samples were spun down 2 minutes at 4°C. To reduce the nonspecific binding, 100 μl of inactive sepharose beads were incubated with the extracts for 30 minutes. Samples were spun again at 7000 rpm for 2 minutes and the supernatants were transferred to 2 μg of antibody left overnight conjugating to Protein G sepharose beads. After incubating at 4°C for 2 hours, the beads were washed twice with 1 ml of 0.5% Triton X100 PBS and once with PBS.

To detach proteins form the beads, 60 μl SDS-PAGE buffer containing 20 mM DTT and 6 M Urea were added to the samples before boiling for 10 minutes at 100°C.

2.3.3 RhoGTPase activation assay G-LISA

For these assays, the cells were transfected with the appropriate siRNAs in 12 well plates, and analysed for levels of active RhoA, Cdc42 and Rac1 using the respective G-LISA assay kit from Cytoskeleton Inc. Protein concentrations were measured in order to load equal amounts of samples. Protein concentration and HRP conjugated secondary antibodies were measured by absorbance at 490 nm using a FLUOstar OPTIMA microplate reader (BMGLabTech, Offenburg, Germany).

2.4 MICROSCOPY

2.4.1 Immunostaining and confocal microscopy

Hela cells were grown for 5 days and HCE cells for 4 days on glass cover slides in 48 well plates. On the last day, cells were fixed with cold methanol (-20°C) for 10 minutes in the freezer. Methanol was discarded and cells rehydrated with 1XPBS for 5 minutes, then blocked with PBS-0.5%BSA-0.1%NaN_3 for 15 minutes at room temperature. For actin staining, cells were fixed with 3% PFA in PBS, pH 7.4 for 20 minutes at room temperature, permeabilised with 0.5% Triton in PBS-BSA for five minutes and then incubated with 0.5% BSA 20mM Glycine PBS for 5 minutes. For microtubules staining, cells were pre-fixed at 37°C for 15' with PFA 4% diluted in a microtubules stabilization buffer (NaOH-Pipes ph 6.8/ MgCl2 1mM/EGTA 1mM/0.1%Triton/H2O). Then they were left a -20°C in methanol for 3'. Methanol was discarded and cells rehydrated with 1XPBS for 5 minutes, then blocked with PBS-0.5%BSA-0.1%NaN_3 for 15 minutes at room temperature.

Primary Antibodies were diluted in PBS-0.5%BSA-0.1%NaN_3 and incubated 1 hour at room temperature. After washing twice with PBS, secondary antibodies conjugated FITC, Cy3 or Cy5 (Jackson ImmunoResearch Inc) were added (dilution 1:300) and cells were kept in the dark for 1 hour.

For actin staining, 1:2000 fluorescently labelled Phalloidin (Sigma) was mixed with the secondary antibodies. For DNA detection Hoechst 33258 (Invitrogen) was diluted 1:5000 in the secondary antibodies solution. Cells were then washed twice with PBS and mounted on microscope slides with ProLong antifade mounting medium (Molecular Probes). Slides were observed with a Leica DMIRB fluorescent microscope using a 63X objective and processed with Adobe Photoshop version 7.0. For confocal microscopy, or a Leica TCS SPE confocal microscope using Leica Application Suite (LAS) software. For confocal microscopy a 63X objective was used.

Primary Antibody	Source	Species	Dilution	
			IF	IB
α-tubulin	Kreis, T.E., 1987	Mouse	-	1:20
α-tubulin	Abcam	Rabbit	1:200	1:1000
β-catenin	Santa Cruz	Goat	1:200	-
E-Cadherin	BD Biosciences	Mouse	-	1:1000
HA	Daro et al., 1996	Mouse	1:10	-
Occludin	Invitrogen	Mouse	1:2000	1:2000
p120-Catenin	BD Biosciences	Mouse	1:250	1:1000
ZO-1	Benais-Pont et al., 2003	Rabbit	1:100	1:1000
Kif1B	Benthyl Laboratories, Inc	Rabbit	1:50	1:200
Kif1B	Eunjoon Kim, KAIST	Guinea pig	-	1:200
EB1	Santa Cruz	Mouse	1:300	1:300
DLC2	Santa Cruz	Goat	1:200	1:200
α-Catenin	Sigma	Rabbit	1:200	1:1000
Dynein	Sigma	Rabbit	1:200	-
Active Cdc42	Newest Bioscience	Mouse	1:50	-
c-Myc	Matter Lab	Mouse	1:200	-
mDia3	ECMBiosciences	Rabbit	1:200	1:1000
mDia3 (Ser-196)	ECMBiosciences	Rabbit	1:200	1:1000
AuroraB P (T232)	Abcam	Rabbit	1:200	1:1000
Aurora B	Abcam	Rabbit	1:1000	1:1000
Aurora B (IF)	gift by Takeshi Urano	Mouse	1:1000	-
Aurora B (WB)	gift by Takeshi Urano	Mouse	-	1:1000
CREST	seralab		1:1000	-
CDC42	Santa Cruz	Mouse	-	1:100
APC	Santa Cruz	Rabbit	1:200	
phospho-S100 hDsn1	sent by Iain Cheeesman		1:200	-
γ-Tubulin	Sigma		1:1000	-
CENP-A	Santa Cruz	Rabbit	1:50	1:50

Table 2.3 List of antibodies used in this project

2.4.2 Time lapse microscopy

For live cell imaging experiments, cells were plated into 35 mm glass bottom microwell (14 mm, No 1.5 coverglass) dishes (MatTek Corporation) and transfected with siRNAs as described in previous sections. Medium was replaced at least 6hours before filming with L-15/10% FBS. Four-dimensional datasets were acquired with a spinning disc confocal system (Yokogawa) equipped with an electron multiplying charge-coupled device camera (iXonEM+; Andor) and a CSU-22 unit (Yokogawa) based on an inverted microscope (TE2000-U; Nikon). Two laser lines (488 and 561 nm) were used for near-simultaneous excitation of GFP and mRFP, and the system was driven by NIS Elements 3.0 software (Nikon). Time-lapse imaging of z stacks with 0.7 μm steps covering the entire volume of the mitotic apparatus were collected every 2 or 3 min with a plan-apochromat 1.40 NA 60x immersion oil objective[142]. Phase contrast microscopy was performed on a Nikon Eclipse TE2000-U microscope driven by NIS Elements 3.0 software with 63x or 100x objectives. Time-lapse was performed every 30sec, 1min or 2min, depending on the type of experiment.

2.4.3 Quantitative analysis of spindle angle and length, astral and kinetochores fibre length, and fluorescence intensity

Quantification of spindle angles and length was performed using ImageJ. Images were collected by taking z-stacks with a step of 0.01 μm covering the entire volume of the mitotic spindle, for the angle measurements, every 0.5 um for the length analysis. Mitotic spindle length was calculated as distance between the two spindle poles. The angle between the spindle axis and the substrate was defined as the angle between a line parallel to the substrate and the line crossing the two spindle poles.

Length of microtubules was measured in monastrol treated cells. Cells were stained with markers specific for astral or kinetochore fibres, then, pictures were take with confocal microscopes and finally analysed in ImageJ. Length was measured from the spindle poles grouped in the middle of the monopolar spindle to the end of the visible fibre. Pictures were maximum intensity projections of 0.5µm step stacks covering the whole cell height.

Aurora B target fluorescence intensity analysis was performed by selecting 5 kinetochore areas, repeated over 10 pictures. Background was subtracted to the intensity mean. Normalized values were compared among control and knockdown conditions. The maximum value in control was identified and used as a threshold to define how many kinetochores show higher intensity in the knockdown cells.

2.4.4 Comet tracking

GFP-EB3 stably transfected HeLa cells were imaged every 2' with the spinning disk microscope. Individual comets were manually tracked using the "Manual Tracking" plugin of ImageJ. Comets were followed continuously until the fluorescent signal disappeared. Three parameters were extracted from the tracking: comet total speed, total distance and total time. The comet time is defined as the continuous time a single comet track is followed (in seconds). The comet distance is the distance the comet travelled until the signal disappeared (μm). The comet speed is defined by the formula v=mean distance (μm)/time (sec) and it represents the mean velocity a comet travels between consecutive time frames.

2.4.5 Statistical analysis and data presentation

In charts where data are represented as box-whisker plots, the box size represents 75% of the population and the line inside the box represents the median of the sample. Maximum (in the upper quartile) and the minimum (in the lower quartile) values are represented by the size of the bars (whiskers). A parametric one-way analysis of variance (ANOVA) was used to perform statistical analysis for multiple groups. These statistical analyses were performed using SigmaStat 3.5 (Systat Software, Inc.). In the case that only two experimental groups were compared, parametric *t* test was used.

2.4.6 Micro-contact printing and cell patterning

Micropatterned dishes were kindly provided by Matthieu Piel[151]. The micropatterned dishes used had parallel fibronectin lines (12μm wide) printed. Cells were trypsinized and resuspended in fresh medium at a density of 104 cells/ml before seeding onto the micropatterned coverslips. After 30 min of seeding, HeLa cells had attached to fibronectin. Non-adherent cells and debris were removed by replacing the medium with fresh medium.

CHAPTER 3:
IDENTIFICATION OF DLC2 AND DESCRIPTION OF DLC2 KNOCKDOWN PHENOTYPE

CHAPTER 3: IDENTIFICATION OF DLC2 AND DESCRIPTION OF DLC2 KNOCKDOWN PHENOTYPE

3.1 IDENTIFICATION OF DLC2 IN AN CELL-CELL JUNCTION INTEGRITY SIRNA SCREENING

The importance of small GTPase regulation for the maintenance of cell-cell junctions and epithelial tissue integrity has been investigated in the Matter and Balda laboratory since several years. To gain a genome-wide view of which small GTPase regulators and effectors are involved in cell-cell junction formation and maintenance, a functional siRNA screen was carried out. The screen comprised 265 genes: these included 20 small GTPases, various small GTPases regulators and effectors as well as some actin regulatory and binding proteins[54] (Zihni et al. and Karl Matter, unpublished data). One of the cellular systems chosen as experimental model was a Human Corneal Epithelial cell line, HCE cells. These cells are a good model to study junction formation and maintenance because they form functional epithelial junctions and express many of the major junctional and polarity markers.

After the siRNA library transfection, all 265 genes were analysed by immunofluorescence and classified on the basis of their effect on markers of cell-cell junctions: β-catenin for AJs and ZO1 for TJs. Moreover, giantin was used to monitor the distribution of the Golgi, and Hoechst dye for nuclei detection. Candidates were split in three categories based on phenotype: no, weak and strong effects. DLC2, a Cdc42 and RhoA GAP protein was identified as having a weak effect on cell-cell junctions. Despite the weak phenotype, DLC2 is an interesting candidate because it had been reported to act as a tumour suppressor in several types of cancers[130,137]. The mechanism underlying the tumour suppressor activity is not clear, but it has been suggested to function as a regulator of migration, which may affect metastasis formation.

When I joined the lab, I repeated the experiment to confirm the phenotype observed in the screen. I transfected a pool of 4 different siRNAs, specific for different regions of the DLC2 mRNA. These siRNAs had also been used in the screen. I also deconvoluted this siRNA pool by transfecting each siRNA alone and

compared the resulting phenotypes with cells transfected with a non-targeting siRNA. This was done to rule out off target effects.

By comparing non-targeting and DLC2 siRNA transfected HCE cells, I noticed that DLC2 depletion caused an effect on E-cadherin and β-catenin localisation: it perturbs the countinous staining along the cell membrane (Figure 3.1). This is particularly evident for E-cadherin, whereas it is not so intuitive for β-catenin. This is due to the fact these pictures were taken with an epifluorescent microscope, and I could not focus on the plane of the junctions to get a neat picture. In confocal pictures shown later (Figure 3.5), the phenotype is more evident. Nevertheless, this picture shows that depletion of DLC2 impairs the junctional barriers: in fact, DLC2 depleted cells have opened gaps with the neighbouring cells (see cells with red asterisks). This phenotype was particularly strong in mitotic cells, suggesting the DLC2 might be of functional importance during mitosis. Alongside the broken junctions, the DNA staining often revealed an atypical chromosome arrangement in what I thought it could have been metaphase. At this stage I cannot define it is a defect of late promethaphase, or metaphase yet, but I decided to quantify this aberrancy to see if there was a significant increase in comparison with the Control. I counted structure where I could detect a straight and main line of chromosomes embedded in a bipolar spindle structure, with chromsomes aligned outside, in a secondary like plate. Hence, DLC2 depletion may not only affect junction maintenance but also the distribution and alignment of chromosomes. I have not yet established a direct correlation between spindle phenotype and junction aberration. I think it would have been good quantifying the number of cells that showed both phenotypes in the same cells.

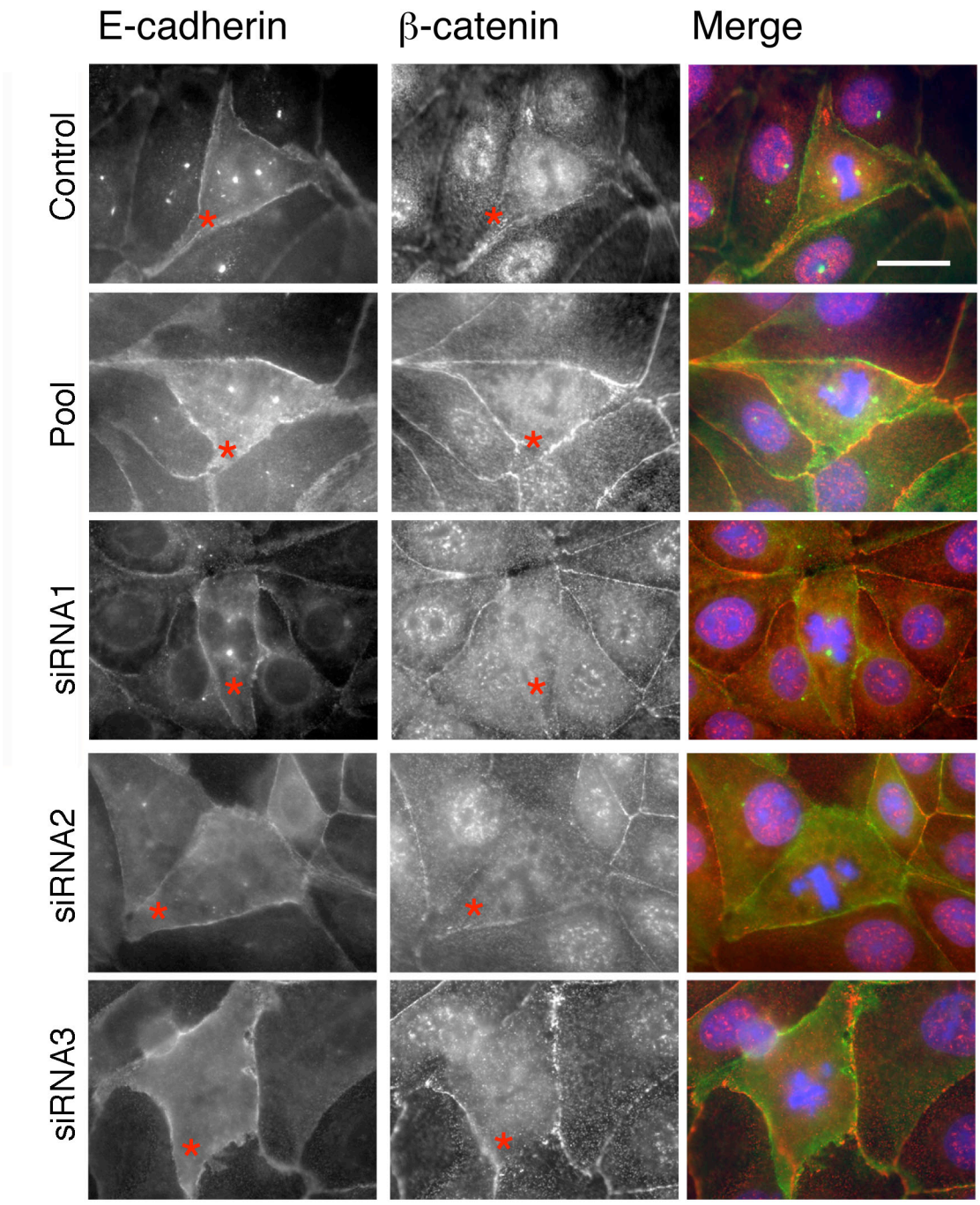

Figure 3.1 DLC2 KD affects cell-cell junctions

HCE cells transfected with control or DLC2-specific siRNAs (pool of those, were stained with AJs marker E-cadherin (green) and β-catenin (red). Red asterisks are pointing to mitotic cells with broken junctions.

Cells were fixed with methanol. Shown are epifluorescence microscopy images.

White bar represents 20μm.

By counting mitotic cells showing an abnormal chromosome alignment, it was evident that the misalignment phenotype is consistent for DLC2 depletion as it was observed with all four individual siRNAs (Figure 3.2).

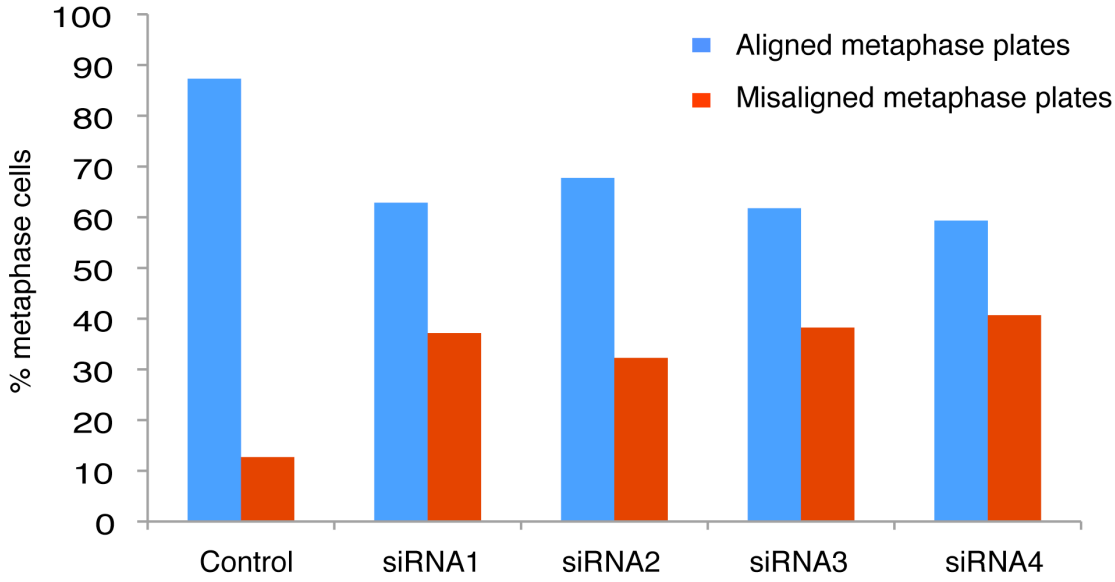

Figure 3.2 DLC2 regulates metaphase plate alignment

Independent transfection of 4 different DLC2 targeting siRNAs causes an increase of aberrant metaphase plates (red bars) and a decrease of normal ones (blue bars), compared with the control cells.

When I validated the efficiency of DLC2 depletion by WB (Figure 3.3), I confirmed that both pool and individual siRNAs decreased DLC2 protein level. Since siRNA 4, despite of having trying to load several times an equal amount of lyasate (estimated by α-tubulin level), it fluctuated too much for α-tubulin level. showed a slight toxic effect on the cells (this was determined by looking at α-tubulin levels when equal amounts of lysates were loaded), I decided to exclude it from the subsequent experiments and a new pool formed by oligo 1, 2 and 3 was established.

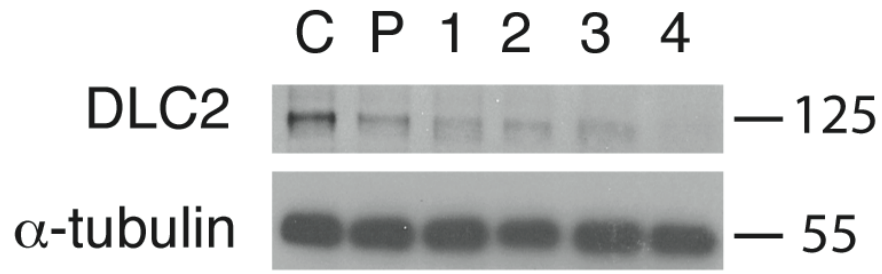

Figure 3.3 WB for validation of DLC2 KD in HCE cells

WB for DLC2 expression in HCE cells: C control, P pool of four siRNAs, 1 siRNA 1, 2 siRNA 2, 3 siRNA 3, 4 siRNA 4. α- tubulin was used as a loading control.

Since the most evident junctional phenotype was in mitotic cells, I looked at the mitotic spindle structure in HCE cells, to see if I could detect abnormal structures. Figure 3.4 shows that depletion of DLC2 (pool or individual siRNAs) impaired the formation of mitotic spindles with a normal morphology, but does not alter the number of centrosomes. Pictures in Figure 3.4 are epifluorescence microscopy, but one can spot two centrosomes per cell. It would have been better having confocal pictures, for a finer and more precise description of this phenotype. In the same picture, as the α-tubulin staining revealed, microtubule fibres were no longer arranged in the typical diamond-shape structure seen in control cells. Hence, depletion of DLC2 seems to affect either spindle formation or maintenance.

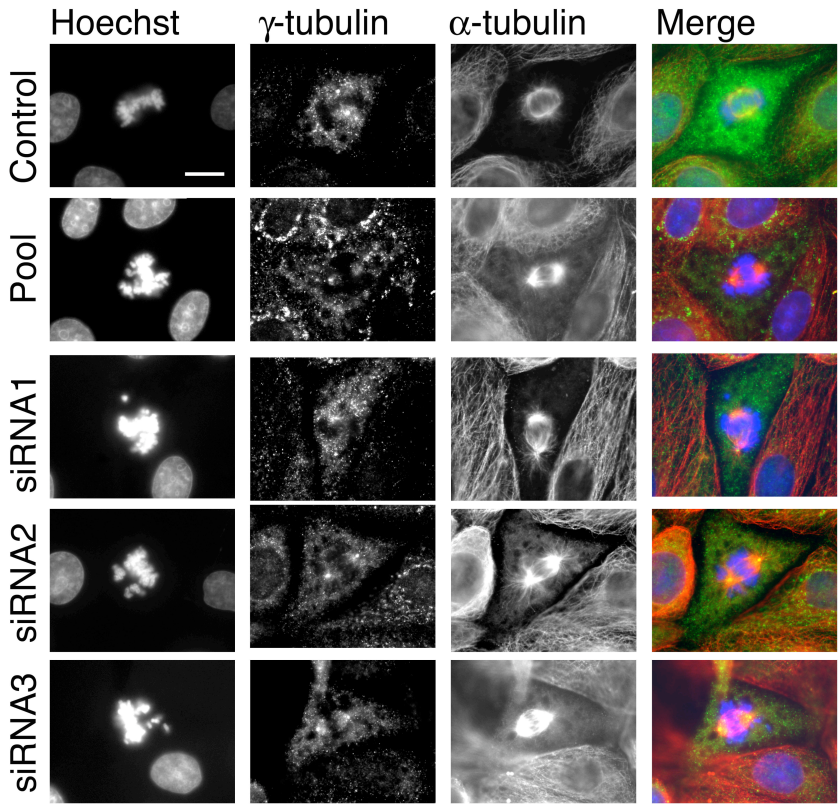

Figure 3.4 DLC2 KD affects spindle morphology

HCE cells transfected with control or individual siRNAs specific for DLC2 were stained with mitotic spindle markers: γ-tubulin (green) and α-tubulin (red).

Cells were fixed with methanol. Shown are epifluorescence images.

Bar represents 20μm.

3.2 FURTHER VALIDATION AND ANALYSIS OF DLC2 KD PHENOTYPE

I next asked whether the junctional phenotype observed in the first sets of experiments was specific for the markers investigated or could also be observed with other types of junctional markers. Figure 3.5 shows that there was a strong effect on both occludin and ZO1 (Figure 3.5A) (TJ markers), and on E-cadherin/α-catenin (Figure 3.5B) and p120Catenin (AJ markers). From these data, the junctional defect does not appear to be constrained to a particular subgroup of components of the junctional complex.

As shown previously, the strongest effect appeared in mitotic cells (Figure 3.6), where impairment of cell-cell junctions (represented by α-catenin staining) correlated with the appearance of aberrant mitotic spindle structures (α-tubulin staining). Quantification of misaligned metaphase chromosomes showed that depletion of the DLC2 KD significantly increased the number of cells with misaligned metaphase plates (Figure 3.7).

By looking in detail at the mitotic spindle structure, it was also evident that MTs (α-tubulin and EB-1 -plus-ends marker of microtubules- staining) were affected. DLC2 depletion altered the structure of the mitotic spindle, with microtubules no longer trapped in the diamond-shape structure and chromosomes misplaced outside of the metaphase plate (Figure 3.8).

Previous work demonstrated that p120catenin mediates the anchorage of astral microtubules at cell-cell junctions. Astral MTs are the microtubules nucleated at centrosomes that spread towards the cell cortex and are responsible for the positioning and orientation of the mitotic spindle throughout mitosis. In Figure 3.5, I have shown that p120catenin was mislocalized from the cell cortex region upon DLC2 depletion, indicating that the linkage between MTs and the cell cortex was impaired. Another key component in the MTs anchorage at the cell-cell junctions is APC. Figure 3.9 shows that DLC2 depletion affected dramatically APC localization and that the effect was equally strong on interphase cells and mitotic one: figure 3.9 shows indeed that the thick ring of APC at the cell cortex is widely reduced in DLC2 depleted cells, or completely abrogated. I observed previously that also p120catenin localization was heavily perturbed in both mitotic and interphase cells. This might imply that MTs attachment and therefore dynamics are impaired in interphase cells too.

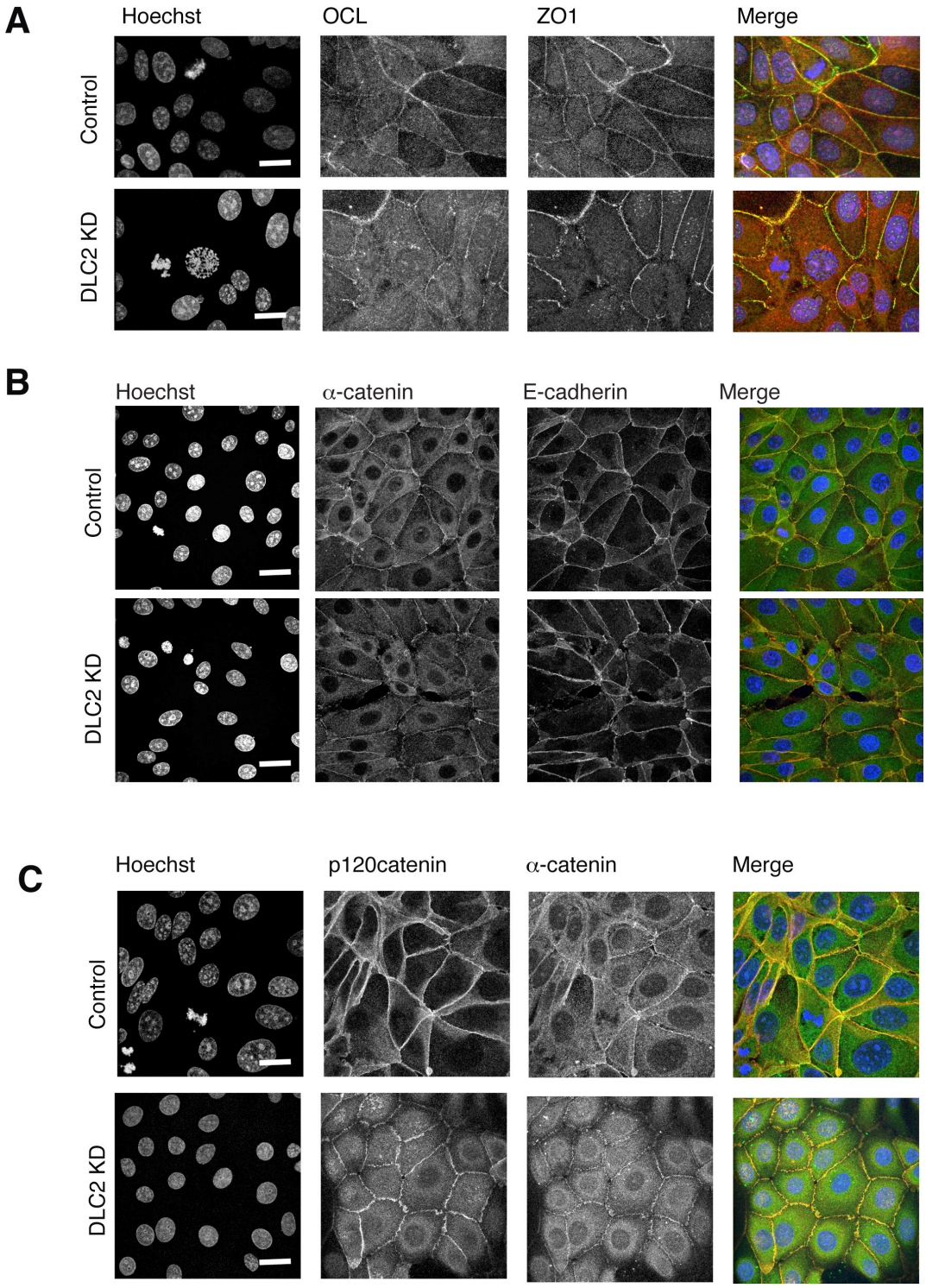

Figure 3.5 DLC2 KD affects cell-cell junctions

Control and DLC2 KD HCE cells stained with AJs markers E-cadherin red and β-catenin occludin (OCL) red and ZO1 green (A), AJs markers E-cadherin red and α-catenin (B), p120catenin red and α-catenin (C).

Cells were fixed with methanol. Shown are confocal images.

Bar represents 10μm.

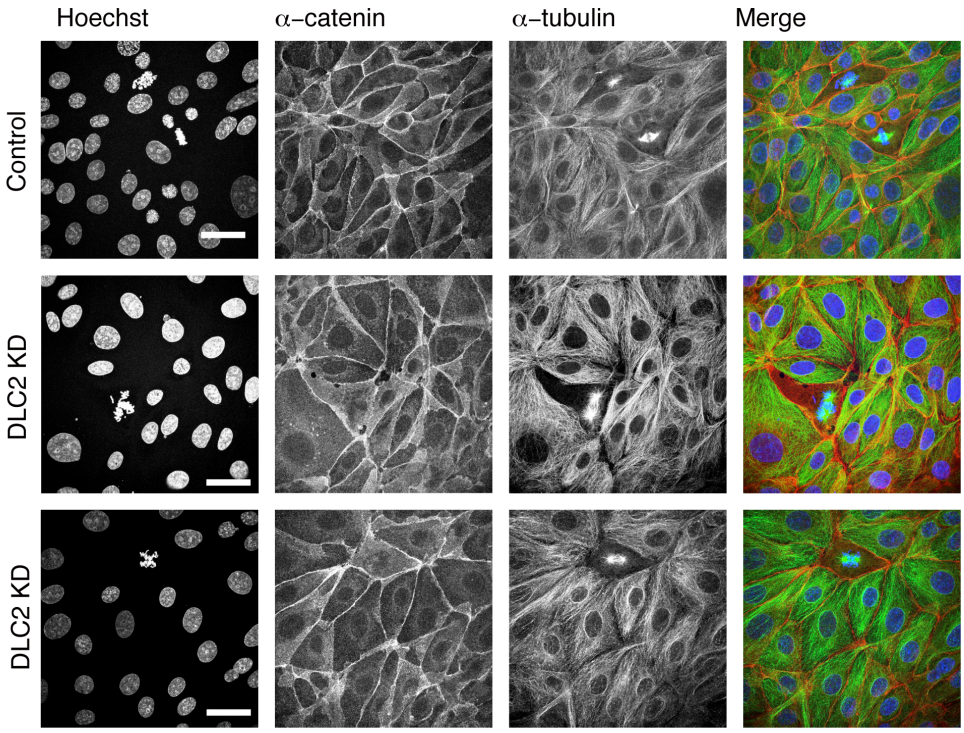

Figure 3.6 DLC2 KD affects spindle stability

This figure shows the effect on the mitotic spindle in HCE cells when DLC2 was depleted (α-tubulin in green). These cells were stained with α-catenin in red. Cells were fixed with methanol. Shown are confocal microscopy images.

Bar represents 20μm.

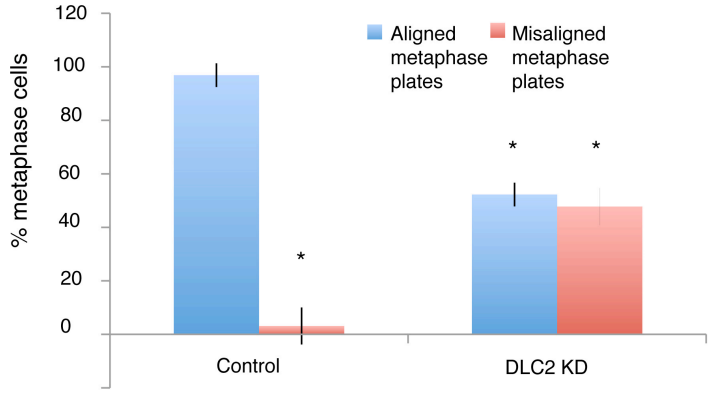

Figure 3.7 DLC2 regulates metaphase plate alignment

Transfection of a pool of 3 DLC2 targeting siRNAs in HCE cells caused an increase of aberrant metaphase plates (red bars) and a decrease of normal ones (blue bars), compared with the control cells.

Bars represent means of 3 independent experiments. Over 60 cells were counted per condition.

* $p<0.05$. Error bars represents standard deviations.

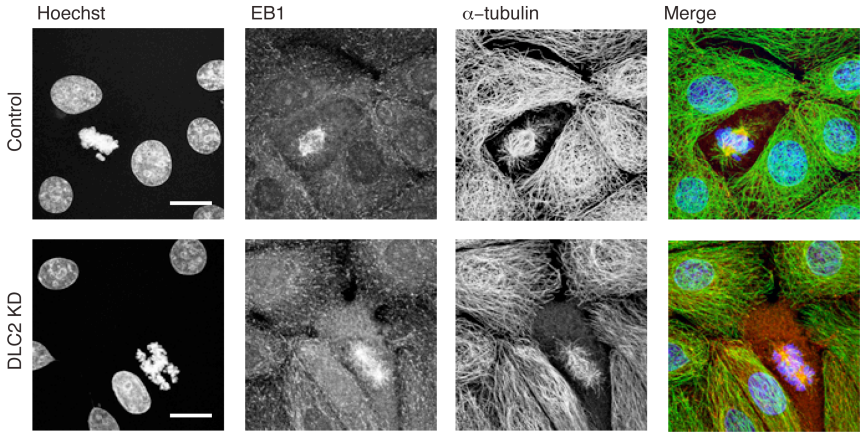

Figure 3.8 DLC2 KD affects spindle architecture

This figure shows the effect on the mitotic spindle in HCE cells when DLC2 was depleted (α-tubulin in green). Cells were stained for EB1 (plus-end marker) in red. Cells were fixed with 4% PFA and methanol. Shown are confocal microscopy images.

Bar represents 10μm.

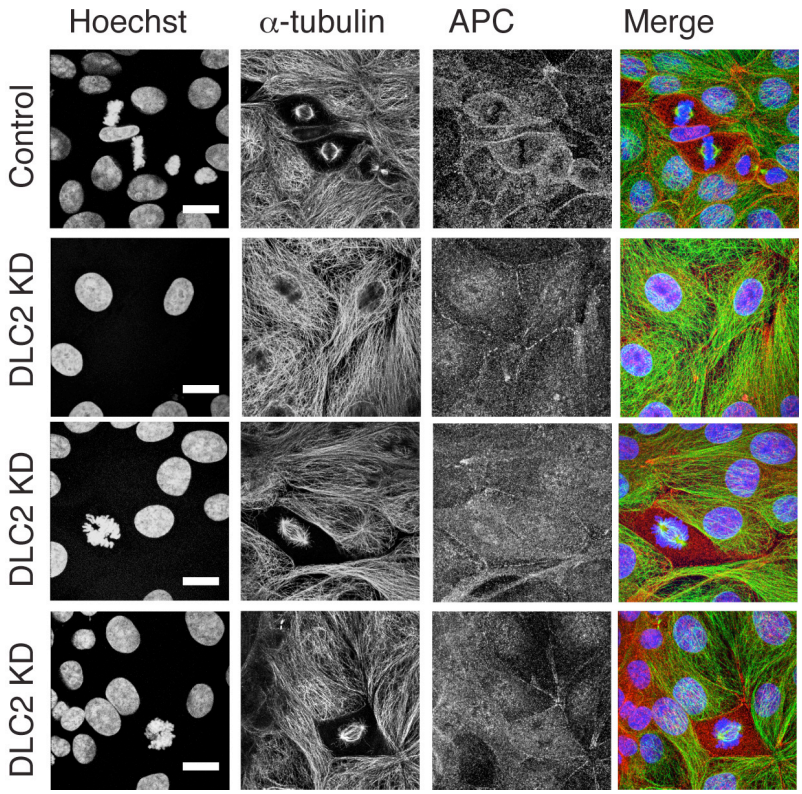

Figure 3.9 DLC2 KD affects localization of APC at cell-cell junctions

Control and DLC2 depleted HCE cells were stained for APC in red and α-tubulin in green. Cells were fixed with methanol. Shown are confocal microscopy images.

Bar represents 10μm.

3.3 DLC2 KD AFFECTS THE DE NOVO JUNCTION FORMATION AND THIS CORRELATES WITH CHROMOSOME MISALIGNMENT

To test if there is a correlation between junction formation and chromosome misalignment in metaphase, I performed a calcium switch experiment. In this assay, cells are resuspended in low calcium media. The initial calcium depletion disrupts junctional complexes; by adding calcium back to the cells, junction formation is induced.

Figure 3.10 shows control cells in low calcium also had misaligned metaphase plates at a percentage similar to DLC2 depleted cells in normal calcium medium (~40%). Upon adding calcium to the control cells, this number decreased gradually through time until the 24 hour time-point when junctions were perfectly formed. On the contrary, the percentage of DLC2 depleted cells with misaligned metaphase plates remained high (Figure 3.10C).

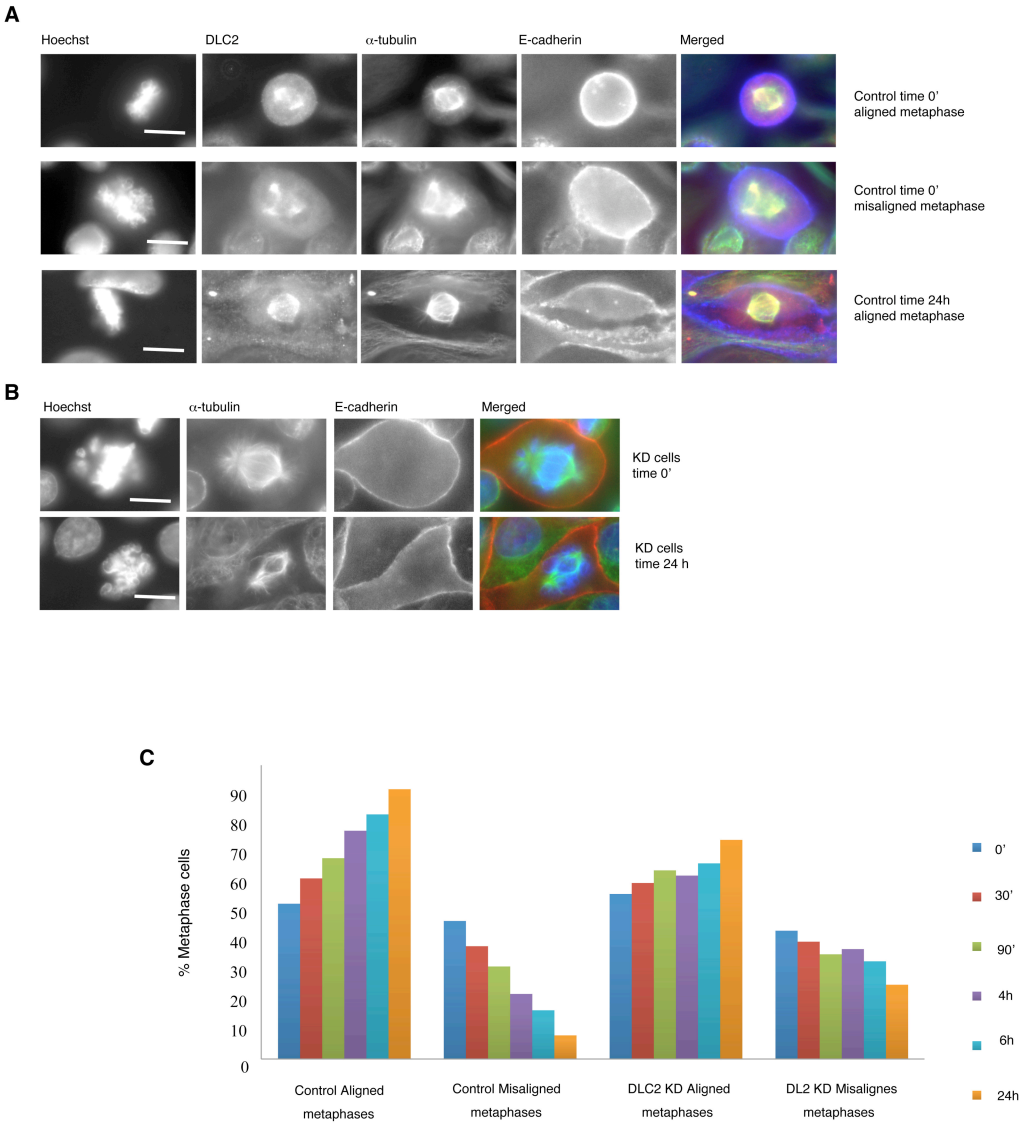

Figure 3.10 Spindle stability correlates with junction assembly

(A) Examples of aligned and misaligned metaphase control HCE cells at time 0′ and aligned metaphase control cells 24 hours after calcium addition. (B) Examples of misaligned metaphase DLC2 KD HCE cells at time 0′ and 24 hours after calcium addition. In panels A and B, cells transfected with siRNAs were stained for DLC2 (red), α-tubulin (blue) and E-cadherin (green) after performing the calcium switch protocol. Shown are epifluorescence microscopy pictures. Bar represents 10μm. (C) Quantification of Calcium switch assay: control normal metaphase, first group of bars; control misaligned cells, second group of bars; DLC2 KD normal metaphase, third group of bars; DLC2 KD misaligned cells, fourth group of bars. Bar colour represents different time points after calcium addition: dark blue 0′; red 30′; green 90′; purple 4h; light blue 6h; orange 24h. Bars represent mean of values**.** Over 60 cells per conditions were counted.

3.4 CELLS OVEREXPRESSING DLC2 DO NOT ENTER CELL CYCLE

To further confirm the DLC2 depletion phenotype specificity, I aimed to transfect DLC2 and non-targeting siRNAs into HCE cells and to rescue depletion with a mouse version of DLC2. The construct transfected well and could easily be detected; however, despite many transfected cells were detected, no transfected mitotic cells were found, indicating that DLC2 overexpressing cells may not proliferate.

To rule out the possibility that the absence of transfected mitotic cells was due to a technical issue, I tried to optimize the conditions of transfection. Firstly, cells were transfected with mouse DLC2-HA and were then treated overnight with Nocodazole to promote synchronization of cells in prophase. The cells were then fixed and prepared for analysis. Once again, no transfected mitotic cells were detected (Figure 3.11).

Next, I transfected cells with a form of DLC2 under a promoter responsive to the tetracycline repressor and co-transfected a plasmid encoding the tetracycline repressor. In these conditions, only the addition of tetracycline activates DLC2 expression. These allowed me to control precisely the moment the cells should have expressed transfected DLC2. Alongside the transfection, cells were treated with Nocodazole overnight, to increase the number of mitotic cells. Four hours before fixation, tetracycline was added to the cells to allow DLC2 expression. Despite DLC2 expression was induced in cells in mitosis, no transfected mitotic cells were found (Figure 3.11).

There could have been other approaches I had not tried, that could have helped me in overexpressing DLC2 in mitotic cells. I could have titrated more the DLC2 cDNA concentration more, for instance, and also I cannot exclude the tag itself does not obstacle the right localization and expression of DLC2 construct.

Overall, these data suggest that DLC2 overexpression inhibits the entry in mitosis and may even trigger the exit of cells from the cell cycle if overexpressed during the cell cycle.

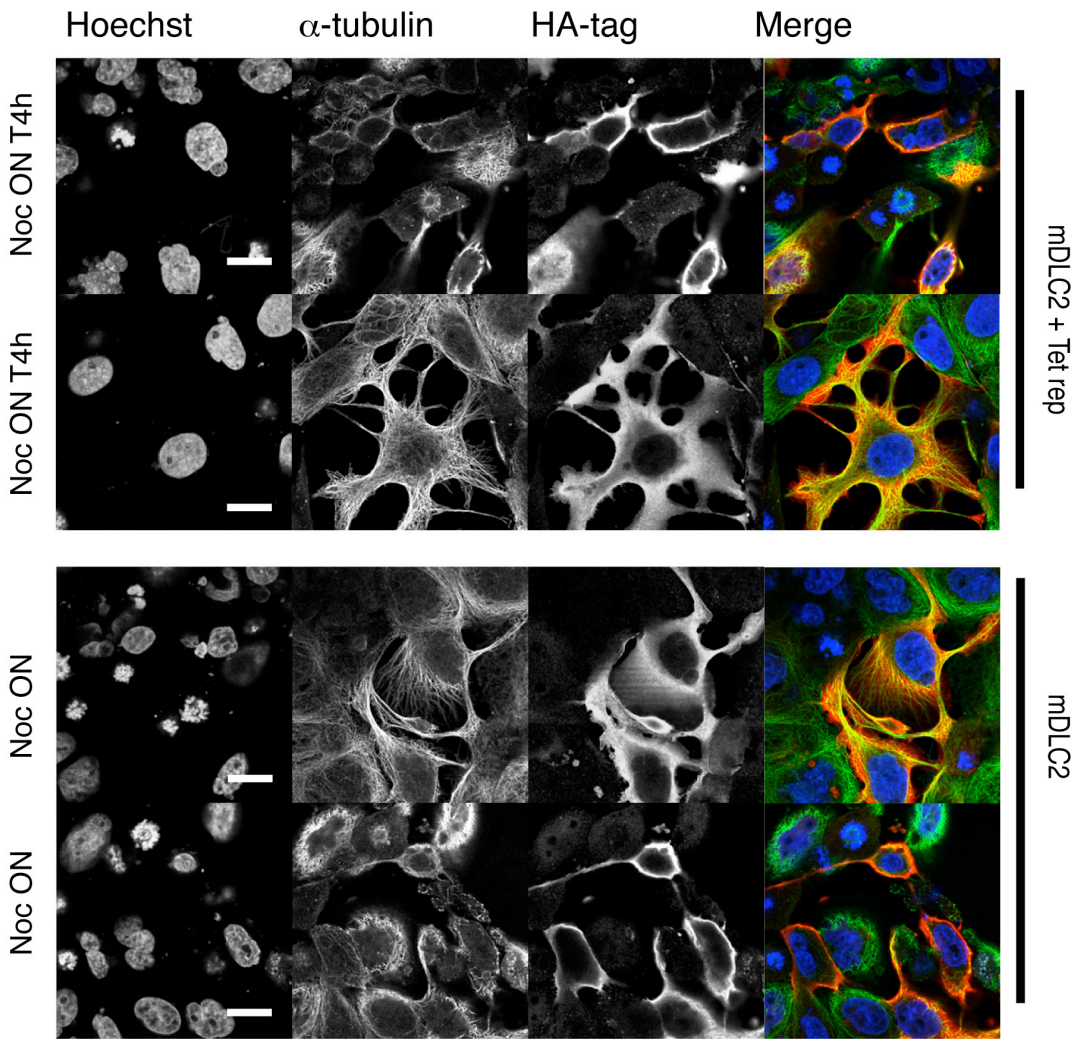

Figure 3.11 Transfection of DLC2 cannot be used to demonstrate rescue

HCE cells were treated with nocodazole ON and then transfected for 6h, or cotransfected with DLC2-HA and Tet-repressor constructed, synchronized ON and treated with tetracycline for 4h to induce DLC2 expression. The cells were then stained with Hoechst dye, HA to detect transfected DLC2 (in red) and α-tubulin in green. Note, in none of these cases mitotic cells overexpressing DLC2 were found. Shown are confocal microscopy pictures.

Bar represents 10μm.

3.5 DISCUSSION

Initially DLC2 was picked as a candidate in a cell-cell junction integrity screen. Here, I showed that DLC2 is important for epithelia in a dual manner: first, junctions are destabilized and this is particularly evident in mitotic cells. As I discussed in the introduction, it is paramount that a cell retains cell-cell junctions in mitosis since this guides cell division in the correct tissue plane, and it prevents cells from escaping the epithelial layer. On the other hand, mitotic cells showed aberrant mitotic spindle structures with scattered chromosomes and microtubules not tidily organized in the typical diamond-shape machinery.

Interestingly junction stability and chromosome alignment need to be finely orchestrated to ensure correct cell division. The calcium-switch experiment demonstrated that when junctions are disassembled due to lack of calcium, the number of misaligned metaphase plates increased in control cells. This number decreased with the re-addition of calcium, indicating that junction stability is essential for chromosome alignment in metaphase. However, DLC2 depleted cells failed to rescue chromosome alignment after calcium re-addition, indicating that DLC2 is important for the regulation of chromosome alignment and junction stability in mitosis.

I can speculate, so far, that DLC2 phenotype seems to be connected to a defect in astral MT anchorage. This is supported by the evidence that p120catenin and APC (mediators of MT anchorage at the cell cortex) are mislocalized from the cell cortex upon DLC2 depletion. It seemed to me that APC mislocalization is actually stronger than the one observed for p120catenin and is evident in interphase cells as well. This would need to be proved by quantifying the signal intensity. Nevertheless, the observed defect on APC and p120catenin raises the possibility that there might be an effect on MT anchorage at the cell cortex in interphase cells.

CHAPTER 4:
DLC2 REGULATES CDC42 IN METAPHASE

CHAPTER 4: DLC2 REGULATES CDC42 IN METAPHASE

4.4 DLC2 IS A GAP FOR CDC42 AND RHOA

In 2003, DLC2 was reported to have GTPase activating protein (GAP) activity for Cdc42 and RhoA, but not Rac[104]. When small GTPases were originally characterized, they were distinguished on the base of their effect on actin[45]. In particular, overactivation of RhoA was shown to induce formation of stress fibres. Since DLC2 was reported as a GAP for RhoA, firstly I confirmed this by checking if DLC2 depletion could cause an increase in stress fibre formation. Figure 4.1 shows DLC2 depletion indeed led to increased stress fibre formation in interphase cells, suggesting that RhoA was more active. Primarily in mitotic cells, I also observed an increase in membrane spikes reminiscent of filopodia, suggesting that DLC2 depletion might also lead to increased levels of GTP-bound Cdc42. Pictures shown are projections of the whole z-stack. HCE cells in control situation barely forms stress fibres or filopodia. They are extremely flat and therefore I have decided to show and analyze the whole z-stack, rather than showing a single basal section.

I next used a G-LISA assay to measure levels of activated small GTPases. By comparing control and DLC2 depleted HCE cells, it was evident that DLC2 depletion induced an increase in GTP-bound RhoA and Cdc42, but not Rac (Figure 4.2 A).

In the previous chapter, I had shown that the most dramatic phenotype of DLC2 KD appeared in metaphase. I therefore tested small GTPase activation levels upon DLC2 depletion in mitotic cells. In order to do this, I used a method validated and published previously. Kimura *et al*. had shown that after synchronization of cells in prometaphase with Nocodazole (Noc) treatment (100 nM) followed by wash-off, it is possible to trigger synchronized entry into mitosis with a peak of metaphase/anaphase cells at 45 minutes, and telophase cells after 90 minutes after release of the block[141]. Performing G-LISA assays at these time-points and comparing with cells still arrested revealed that only GTP-bound Cdc42 was increased in metaphase cells upon depletion of DLC2 (Figure 4.2B and C).

This method had been changed for the original protocol adopted by Kimura et all. I am aware that the lack of initial block in S-phase and the lack of mitotic shake-off after nocodazole treatment might represent an issue since the rest of the cells in interphase will have an effect on the measurement. Taken this into account, it must be said that we can exclude the difference I see I metaphase upon DLC2 depletion has to be attributed to the interphase cell population. This is because if this was true, I most likely would have observed this change at the other time point too, since the percentage of non dividing cells is the same of that present at the 45'. Therefore, the lack of effect at the other time-point is an indication that Nocodazole treatment per se does not change the level of active RhoA or Cdc42 in HCE when DLC2 is depleted, compared with the control. This made me confident in further using this short version of the method also in other experiments I describe afterwards in this thesis. In any case, to be extremely sure it would have been interesting performing the same experiments, by increasing the pool of mitotic cells by collecting the prometaphases and then release them from the Nocodazole block (mitotic shake off).

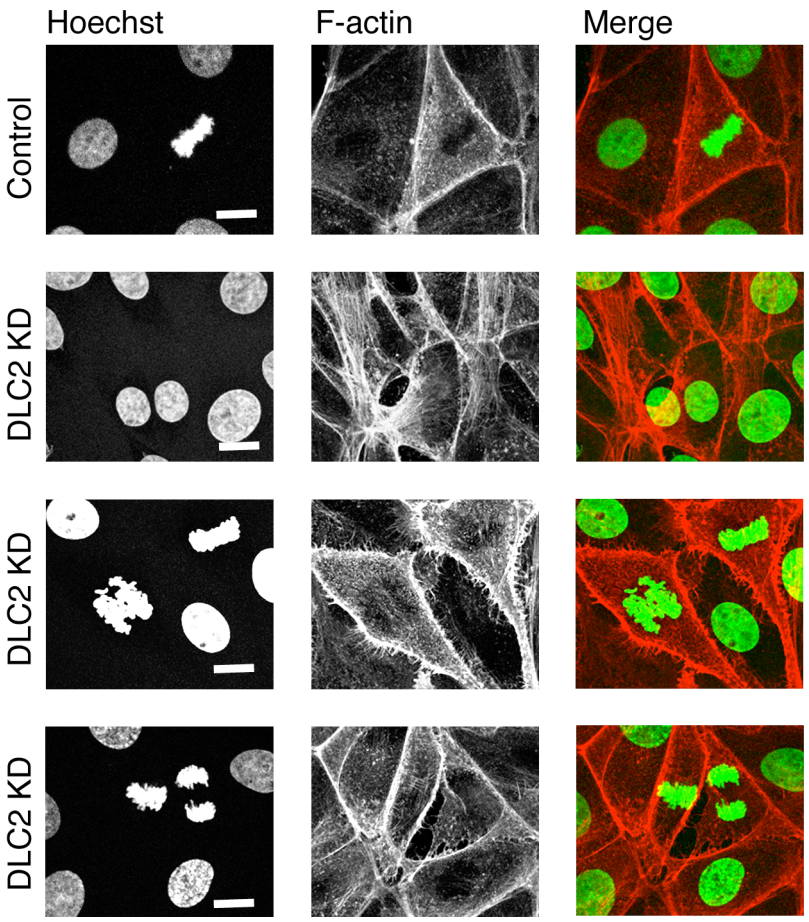

Figure 4.1 DLC2 KD induces increases in actin stress fibres

Control and DLC2 KD HCE cells stained with Hoechst and phalloidin. Note, DLC2 KD increased stress fibres along the base of cells and spikes along the lateral membrane. The picture are projections of the whole z-stack.

Shown are confocal microscopy pictures.

Bar represents 10μm.

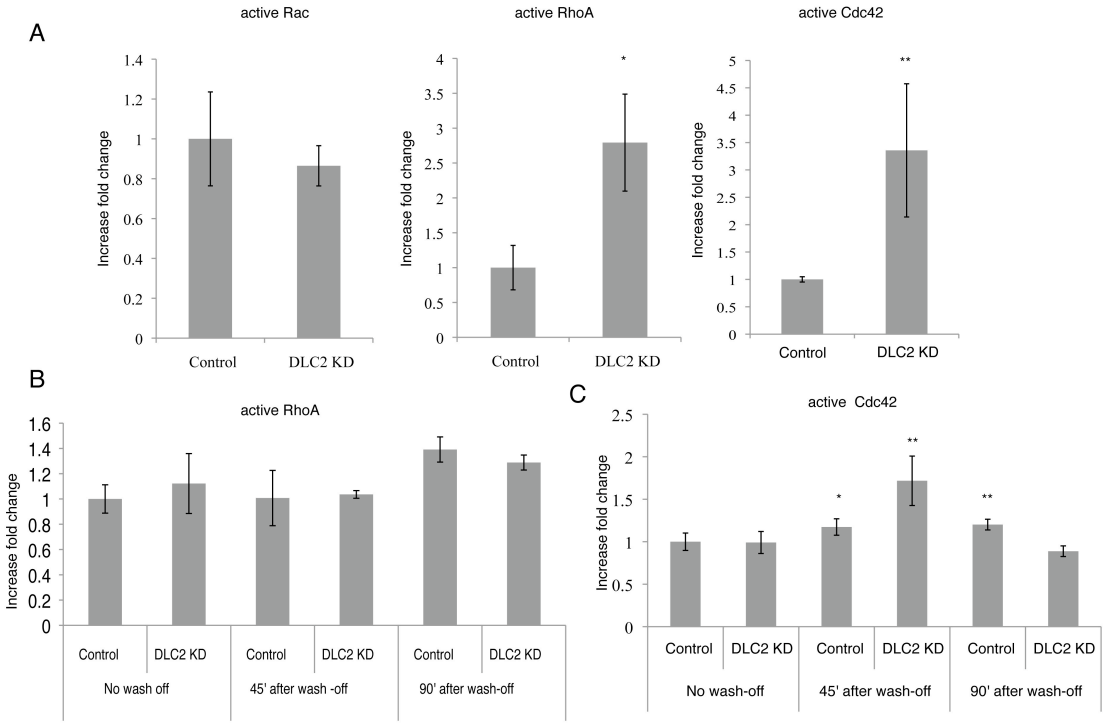

Figure 4.2 DLC2 KD affects GTP-bound Cdc42 levels in mitosis

(A) Cdc42, RhoA and Rac G-LISA assays were performed with non-synchronised cells. DLC2 KD resulted in an increase of active RhoA and Cdc42 but not Rac.

(B) RhoA G-LISA of HCE cells treated with Nocodazole. Time points analysed: 0, 45, and 90 minutes. At 45 minutes (metaphase peak), DLC2 depletion did not effect RhoA activity in mitosis.

(C) Cdc42 GLISA of HCE cells treated with Nocodazole. Time points analysed: 0, 45, and 90 minutes. At 45 minutes (metaphase peak), DLC2 depletion resulted in increased levels of GTP-bound Cdc42.

All bars represent means of values of three experiments. *<p0.05 ** p<0.01.

4.5 DLC2 DEPLETION-INDUCED CHROMOSOME MISALIGNMENT OCCURS VIA DEREGULATION OF CDC42

The G-LISA experiments revealed DLC2 as a specific regulator of Cdc42 in metaphase. Considering that I observed a defect in chromosome alignment in metaphase, I speculated that misregulation of Cdc42 could be the primary cause for the chromosome misalignment defect detected in DLC2 depleted cells. However, at this point I could also not rule out a contribution of RhoA despite that I had seen no difference in levels of active RhoA, differential spatial regulation may not be evident in assays measuring total active GTPase levels. To establish more clearly which small GTPase was implicated in the observed chromosome misalignment phenotype, I performed a double knockdown with Cdc42/DLC2 or RhoA/DLC2 and counted the number of aligned and misaligned metaphase cells. As shown in Figure 4.3, only the simultaneous depletion of DLC2 and Cdc42 resulted in a similar number of misaligned metaphase cells than control, indicating that co-transfection of Cdc42 siRNAs could rescue the DLC2 phenotype. Figure 4.4 shows that DLC2 was equally well depleted in single and double siRNA transfections, indicating that rescue was indeed due to depletion of Cdc42.

To further prove that RhoA was not involved the chromosome misalignment phenotype, I adopted a parallel strategy. I treated both control and DLC2 depleted HCE cells with C3 transferase (RhoA-C inhibitor). Although C3 treatment inhibited RhoA activity – as indicated by the decrease in stress fibres induced by DLC2 depletion (Figure 4.5A) - it did not result in a decrease of cells with misaligned chromosomes (Figure 4.5B). Hence, the mitotic DLC2 phenotype cannot be rescued by RhoA inhibition.

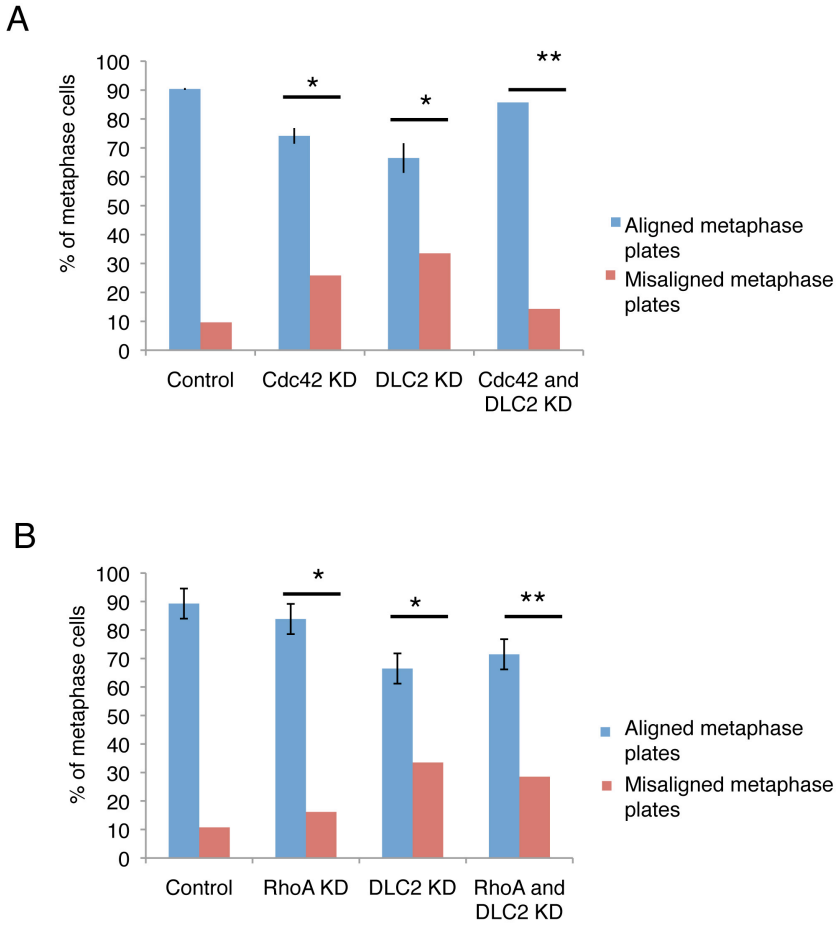

Figure 4.3 Cdc42 but not RhoA is involved in the misalignment phenotype caused by DLC2 depletion.

HCE cells were transfected with Control, Cdc42, DLC2, Cdc42/DLC2 specific siRNA, or control, RhoA, DLC2 and RhoA/DLC2 siRNA. Cells were analyzed for metaphase plates misalignment defects. Panel A and B represent percentage of aligned metaphase plates (blue bars) and misaligned metaphase plates (red bars).

All bars represent means of values of three experiments. *<p0.05 ** p<0.01.

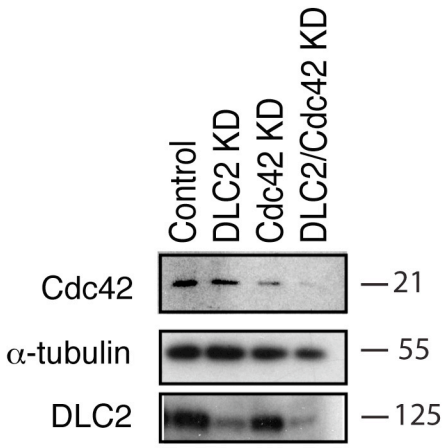

Figure 4.4 WB of Cdc42/RhoA KD and transfection of Cdc42 constructs

HCE cells were transfected with siRNAs as indicated. The cells were then lysed and expression of the indicated proteins determined by WB.

α-tubulin was used as an internal loading control.

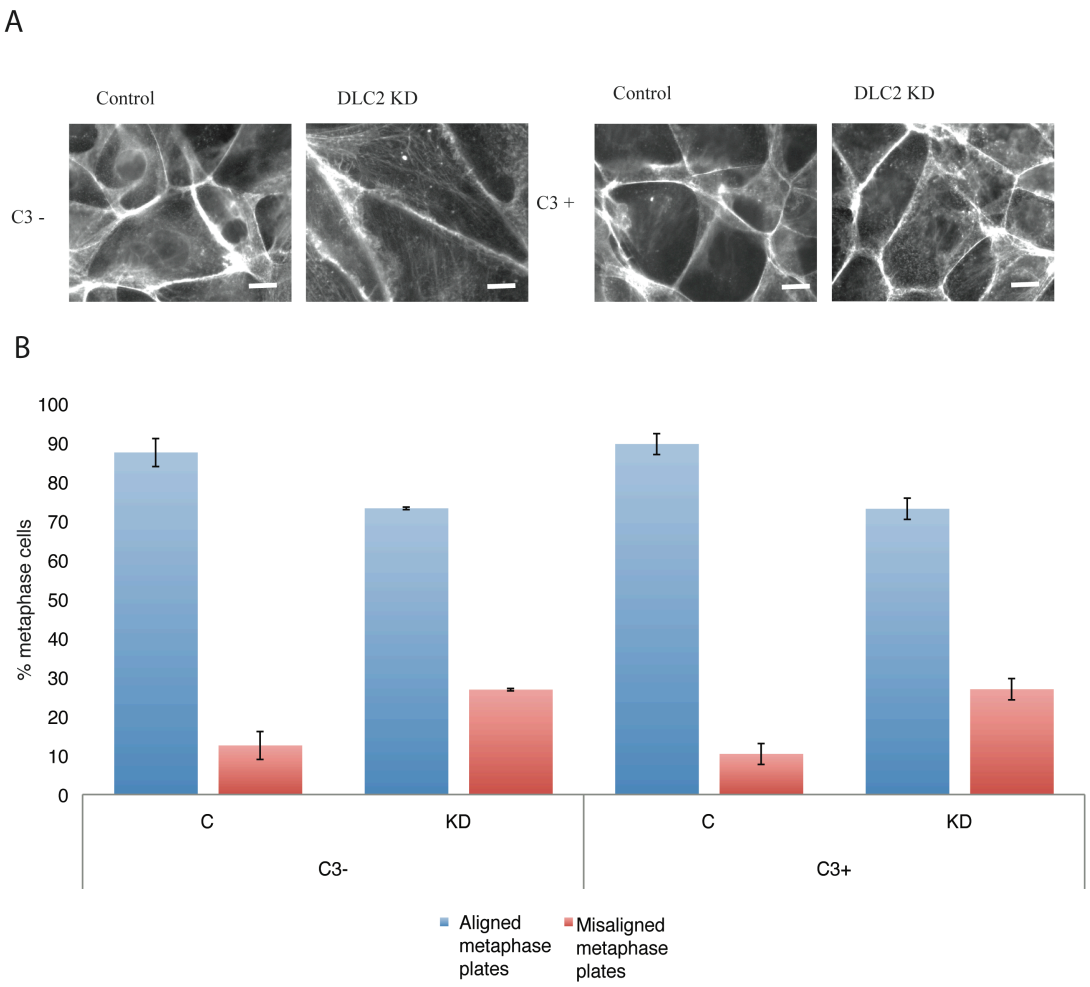

Figure 4.5 RhoA is not involved in the misalignment phenotype caused by DLC2 depletion.
(A) Epifluorescence microscope pictures of actin staining in of Control and DLC2 siRNA transfected HCE cells that were treated with C3 transferase as indicated. Control cells did not have active stress fibres, but DLC2 depletion induced actin stress fibres and these were abolished upon C3 transferase treatment.
(B) Count of misaligned/normal metaphase HCE cells upon transfection of Control (C) and DLC2 siRNAs followed by treatments with C3 transferase as indicated. Values in the graph are an average of 2 experiments.
Bar represents 10μm.

4.6 DLC2 LOCALIZES ALONG MTS

I next stained cells for DLC2 to identify the subcellular localization of the protein. I used a commercially available antibody (see Material and methods) that recognised DLC2 specifically in immunoblots. As Figure 4.6 shows, the DLC2 antibody labelled microtubules in interphase and metaphase cells. In metaphase, DLC2 decorated the mitotic spindle, suggesting that DLC2 associates with microtubules in interphase and mitotic spindle cells. Here, the pattern looks quite dotted suggesting that perhaps DLC2 does not decorate smoothly microtubules, but maybe parts of them where vescicles are attached. The two-hybrid screening results suggest that the nature of the interaction is direct, but nevertheless DLC2 can localize in patches, resembling a vescicular localization. In mitosis, DLc2 localises specifically along the MTs within the spindle. It is hard to detect it along the astral MTs, but I have seen DLC2 localizing with microtubules along the cell cortex (Fig 4.6 A). This suggests that despite astral MTs are usually less dense and bright, DLC2 is able to associate with other MTs, apart from those within the spindle. The microtubule staining was strongly reduced upon transfection of DLC2 siRNAs (Fig 4.6 B). Hence, DLC2 seems to interact, directly or indirectly, with microtubules.

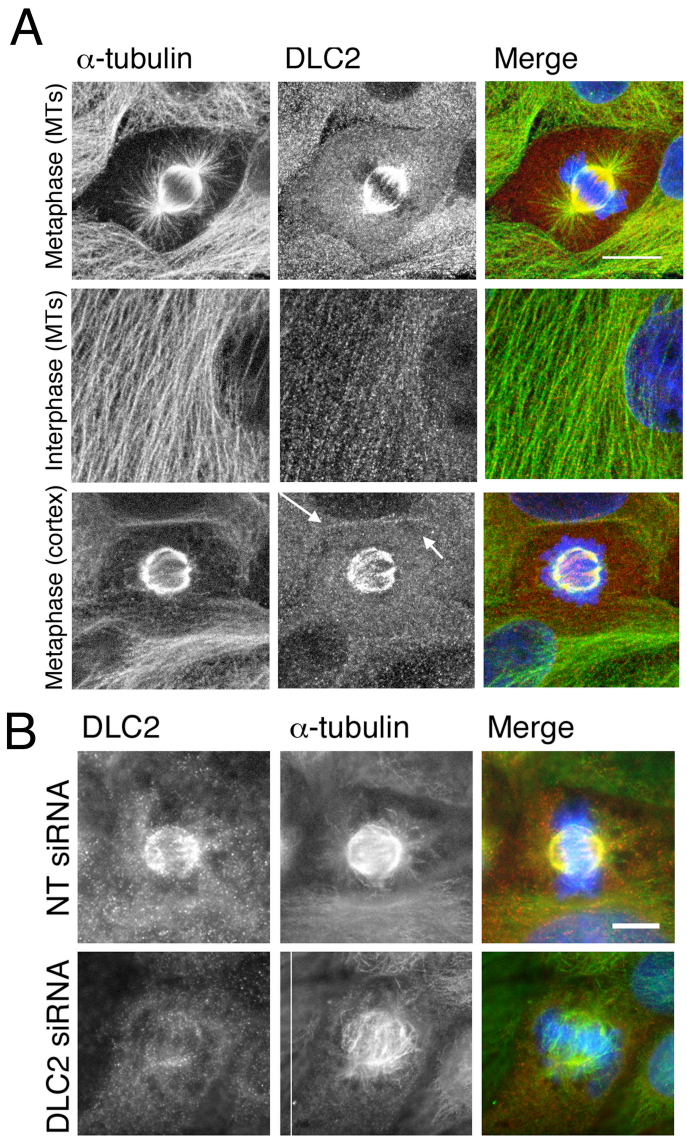

Figure 4.6 DLC2 localizes on the mitotic spindle

(A) HCE cells were stained for α-tubulin and DLC2 in red. Cells were fixed with 4% PFA and methanol. Shown are confocal images.

(B) DLC2 staining disappears in HCE cells transfected with DLC2 specific siRNA, compared with control.

Bar represents 10μm.

Identifying interaction partners is fundamental for the identification of the molecular mechanism by which DLC2 regulates mitotic spindle organisation. By performing co-immunoprecipitation assays, I found that DLC2 interacts with α-tubulin, EB-1 (a marker of the plus end of the MTs), and the AJ markers

p120catenin and E-cadherin (Fig. 4.7). TJs proteins were not found to co-immunoprecipitate (Figure 4.7 right panel), and also β-catenin.

I have performed this IPs not on cold, to prevent MTs from depolymerising, since from DLC2 staining I have never observed DLC2 dots associated with singe subunit of tubilin (e.g. in the proximity of tips of MTs next to cells cortex). This experimental procedur choice could interfere a little with the results because the lack of depolymerization might drive aspecific immuniprecifitation of MT interactors, such as motor proteins or scaffolds, which are not interacting or forming necessarily a complex with DLC2. Perhaps, to enforce the specificity of my assay I should have tried to test the presence of other interactors, such as GEF-H1 which is unlikely to bind DLC2, or other molecules (dynein or CLASPs). Nevertheless, this experiment suggested that DLC2 might be involved in the regulation of the interaction between the plus end tips of MTs E-cadherin-based cell-cell contacts.

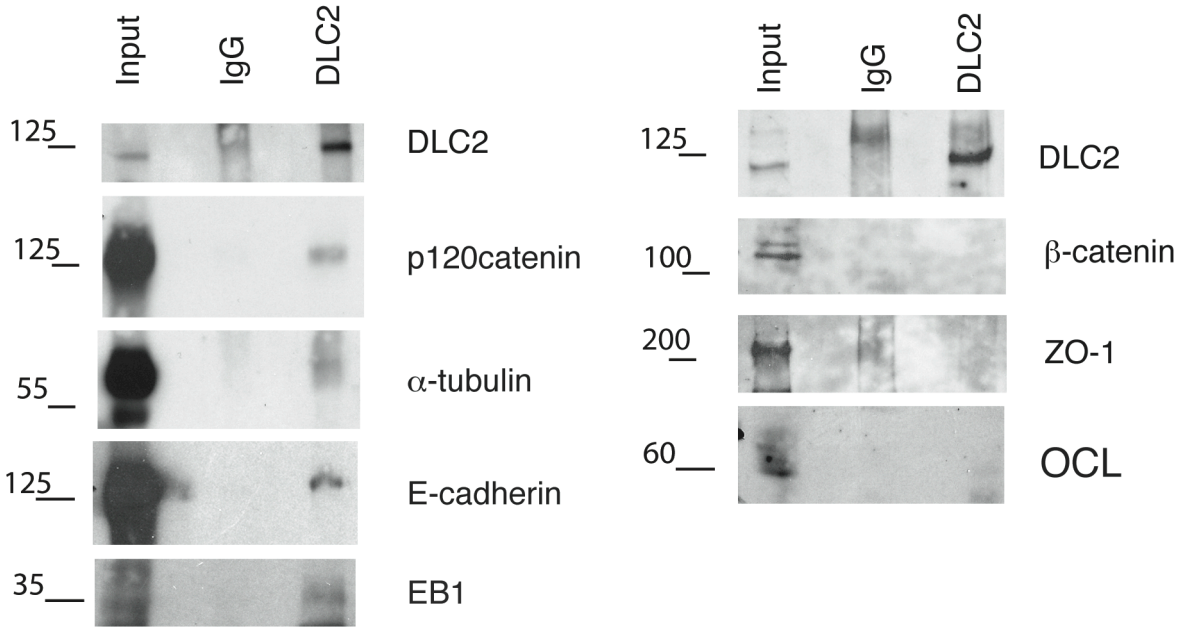

Figure 4.7 Identification of candidate interaction partners

Immunoprecipitates of DLC2 from HCE cell extracts were analyzed by WB against α-tubulin, EB1, E-cadherin and p120catenin (left panel) and OCL, ZO-1 and β-catenin (right panel).

4.7 DISCUSSION

In this chapter I have shown that DLC2 is a functionally relevant GAP for both Cdc42 and RhoA in non-synchronised HCE cells, but only relevant for the maintenance of active Cdc42 levels during mitosis. Moreover, Cdc42 is the GTPase relevant for chromosome alignment downstream of DLC2. This was supported by the observation that double knockdown of DLC2 and Cdc42 is able to rescue the number of misaligned metaphase cells induced by single depletions of either Cdc42 or DLC2. Double depletion DLC2/RhoA or C3 transferase treatment failed to rescue the DLC2 KD phenotype, further supporting the functional specificity of Cdc42.

During metaphase, chromosomes should be stably attached to kinetochore fibres and be aligned properly into a metaphase plate. I have not yet explained how DLC2 causes the observed chromosome defect, but the fact that endogenous DLC2 staining reveals a localization along the microtubules inside and outside the mitotic spindle supports the already mentioned idea that DLC2 regulates microtubules dynamics via regulation of Cdc42 levels in metaphase. Once again, I cannot rule out DLC2 plays a role in microtubule regulation outside mitosis. In contrast, G-LISA results show that DLC2 regulates level of active Cdc42 also in interphase cells; however, the roles of DLC2 in interphase might be more complex since at this stage also RhoA is regulated by DLC2. Moreover, if DLC2 also regulates microtubules in interphase cells, this function is not as important as during mitosis, as cell-cell adhesion is not as obviously affected in interphase as in mitotic cells.

Nevertheless, the immunoprecipitation experiment re-enforces the idea that DLC2 is involved in anchorage and stabilization of microtubules in epithelial cells. DLC2 is able to form complexes with AJs components such as E-cadherin and p120catenin (the latest is directly connected to the plus ends of the microtubules via EB1) and also co-immunoprecipitates α-tubulin and EB1.

CHAPTER 5:
KIF1B IS A KEY ELEMENT OF THE DLC2 PATHWAY

CHAPTER 5: KIF1B IS A KEY ELEMENT OF THE DLC2 PATHWAY

5.1 Introduction to forces acting on the mitotic spindle

The mitotic spindle is not a steady structure; on the contrary, it is highly dynamic and constantly under change. The typical diamond shape structure detectable in mitosis is the result of a complicated network of many and different types of microtubules organized in a unique and finely balanced manner. There are three major categories of microtubules contributing to the mitotic spindle: kinetochore microtubules, responsible for chromosome attachment and alignment onto the metaphase plate; non-kinetochore fibres, fundamental for stabilization of chromosomes inside the spindle and their segregation during anaphase; and astral microtubules that anchor the mitotic spindle to the cell cortex.

In 2009, Dumont and Mitchison reviewed forces acting on the mitotic spindle in mammalian cells[152]. They identified five major force-generating mechanisms: the first is based on kinesin-5 family members, which are motors cross-linking microtubules in the spindle that are responsible for pushing microtubules apart by outward force and are required for bipolarity in most spindles; the second involves microtubule depolymerisation at the kinetochores; the third is found at the poles and involves dynein and/or minus-end kinesins, which organize and focus minus-ends; the fourth involves chromosome arms and plus-end-directed chromokinesins, which push microtubules, exerting away-from-the-pole force; the last mechanism is located at the cortex and involves dynein and kinesin 1 family members, which pull on astral MTs (Figure 5.1).

Figure 5.1 Forces acting on the mitotic spindle

Cartoon representing forces acting on the mitotic spindle. Five different categories of forces can be identified: (1) the first is based on kinesin-5 family members, motors cross-linking microtubules in the spindle, responsible for pushing microtubules apart by outward force; (2) the second involves depolymerization at the kinetochores; (3) the third is found at the poles and is controlled by dynein and/or minus-end kinesins; (4) the fourth involves chromosome arms and plus-end-directed chromokinesins, which push microtubules, exerting away-from-the-pole force; (5) the last mechanisms is located at the cortex and involves dynein and kinesin 1 family members, which pull on astral MTs (adapted from Dumont and Mitchison, 2009)[152].

5.2 DLC2 KD does not effect dynein but alters Kif1B localization

Since DLC2 depletion resulted in increased misaligned metaphase plates and a distortion of the mitotic spindle itself, I raised the question of how forces acting on the mitotic spindle are altered upon DLC2 depletion.

Four out of five classes of forces identified in the previous section are instigated by motors; therefore, I decided to test whether DLC2 depletion had an effect on kinesins or dyenin. Staining for dynein in control and depleted cells revealed that dynein localisation was not altered upon depletion of DLC2 (Fig 5.2). This suggests that DLC2 does not have an evident effect on dynein localization in the mitotic spindle. In fact, dynein staining simply reflected the distorted microtubules patterned caused by DLC2 depletion. Moreover, dynein is a motor protein that walks towards the minus end of the microtubules, and the defect observed in DLC2 depleted cells could be thought of as directly connected to the plus-ends. It is indeed the plus-ends of the microtubules that connect the mitotic spindle to the cell cortex on one hand, and, on the other hand, they are responsible for capturing chromosomes. This gave me reasons to believe that I should investigate kinesins, which are plus-end directed motor proteins.

Interestingly, one of the first papers published on DLC2 showed a yeast two-hybrid screen in which they used DLC2 as a bite[139]. They found a member of the kinesin 3 family, Kif1B, to interact with DLC2. Interested in verifying if this kinesin was a part of the jigsaw I was trying to resolve, I first tested whether Kif1B interacts with DLC2 by co-immunoprecipitation. Indeed, the two proteins efficiently co-immunoprecipitated with each other, indicating that they also form a complex in epithelial cells (Figure 5.3).

I next looked at Kif1B localization and asked if and how its localization was affected by DLC2 KD. Figure 5.4 illustrates that in control cells Kif1B localized at the cell cortex, suggesting it might be implicated in astral MT anchoring and pulling. Upon DLC2 depletion, Kif1B was dramatically decreased at the cell cortex, indicating that DLC2 is important for Kif1B localization. By WB, Kif1B protein levels were decreased upon DLC2 depletion, further supporting the importance of DLC2 for Kif1B (Figure 5.5). As Kif1B is a motor protein and my data show that it localises to the cell cortex, these observations are compatible with the hypothesis that depletion of DLC2 affects the balance of forces that act on the mitotic spindle.

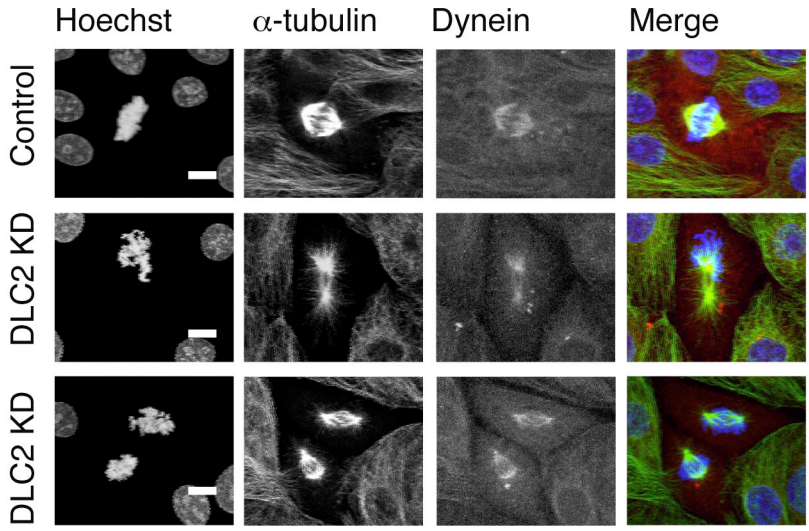

Figure 5.2 Dynein is not affected by DLC2 depletion

Control and DLC2 depleted cells were stained for α-Tubulin (green) and dynein in red. Cells fixed with 4% PFA and methanol. Shown are confocal microscopy images.

Bar represents 10μm.

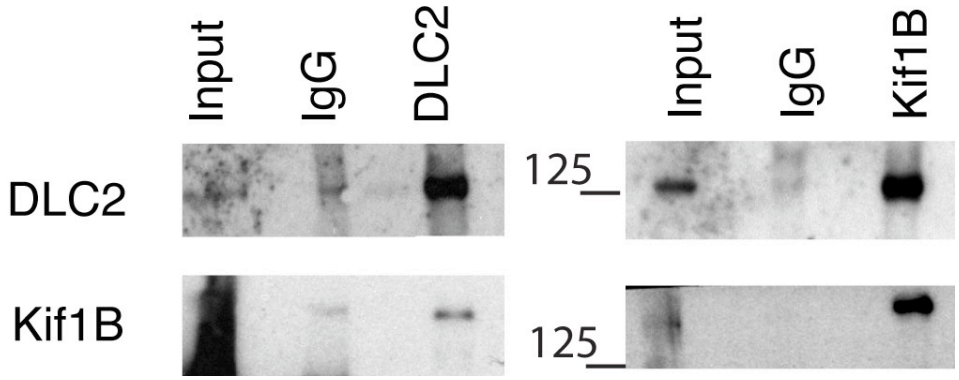

Figure 5.3 Identification of DC2-Kif1B interaction

Immunoprecipitates of DLC2 or Kif1B were analysed by WB with antibodies against the two proteins.

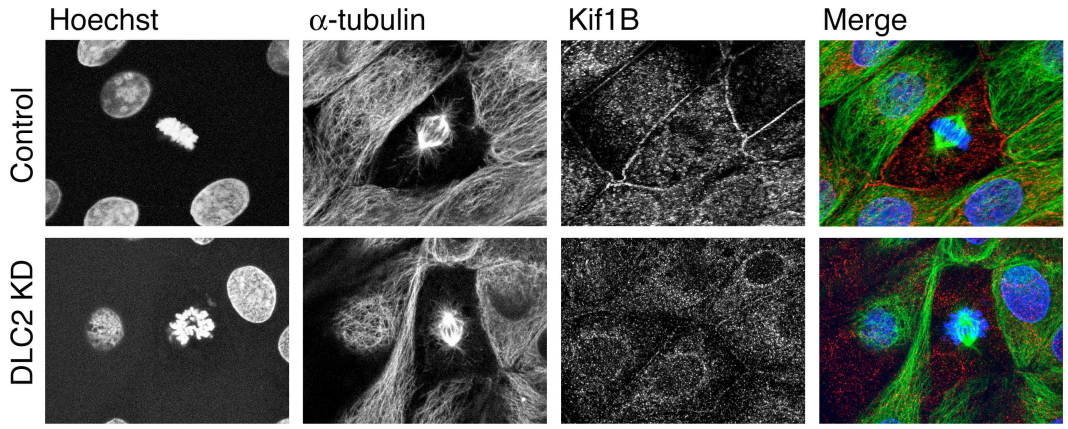

Figure 5.4 Cortical Kif1B is delocalized upon DLC2 depletion

Control and DLC2 depleted cells were stained for α-tubulin (green) and Kif1B in green. Cells were fixed with methanol. Shown are confocal microscopy images.

Bar represents 10μm.

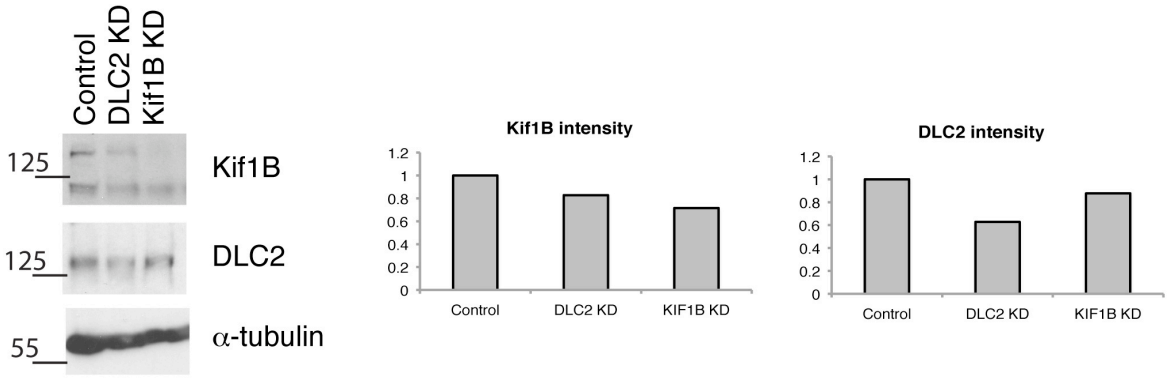

Figure 5.5 DLC2 depletion affects Kif1B protein levels

WB for DLC2 and Kif1B in HCE cells transfected with control, DLC2 or Kif1B siRNAs. DLC2 affects Kif1B total level. α-tubulin was used as a loading control.

The two charts show quantification of Kif1B and DLC2 signal intensity as a protein/α-tubulin ratio normalized against the control ratio. This is the quantification of the blot shown in this picture. According to this picture, DLC2 depletion results in a 20% reduction of Kif1B protein level. It would be good to quantify other blots and estimate an average. A similar effect is also supported by the Figure 6.6.

5.3 What is known about Kif1B?

Until this point, I did not know much about Kif1B and there is only limited information available in the literature. Kif1B was initially identified as mutated and functionally impaired in the neurological disease Marie-Charcot-Tooth[153], and it was recently reported that mutations in Kif1B are associated with an increased risk of hepatocellular carcinoma[154]. Hepatocellular carcinoma is also the first type of tumour that had been linked to DLC2. As I described in the introduction, DLC2 was reported to be frequently underrepresented in mRNAs isolated from hepatocellular carcinomas. Hence, Kif1B and DLC2 might be involved in the same pathway, and reduced expression of either protein might promote formation of hepatocellular carcinomas in a similar manner.

Kif1B is a kinesin belonging to sub-family 3 of kinesins. It was reported to exist in two isoforms: KIF1Bα and KIF1Bβ, which are alternatively spliced products of the KIF1B gene located on 1p36.2. KIF1Bα is distinct from KIF1Bβ in the C-terminal cargo-binding domain; however, they have the same N-terminal motor domain[155]. Both isoforms were reported mutated in Marie-Charcot-Tooth disease and both were linked to hepatocellular carcinomas; however, only the longer one, beta, was reported to interact with DLC2 in the two hybrid analysis.

Isoform β was also shown to direct transport of mitochondria[156] and to regulate axonal transport of presynaptic regulator Rab3[157]. It still remains unclear how Kif1B is linked to the Marie-Charcot-Tooth disease or hepatocellular carcinoma.

I am going to discuss further the role of Ki1Bβ in the next chapters, but I will always call it Kif1B for simplicity.

5.4 Depletion of Kif1B resembles DLC2 KD phenotype

Since Kif1B localization was altered by DLC2 depletion, I wondered if Kif1B also played a role in mitosis. To investigate this, I first tested the specificity of three siRNAs against Kif1B (Sigma) and validated them by WB. Figure 5.6 shows that individuals and a pool of the three siRNAs were able to reduce Kif1B protein levels.

By staining for DLC2 in HCE cells depleted of Kif1B, it was evident that Kif1B did not affect DLC2 localization, despite that the mitotic spindle showed an aberrant shape. This suggested that Kif1B might play a role downstream DLC2, since its depletion did not have an effect on either DLC2 protein levels or localization (Figure 5.7).

By staining for α-tubulin and E-cadherin, I observed that transfection of individual and pooled siRNAs resulted in fragmented junctions in mitotic cells and misaligned metaphase plates. The effect on junctions was not as strong as the DLC2 KD but mitotic spindles were affected in a similar manner (Figure 5.8). Quantification of aberrant metaphase cells revealed that Kif1B depletion induced a significant increase in the number of misaligned metaphases cells (Figure 5.9).

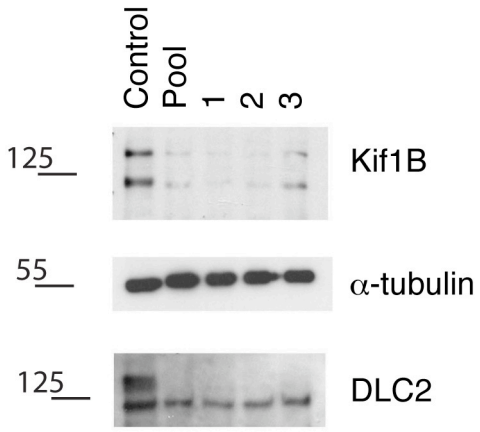

Figure 5.6 WB for validation of Kif1B KD

WB for Kif1B expression in HCE cells transfected with siRNAs: C control, P pool of three siRNAs, 1 siRNA 1, 2 siRNA 2, 3 siRNA 3. DLC2 is not altered upon depletion of Kif1B. α-Tub (α-tubulin) is used as internal control.

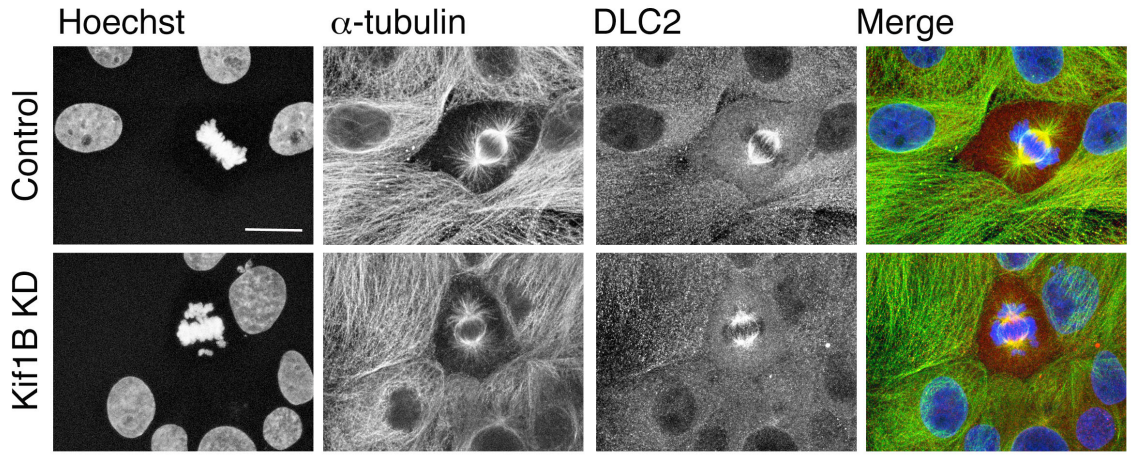

Figure 5.7 Kif1B KD does not alter DLC2 localization

HCE cells transfected with Kif1B specific siRNA pool were compared with control HCE cells transfected with a non-targeting siRNA. The cells were stained with DLC2 (red) and α-tubulin (green).

Cells fixed with 4% PFA and methanol. Shown are confocal microscopy images.

Bar represents 10μm.

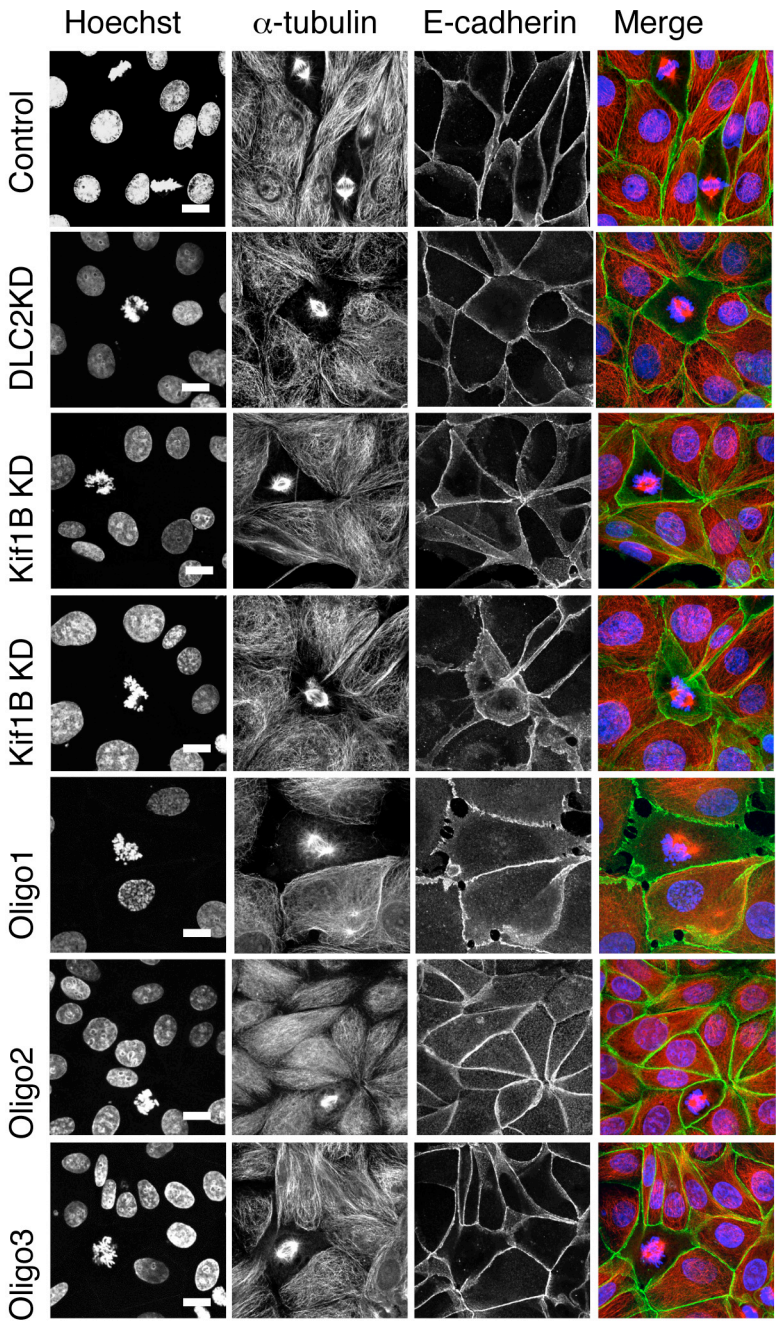

Figure 5.8 Kif1B depletion phenocopies the DLC2 KD

HCE cells transfected with individual siRNAs specific for Kif1B or a pool of those were compared to Control HCE cells transfected with a non-targeting siRNA and HCE cells transfected with a DLC2 siRNA pool. These cells were stained for the AJs marker E-cadherin (green) and α-tubulin (red).

Cells were fixed with methanol. Shown are confocal microscopy images.

Bar represents 10μm.

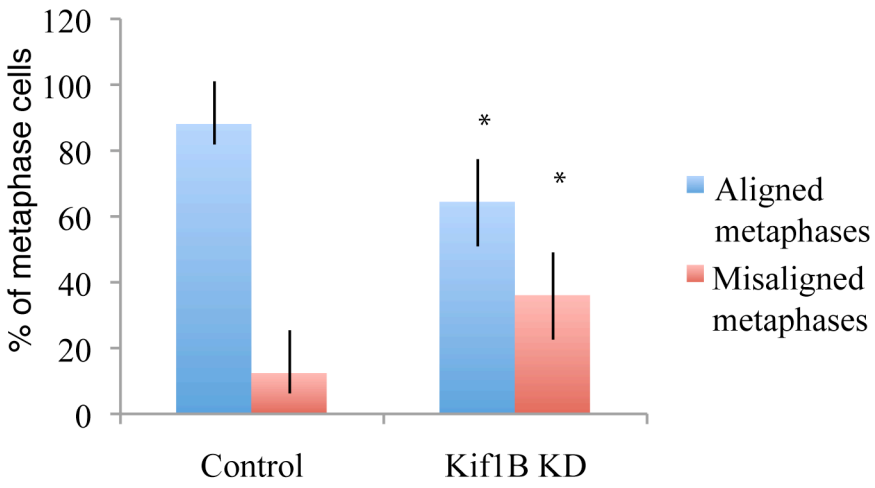

Figure 5.9 Kif1B regulates metaphase plate alignment

Transfection of a pool of 3 Kif1B targeting siRNAs causes an increase of aberrant metaphase plates (red bars) and a decrease of normal ones (blue bars) compared with control cells. Over 60 cells per experiment were counted. Bars represent mean values of three experiments. * $p<0.05$ Error bars represent standard deviations.

5.5 Kif1B interacts with AJ components in a DLC2-dependent manner

To determine whether Kif1B also forms complexes with cortical components, I performed a set of immunoprecipitations and looked at candidates I had previously identified to co-precipitate with DLC2 (components of AJs and α-tubulin). Figure 5.10 shows that Kif1B antibodies co-immunoprecipitate p120catenin and E-cadherin, and α-tubulin. These results re-enforce the hypothesis that DLC2 and Kif1B act in the same pathway. TJ components (ZO-1 and OCL) and β-catenin were not immunoprecipitated.

At this point, I was interesting to know the role of Kif1B and DLC2 in complex formation. To answer this question, I performed immunoprecipitations of DLC2 upon depletion of Kif1B and looked at the co-immunoprecipitating protiens. I also performed an IP for Kif1B upon depletion of DLC2. Control immunoprecipitations were kept as a reference to study the effect of one or the other depletion (Figure 5.11). Interestingly, Kif1B was no longer able to interact with α-tubulin or AJs components upon DLC2 depletion. On the contrary, DLC2 interactions were not affected by Kif1B depletion. Once again, this suggests a role for Kif1B more downstream of DLC2, and that formation of Kif1B complex with AJ components and α-tubulin are dependent on DLC2. Again, in none of the depleted conditions, TJ components (ZO-1 and OCL) and β-catenin were not immunoprecipitated.

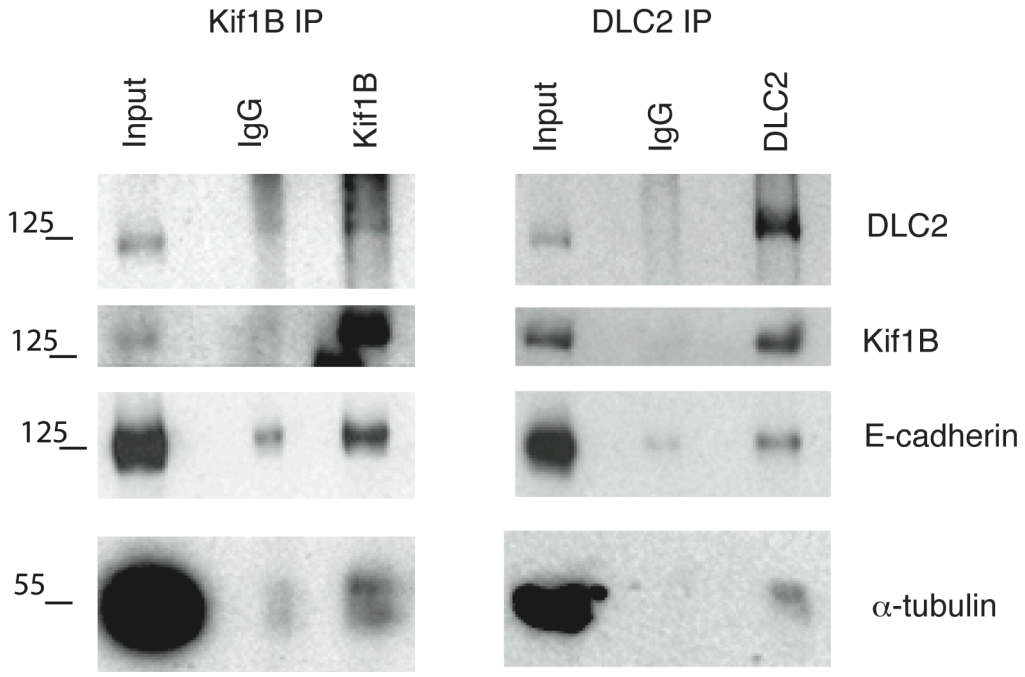

Figure 5.10 Identification of candidate interaction partners

Immunoprecipitates of Kif1B and DLC2 from HCE cell extracts were analysed by WB against α-tubulin, E-cadherin and p120catenin, DLC2 and Kif1B.

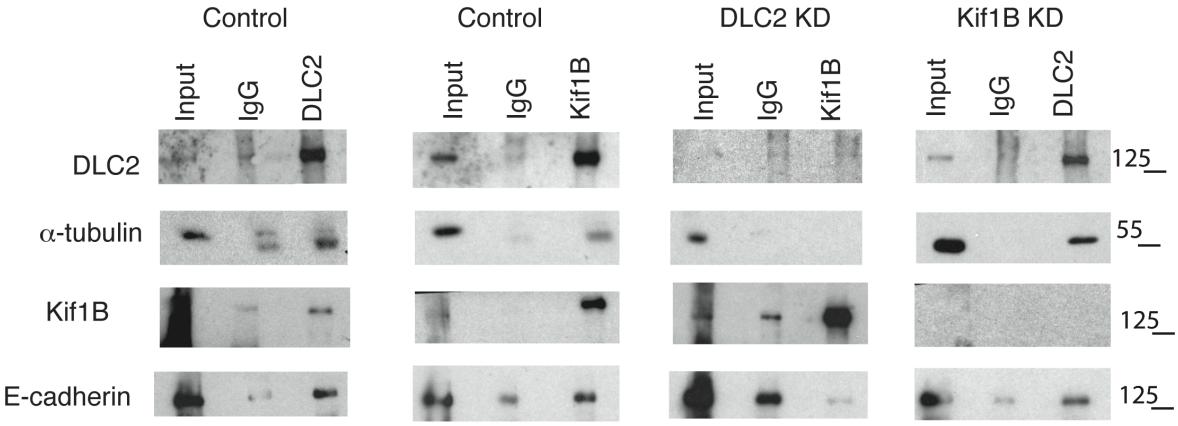

Figure 5.11 Identification of candidate interaction partners

Immunoprecipitation of Kif1B and DLC2 in Control cells and in respectively DLC2 KD and Kif1B KD cells. WB against α-tubulin and E-cadherin. DLC2 and Kif1B.

5.6 Kif1B KD stimulates higher levels of active Cdc42

To better understand the correlation between Kif1B and DLC2 I decided to look at active Cdc42 levels upon Kif1B depletion. Although this kinesin does not have GAP or GEF activity, it might contribute to Cdc42 regulation via its interaction partner DLC2. G-LISA performed on HCE cells showed that Kif1B depleted cells had higher levels of active Cdc42 in nonsynchronised cells (Figure 5.12A), suggesting that Kif1B is indeed important for DLC2 function. Upon synchronized entry into mitosis, Kif1B depletion again led to increased Cdc42-GTP levels after 45' of Nocodazole washout, corresponding increased Cdc42 activity in metaphase as I had observed for DLC2 depleted cells (Figure 5.12B). Hence, Kif1B is also required for normal control of Cdc42, suggesting that it might exert a regulatory role on DLC2. However, I cannot rule out a contribution by another Cdc42 regulator at this time.

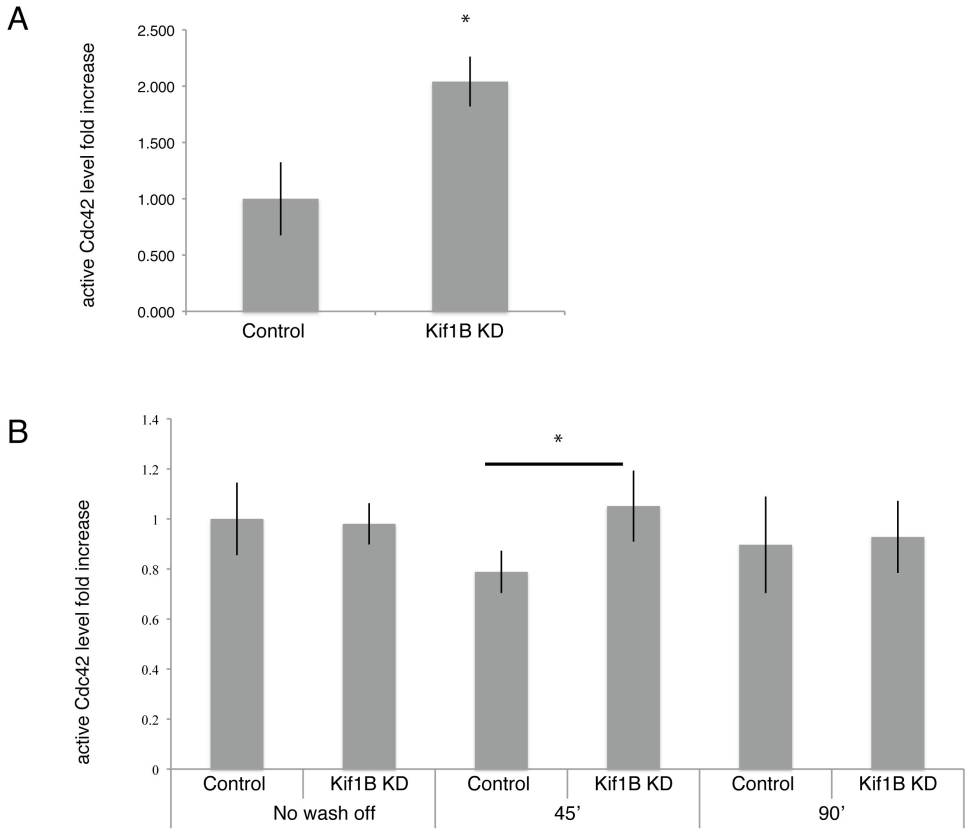

Figure 5.12 Kif1B KD leads to increased active Cdc42 levels

(A) Cdc42 G-LISA assay. Kif1B KD results in an increased Cdc42 activity.

(B) Cdc42 G-LISA of HCE cells treated with Nocodazole. Timepoints analyzed: 0', 45 minutes, and 90 minutes. At 45 minutes (metaphase peak) Kif1B depletion results in an increased level of Cdc42. Bars represent mean values of three experiments. * $p<0.05$ Error bars represent standard deviations. The chart is an average of three experiments.

Since DLC2 depletion induced increased levels of Cdc42 activity and in this condition Kif1B localization was dramatically perturbed, I wondered if Kif1B localization is regulated by active Cdc42 levels. To tackle this question, I expressed CA (Q61L) and DN (T17N) constructs of Cdc42 in control or DLC2 depleted cells. Figure 5.13 shows that overexpressing a DN form of Cdc42 in DLC2 KD cells restored Kif1B localization at the cell cortex. On the contrary, overexpression of CA in control cells led to mislocalization of Kif1B. This highlights the possibility that Kif1B localisation is regulated by Cdc42 activity.

Double depletion Cdc42 and DLC2 restored Kif1B at the cell cortex further supporting the model that DLC2-regulated Cdc42 activity is important for Kif1B function.

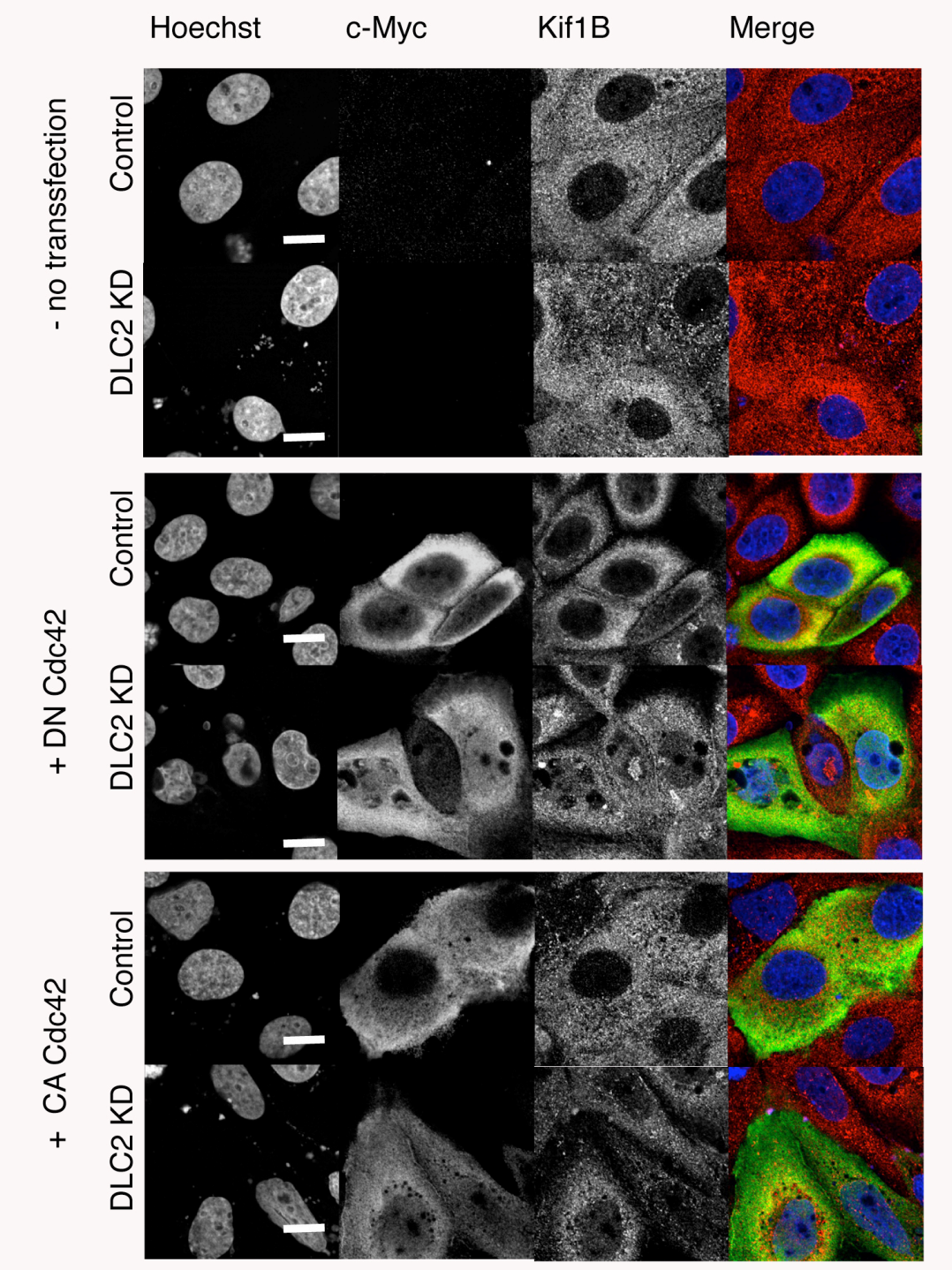

Figure 5.13 Kif1B is at the cell cortex when Cdc42 is inactive

Control and DLC2 KD HCE cells, untransfected or transfected with CA or DN Cdc42 were stained for Kif1B (in red), c-Myc (in green) and with Hoechst. The picture shows that Kif1B is mislocalized upon DLC2 KD, but if DN Cdc42 is overexpressed, Kif1B sits at the cell cortex, indicating Kif1B localization depends on Cdc42 activity.

Bar represents 10µm.

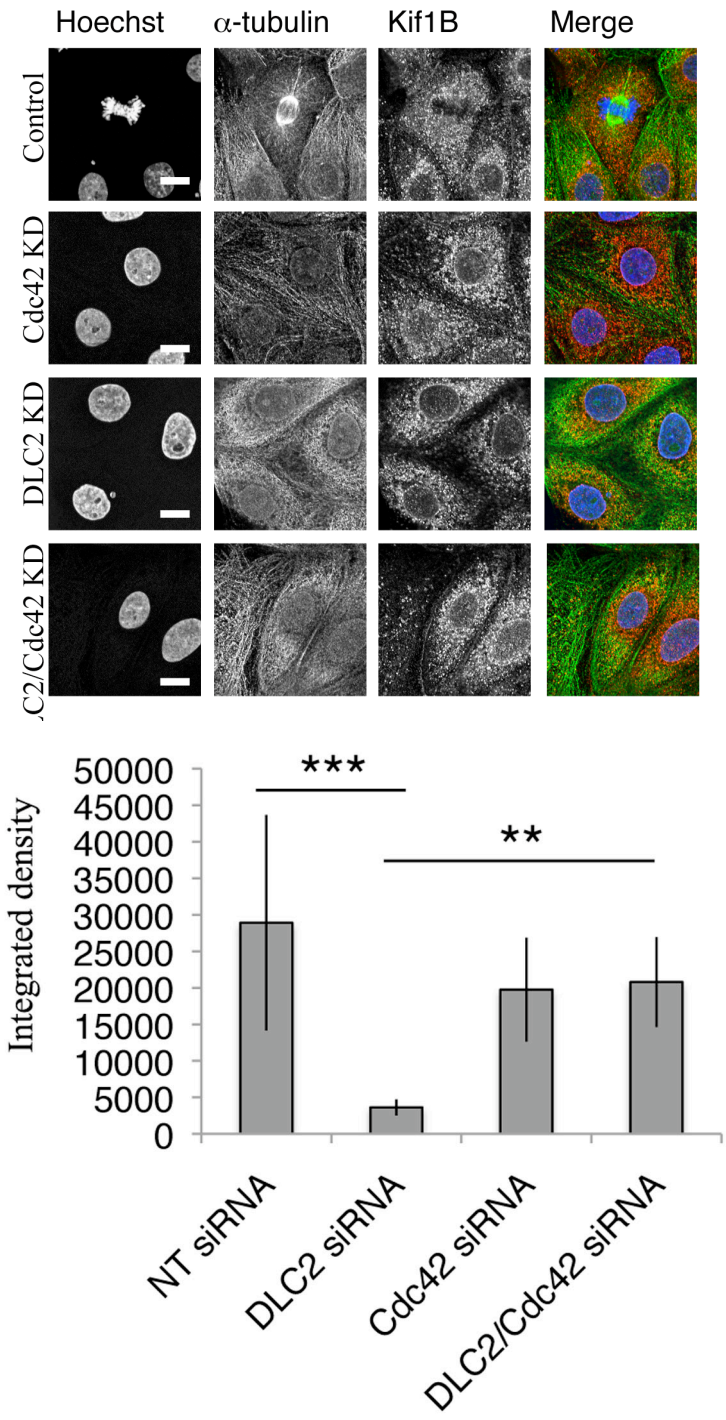

Figure 5.14 Kif1B is recruited at the cell cortex when Cdc42 is not active.

(Top panel) Confocal pictures showing Control, Cdc42 KD and DLC2 KD and Cdc42/DLC2 KD HCE cells stained in the left panel for Hoechst, Kif1B (red) red and α-tubulin (green). Bar represents 10μm

(Bottom panel) Quantification of Kif1B signal at the cell membrane from over 10 cells each condition.

*** $p<0.001$ ** $p<0.01$

5.7 Does Kif1B associate with kinetochores?

Plus-end tips of microtubules are attached at the cell cortex on one end, and at the DNA via the kinetochores on the other side. Since in both cases plus ends of microtubules are involved in anchoring other components to the spindle, and since I observed that Kif1B localized at the cell cortex but also that Kif1B depletion affected chromosome alignment, I wondered if Kif1B could be localized at the plus ends of the kinetochores. Hence, I co-stained cells for Kif1B and the kinetochore marker CREST. Figure 5.15 shows that I could indeed observe some Kif1B dots colocalizing with CREST. These dots were visible in both prometapahse and metaphase, suggesting that Kif1B might localize at the kinetochores during both capture and stabilization of chromosome attachment. To test if these dots were Kif1B specific, I knocked down Kif1B and observed that these dots disappeared (Figure 5.15). However, Kif1B also localizes to mitochondria; hence, there is a considerable amount of cytoplasmic, dotty staining. It is therefore difficult to be certain at this time that the Kif1B dots co-localizing with CREST is indeed due to kinetochore staining. Nevertheless, mitochondria are excluded from the metaphase plates, suggesting that an overlap with the mitochondrial staining is unlikely. Thus, I recognize the evidences for this type of association are little. It would have been helpful trying to use a vector with an appropriate tag to stain in fix cells (perhaps without the portion responsible for localization to mitochondria, which is not known in literature yet, since both the isoforms annotated in literature do localise at the mitochondria[156]). If this information was available, I could have expressed the rest of the protein and trying to see if the other domains are responsible for a localization of Kif1B at the kinetochores. Perhaps, it would have been also interesting performing some live imaging with this construct, to follow up the localization throughout mitosis.

Since I had found that Kif1B recruitment to the cortex occurs when Cdc42 activity is low, I depleted Cdc42 and looked at Kif1B localization. Depletion of Cdc42 emulates an inactive state, and in these conditions it seems to me that I could detect several Kif1B dots co-localizing with kinetochores (Figure 5.16). It seemed to me that depletion of Cdc42 was sufficient to restore Kif1B localization at the cell kinetochores upon double knockdown Cdc42 and DLC2. Unfortunately, to make the data stronger, I should have stained for a kinetochore marker alongside Kif1B. These data might indicate that Kif1B might indeed localize to the

kinetochores and that this association is regulated in the same way by Cdc42 activity as association with the cell cortex.

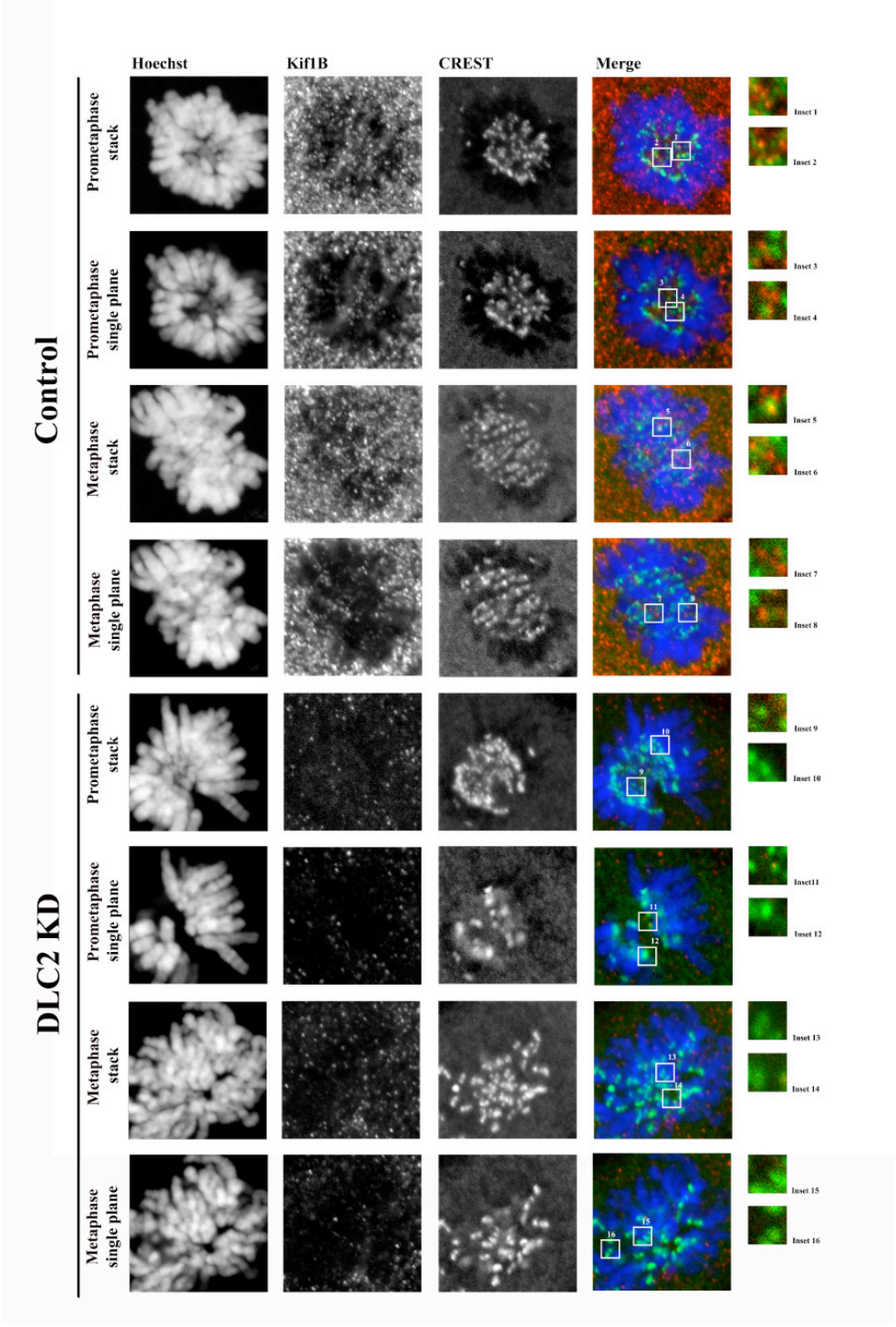

Figure 5.15 Co-localisation of Kif1B with the kinetochore marker CREST

Control and DLC2 KD HCE cells were stained for CREST (kinetochore marker) and Kif1B (red). A single plane or a z-projection of metaphase and prometaphase cells were analyzed for both control and DLC2 KD cells.

Cells were fixed with PFA 4% and methanol. Shown are confocal images.

Bar represents 1µm.

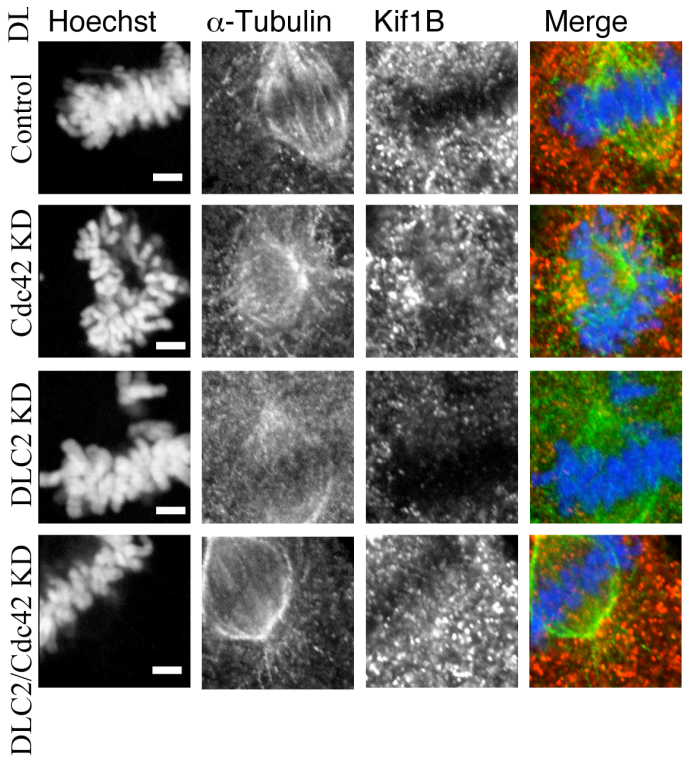

Figure 5.16 Kif1B is recruited when Cdc42 is not active.

Confocal pictures showing Control, Cdc42 KD and DLC2 KD and Cdc42/DLC2 KD HCE cells stained in the left panel for Hoechst, Kif1B (red) red and a-tubulin (green).

Bar represents 5μm.

5.8 DISCUSSION

I presented data in this chapter that indicate that Kif1B is an important DLC2 interactor and component of the DLC2 pathway. In 2004, the interaction between Kif1B and DLC2 was reported in a two-hybrid screen[139]. Here, I confirmed the interaction between the endogenous proteins extracted from HCE cells. Moreover, DLC2 plays a paramount role in controlling Kif1B localization at the cell cortex and its protein levels. On the contrary, DLC2 localization and expression were not influenced by depletion of Kif1B, suggesting that Kif1B might be in a more downstream position in the same pathway. Nevertheless, depletion of Kif1B led to increased Cdc42 activity, suggesting that the kinesis might also play a role in DLC2 regulation. However, I cannot exclude that this effect on Cdc42 involves another mechanism of Cdc42 regulation, such as another regulator or an indirect effect due to a feedback signal since the DLC2 pathway is disrupted. Depletion of Kif1B phenocopies DLC2 chromosome misalignment, indicating that regulation of Kif1B by DLC2/Cdc42 is important for mitosis. How Kif1B participates in regulation of the mitotic apparatus is not clear yet. I can imagine that Kif1B at the cell cortex mediates anchorage of microtubules by docking them at cell-cell junctions. This idea is supported by the co-immunoprecipitation of E-cadherin, p120catenin and α-tubulin with Kif1B. Upon perturbation of DLC2, Kif1B is misplaced and cannot associate anymore with the astral microtubules at the junctions. Since this happens at the plus ends, it is possible that a similar mechanism regulates Kif1B association with the plus ends at the kinetchores of K-fibers. Staining for Kif1B and CREST (kinetochore marker) revealed that Kif1B also might associate with kinetochores. Perhaps here too Kif1B regulates microtubules attachment. This would explain the effect of Kif1B on chromosome alignment. However it could also be that the chromosome defect is due to a defect of MT attachment at the cell cortex that is somehow sensed by the kinetochores.

Noteworthy is the fact that Kif1B seems to 'sense' the active level of Cdc42 within the cell. Presence of too high levels of active Cdc42 is sufficient to misplace Kif1B from the cell cortex. Hence, DLC2 depletion led to a loss of cortical Kif1B and this could be corrected by inactive Cdc42 or Cdc42 depletion. This active/inactive Cdc42 sensing strongly links Kif1B to DLC2. However, Kif1B does not simply act as sensor, since its depletion is sufficient to change active Cdc42 levels. It seems then that the mechanism is not a one-way cascade, but rather a

complicated network with Kif1B influencing DLC2/Cdc42 activation and DLC2 regulating Kif1B localization.

CHAPTER 6:
DLC2 AND KIF1B DEPLETED CELLS SHOW DELAYS IN METAPHASE

CHAPTER 6: DLC2 AND KIF1B DEPLETED CELLS SHOWS DELAYS IN METAPHASE

6.1 DLC2 and Kif1B depletion does not affect spindle orientation

Several reports in literature show that Cdc42 and its regulators are involved in the regulation of mitotic spindle orientation[158–161]. As I discussed largely in the introduction, mitotic spindle orientation is essential to determine where the cell is going to remain in the same layer. This influences the fate of a cell. Therefore, spindle orientation needs to be tightly controlled.

When I started this project and I observed a mitotic phenotype in DLC2 KD cells, I thought that since Cdc42 is misregulated within these cells, the chromosome misalignment could have been due to a spindle misorientation with a consequent failure of the spindle. To test this hypothesis, I compared Control, DLC2 KD and Kif1B KD HCE cells stained for E-cadherin, to determine the junction position, and γ-tubulin, to monitor the plane of the mitotic spindle. I then measured the angle between the line passing through the centrosomes and a line perpendicular to the substrate. As Figure 6.1 shows, DLC2 KD and Kif1B KD cells did not show any increase in cells with misaligned spindles. Hence, the DLC2/Kif1B pathway does not regulate spindle orientation.

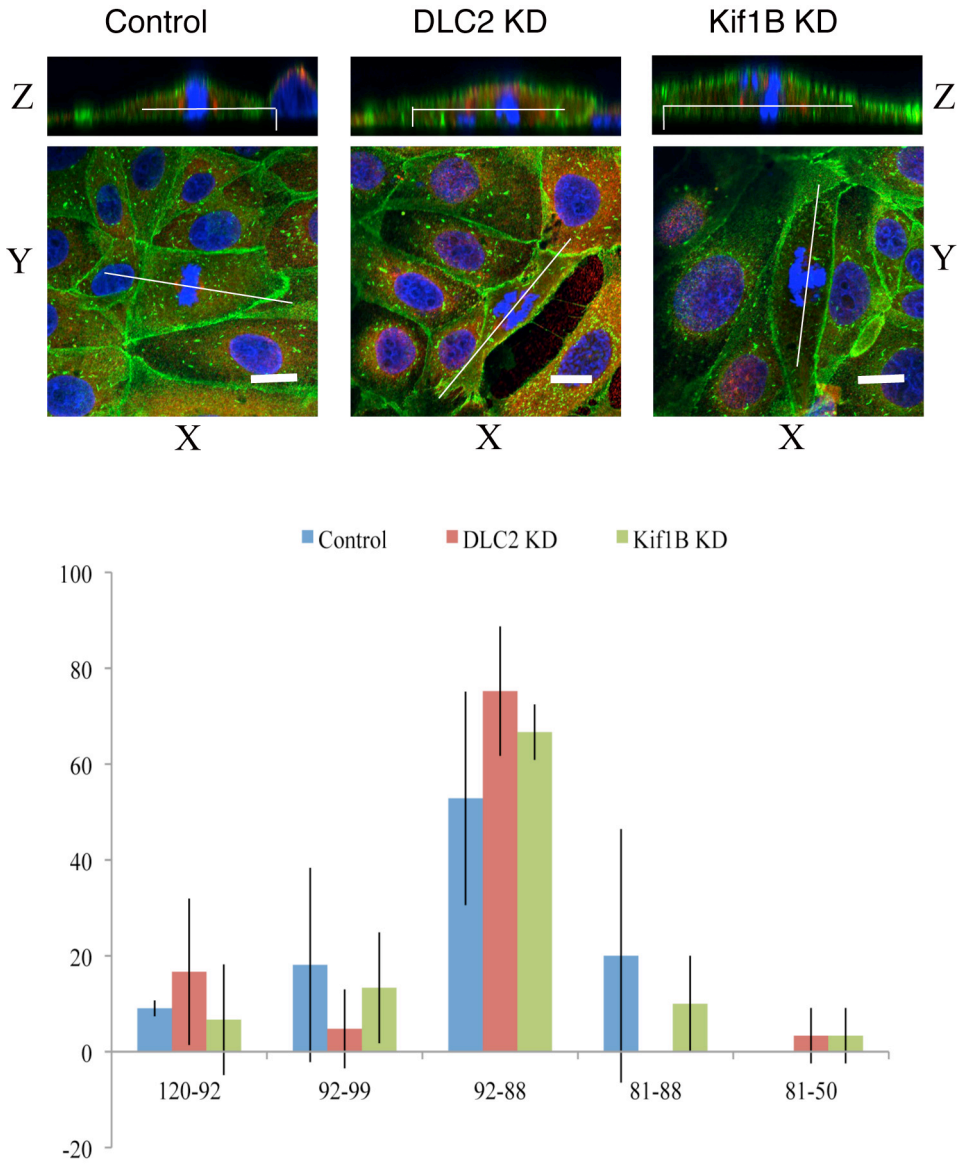

Figure 6.1 DLC2 and Kif1B depletion does not alter the spindle orientation

Control (blue bars), DLC2 KD (red bars) and Kif1B KD (green bars) HCE cells were stained for γ-tubulin in red and E–cadherin in green. A z-line was acquired and lines were drawn passing through the two spindle poles and the cell junctions. Spindle angles were calculated in the z-line picture by measuring the angle between a line perpendicular to the substrate and the line passing through the two spindle poles. 5 groups of angles were counted. Control, DLC2 KD and Kif1B KD cells spread among the 5 categories in a similar way. Bars represent mean values of 3 experiments. Over 30 angles per condition were counted.

Cells were fixed with methanol. Shown are confocal microscopy images. White bars represent 10μm.

6.2 DLC2 and Kif1B depleted cells show delays in metaphase

To better understand DLC2 phenotype and identify at which step of mitosis the defect is initiated, I decided to use live cell. For this purpose, HeLa cells stably transfected with α-tubulin and H2B (DNA marker) were imaged on a spinning disc confocal microscope and followed from the beginning of mitosis (prometapahse) to the end of it (cytokinesis). Using the structure of the mitotic spindle as a reference, I calculated the length of prometaphase/metaphase (defined as the time from the nuclear envelop break-down to the appearance of the metaphase plate) and metaphase/anaphase (from the onset of the metaphase plate to chromosome segregation).

Figure 6.2 A shows time-courses of three example cells. Comparing the times required by control cells with DLC2 and Kif1B KD cells, it became clear that there were differences in metaphase. Control cells segregated chromosomes after an average of 40 minutes from the entry into mitosis; DLC2 and Kif1B depleted cells showed delays in metaphase, with spindles not getting misorientated, but enhanced shaking, spinning in the same plane, and rocking from left to right (Watch Videos Chapter6-Control-atub-h2b, Chapter6-DLC2kd-atub-h2b, Chapter6-Kif1Bkd-atub-h2b).

By measuring the length of prometaphase and metaphase, it resulted that DLC2 KD and Kif1B KD cells did not show any primary chromosome alignment defect, but the spindle did not become stabilised and underwent increased dynamic movements, resulting in prolonged times in metaphase and leading to chromosome misalignments. The times in metaphase were indeed almost the double for KD cells than for control cells (Figure 6.2 B). Unfortunatelly, I have not shown a Kif1B KD cell starting from NEB but from already metaphase, since this cell had the most striking defect of misaligned metaphase plate, but it was found already in metaphase, when the movie was started.

Similar results were obtained with fixed HCE cells. By treating HCE cells with Nocodazole as I have shown in Chapter 5 (see Materials and Methods for further information), it is possible to synchronize cells in different phases of mitosis. Keeping in mind that 0′ from the wash out corresponds to a peak of prometaphase, 45′ of metaphase/anaphase, and 90′ telophase, I compared the percentage of cells in specific phases in the different timepoints, in Control, DLC2 KD and Kif1B KD cells. Figure 6.3 shows that at 90′ from the washout, the majority of control cells had reached telophase, DLC2 and Kif1B depleted cells were still in

metaphase. These results are thus in agreement with the live imaging experiments performed with HeLa cells.

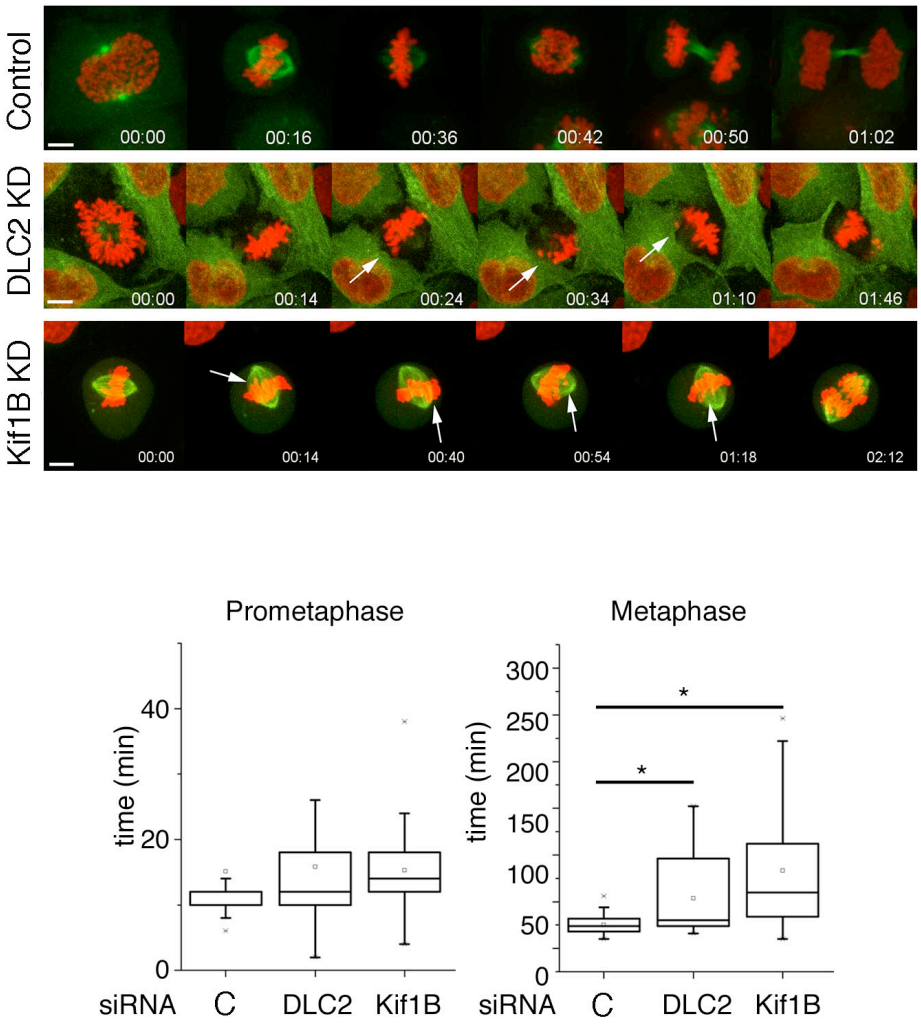

Figure 6.2 Live imaging of DLC2 KD and Kif1B KD HeLa cells

(A) HeLa cells stably transfected with H2B-mCherry and α-tubulin-GFP and transfected with control, DLC2 or Kif1B siRNAs, were filmed throughout mitosis. Pictures have been taken with a Spinning Disc confocal microscope every 2 minutes. Watch Videos Chapter6-Control-atub-h2b, Video Chapter6-DLC2kd-atub-h2b, Video Chapter6-Kif1Bkd-atub-h2b.

(B) Length of prometaphase and metaphase was calculated and plotted in a graph. * $p<0.05$.

In charts where data are represented as box-whisker plots, the box size represents 75% of the population and the line inside the box represents the median of the sample. Over 30 cells were analyzed per condition. Maximum (in the upper quartile) and the minimum (in the lower quartile) values are represented by the size of the bars (whiskers).

Scale bars are 10μm.

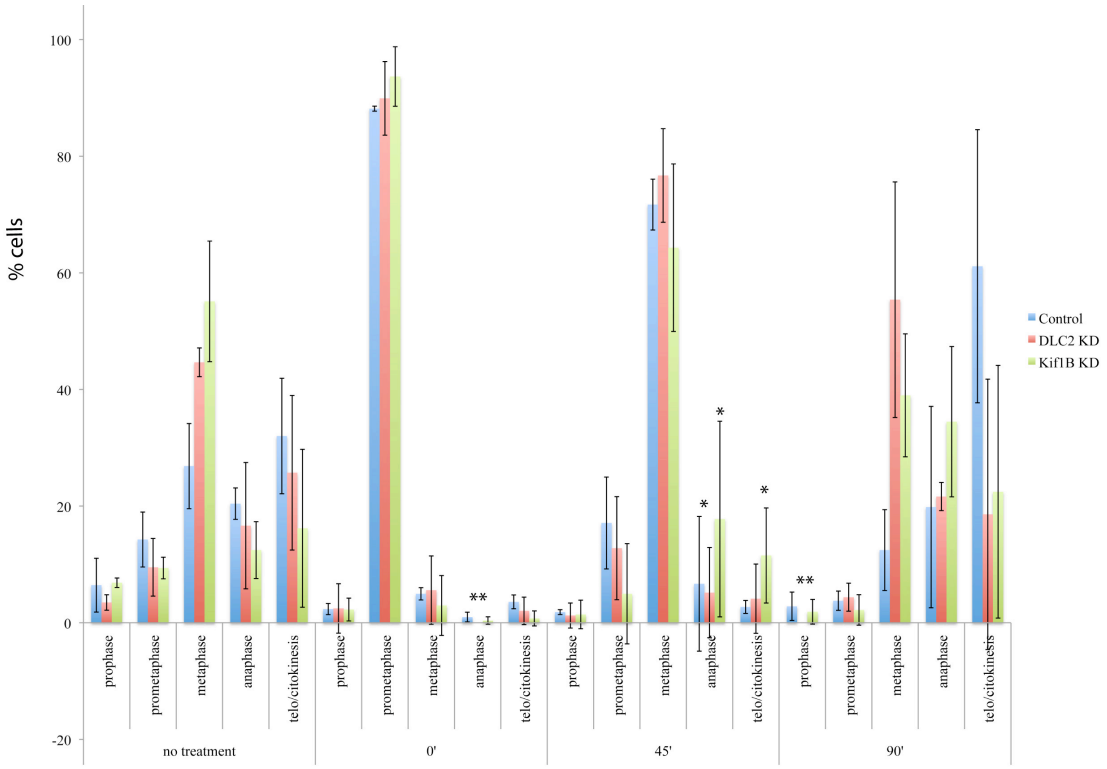

Figure 6.3 Mitotic index analysis reveals DLC2 and Kif1B depleted cells have a delay in metaphase

Control (blue), DLC2 KD (red) and Kif1B KD (green) cells were counted to determine what it is the percentage of the different phases of mitosis among the whole popultion of mitotic cells. Cells were treated with Nocodazole and the following timepoints from the washing-off were analyzed: 0', 45', 90'.

The chart shows that depletion of DLC2 and Kif1B results in an increase of cells delayed in metaphase.

Bars represent mean values of three experiments. * $p<0.05$ ** $p<0.01$ Error bars represent standard deviations.

6.3 The metaphase delay is checkpoint dependent

As I discussed in the introduction, the purpose of mitosis is to equally segregate the duplicated chromosomes between two daughter cells. This task is accomplished by the mitotic spindle and the microtubules within that capture all the chromosomes, align them on a metaphase plate and then split them. To ensure that each daughter cell inherits an identical copy of the genome, a cell has a checkpoint system that is ON to prevent anaphase onset until all the chromosomes are perfectly aligned and anchored. When the checkpoint is satisfied, anaphase can occur.

One of the key elements of the checkpoint is Aurora B, a sensor molecule and kinase that phosphorylates targets downstream when chromosomes are not attached properly[162–164]. Aurora B requires phosphorylation of Ser311 by checkpoint kinase 1 (Chk1) (kinase best known for its role in the DNA damage checkpoint). Aurora B is activated by binding to inner centromere proteins such as INCEP, which triggers the phosphorylation of its own kinase domain. Binding to INCEP generates a gradient of phospho Aurora B localized in metaphase at the kinetochores, and in the middle of the spindle in anaphase

Since DLC2 and Kif1B KD cells showed delays in metaphase, I checked if this was checkpoint dependent or not. I first looked at the global level of phospho-Aurora B in control, DLC2 KD and Kif1B KD cells, untreated and synchronized. As shown in Figure 6.4, whereas control cells at the 90' of the nocodazole washout showed little phospho-Aurora B, DLC2 KD and Kif1B cells still retained high levels of phospho-Aurora B, suggesting that the checkpoint was still on in the delayed metaphase cells.

To further prove that the checkpoint was active, I decided to look at a substrate of Aurora B, Dsn1. P100 is an antibody raised against the Dsn1 phosphorylation site at Ser100, when phosphorylated by Aurora B (gift by Iain Cheeseman). Figure 6.5A shows that upon depletion of DLC2 and Kif1B, HCE cells had high levels of phospho-Dsn1, indicating high levels of activate Aurora B. This was further supported by a quantification of the signal intensity (Figure 6.5 B). These data reinforced the model that in DLC2 and Kif1B depleted cells the checkpoint was maintained active for longer than in control cells.

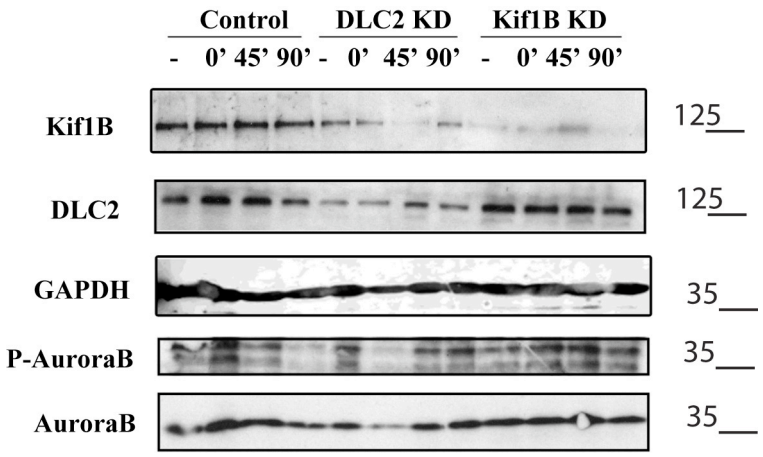

Figure 6.4 DLC2 and Kif1B KD cells retain high levels of phospho Aurora B at the 90′ time point after nocodazole washout.

Control, DLC2 and Kif1B KD HCE cells, treated or untreated with nocodazole, were lysed and analysed by WB as indicated.

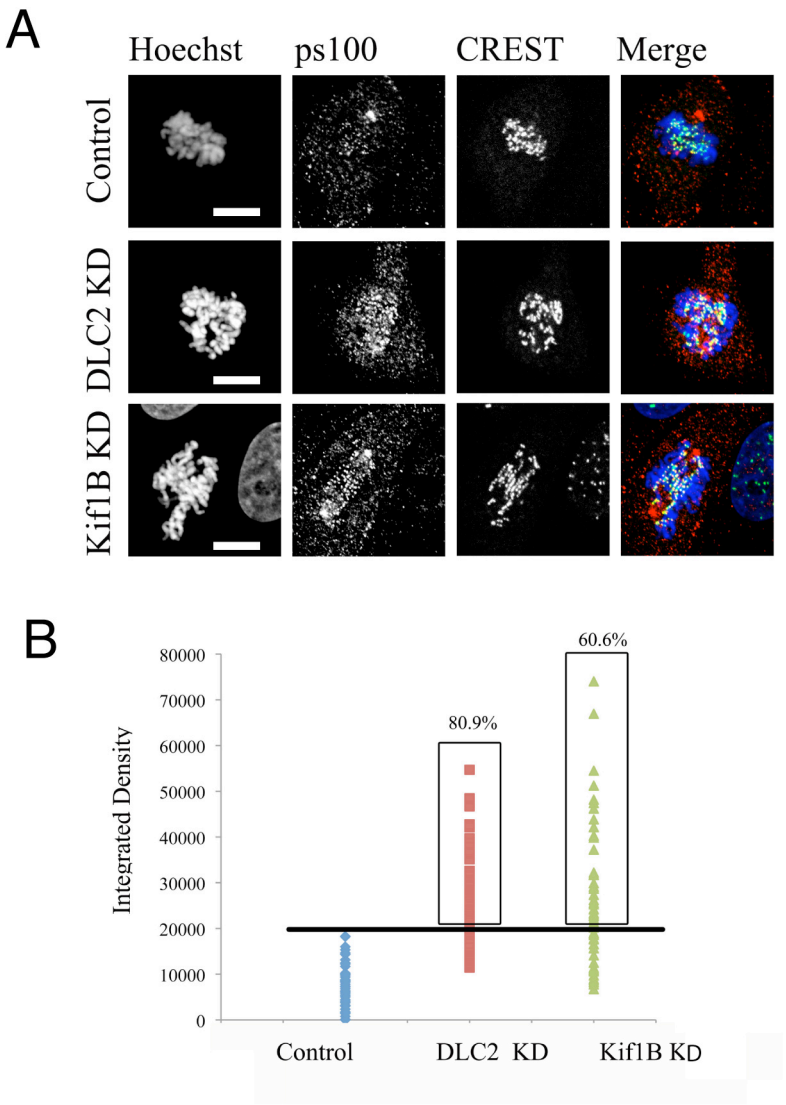

Figure 6.5 DLC2 and Kif1B KD cells retained high levels of phospho-Dsn1

(A) Confocal microscopy pictures showing Control, DLC2 KD and Kif1B KD HCE cells stained for Hoechst, p100 (phospho Dsn1 in red) and CREST (kinetochore marker in green).

(B) Chart representing a typical experiment. Integrated intensities were scattered on the chart. The threshold (black line) was identified as the highest integrated intensity in control cells. Above the values are percentages of how many counted kinetochores show higher density.

6.4 Checkpoint remains active because of unattached kinetochores

The Aurora B checkpoint senses unattached kinetochores. Therefore, I wondered if in the case of DLC2 and Kif1B depletion, the checkpoint was kept on longer because of unattached kinetochores. The most common way to check this is by taking advantage of a protein that sits at the kinetochores when kinetochores are not coupled to MTs: Mad2[165–170].

By staining with a commercial Mad2 Ab, and by quantifying the number of Mad2 dots detected within a cell, I observed that DLC2 and Kif1B depleted cells showed increased numbers of Mad2 positive dots (Figure 6.6). This suggested that in these cells kinetochores were not properly attached.

I confirmed this result by using a live imaging approach with HeLa cells stably expressing Mad2-GFP. As Figure 6.7 and Figure 6.8 A show, DLC2 and Kif1B depleted HeLa cells showed longer in metaphase and with positive Mad2 spots through-out the whole length of metaphase (watch Videos Chapter6-Control-mad2, Chapter6-DLC2kd-mad2, Chapter6-Kif1Bkd-mad2). When the last dot had disappeared, anaphase finally occured. This experiment suggested that DLC2 and Kif1B depleted cells had defects in attaching or keeping attached all chromosomes to MTs.

To determine the checkpoint dependence directly, I used an MPS-1 inhibitor. MPS-1 is involved in the correct recruitment of the Mad1-Mad2 core to kinetochores when they are unoccupied[170,171]. MPS-1 inhibitor treatment of DLC2 KD and Kif1B KD HeLa cells rescued the prolonged metaphase times (Figure 6.8 B), confirming that the delayed metaphase was due to prolonged activation of the checkpoint.

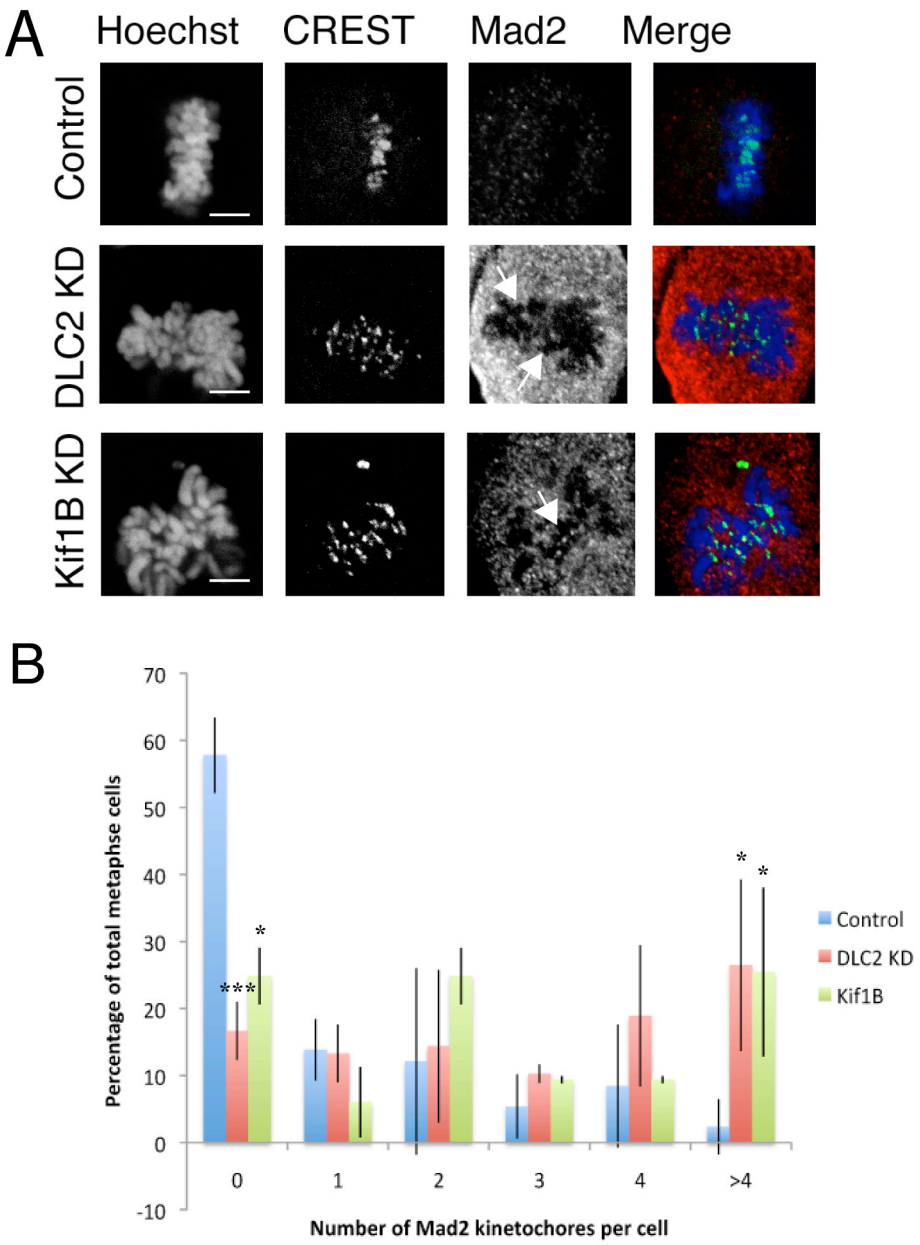

Figure 6.6 DLC2 and Kif1B KD cells retain increased numbers of Mad2 positive kinetochores

(A) Mad2 staining for Control, DLC2 KD and Kif1B KD cells. Bar represents 5μm.

(B) Chart representing the percentage of cells showing a specific number of Mad2-positive dots at the kinetochores. DLC2 and Kif1B KD cells show higher percentages of cells with more than one Mad2-positive dot. Over 50 kinetochores per condition were counted.

Bars represent mean values. * $p<0.05$ *** $p<0.001$ Error bars represent standard deviations.

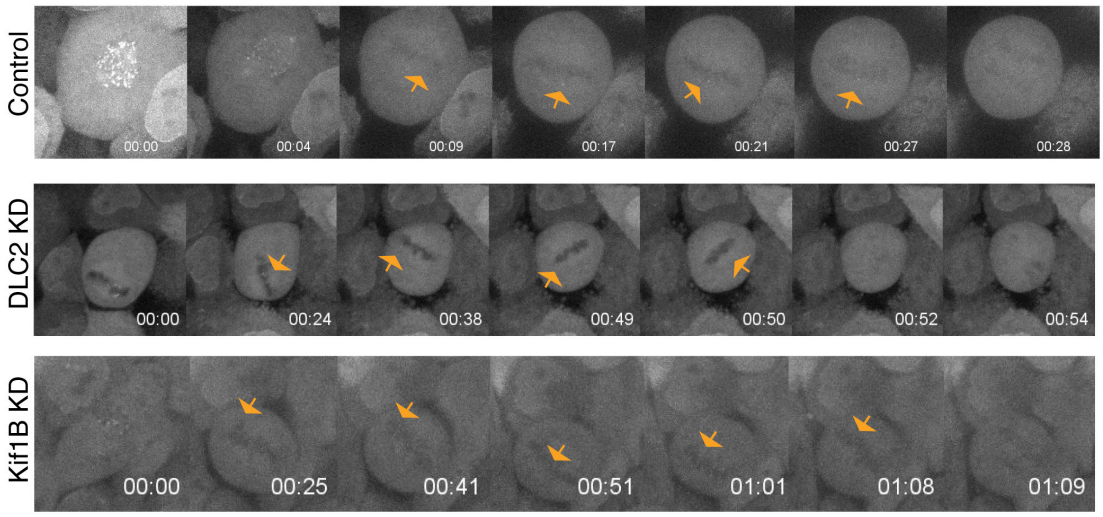

Figure 6.7 Live imaging of DLC2 KD and Kif1B KD HeLa cells Mad2-GFP

HeLa cells stably expressing Mad2-GFP and transfected with control, DLC2 or Kif1B siRNAs were filmed during mitosis. Pictures were taken with a spinning disc confocal microscope every minute. Watch Videos Chapter6-Control-mad2, Chapter6-DLC2kd-mad2, Chapter6-Kif1Bkd-mad2.

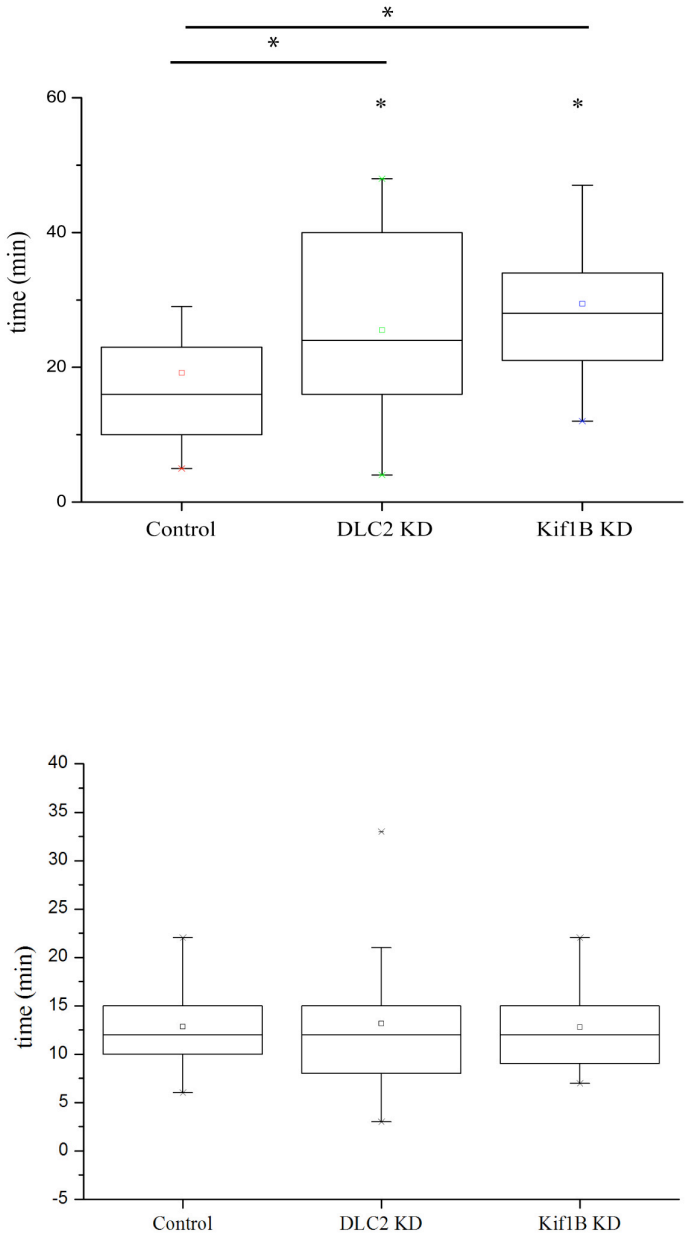

Figure 6.8 DLC2 and Kif1B KD cells retain GFP-Mad2 positive kinetochores for longer

Top chart show the average of minutes cells retain GFP-Mad2-positive dots at the kinetochores. DLC2 and Kif1B KD cells show GFP-Mad2 dots for longer.

Bottom chart show that the longer GFP-Mad2 staining is abolished if cells were treated with MPS-1 inhibitor that blocks the mitotic checkpoint. Over 30 cells per condition were counted.

In charts where data are represented as box-whisker plots, the box size represents 75% of the population and the line inside the box represents the median of the sample. Maximum (in the upper quartile) and the minimum (in the lower quartile) values are represented by the size of the bars (whiskers). * $p<0.05$.

6.5 DISCUSSION

In this chapter, I have shown that the DLC2 spindle defect is not related to the previously reported Cdc42-regulated spindle orientation. On the contrary, cells depleted of DLC2 assemble spindles that have normally orientated spindles. However, these spindle seem have lost their anchorage and they spin inside the cells and shift from left to right throughout metaphase.

I am aware that some of the experiments (live imaging) was done in HeLa cells, and others (mitotic index experiment) in HCE cells. HeLa cells are a model system really different from HCE cells and most importantly do not form any junctions, but I can compare the results on the cell division timing. Interestingly, in both the same line, DLC2 and Kif1B KD slows down metaphase, and moreover, throughout the long spinning and rocking movements, HeLa cells reveal that depletion of either DLC2 or Kif1B results in chromosome misaligned, such as those observed in HCE cells at the beginning of the project. It would have been important to validate the rocking movements in the HCE cell monolayer in live.

The observed delays in metaphase are connected to the fact that DLC2 KD cells do not have chromosomes attached properly. This is sensed by Aurora B and reflected in prolonged activation of the checkpoint. Since some kinetochores are misattached, Mad2 is constantly recruited and only eventually it switches off and cells complete mitosis. At this stage I cannot say whether this affects chromosome segregation. However, I can imagine it is more likely that, strained by the long metaphase, the checkpoint eventually turns off and chromosomes are distributed unevenly between the two daughter cells. This has previously been described as chromosome fatigue.[172] In this condition, cells adopt the strategy of exiting mitosis despite of the checkpoint and kinetochores remain misattachment in order to ensure cell survival, although the new cells will be aneuploid. Aneuploidy is one of the possible ways cancer is triggered, as the excess or lack of DNA information can instruct a cell to a wrong behaviour, which can degenerate to cancer[173,174].

CHAPTER 7:
MDIA3, AN EFFECTOR OF CDC42 IN THE DLC2 PATHWAY

CHAPTER 7: MDIA3, AN EFFECTOR OF CDC42 IN THE DLC2 PATHWAY

7.1 On the quest of a Cdc42 effector

When small GTPases are active, they transmit signals by binding directly their effectors. Through specific binding to a particular effector, small GTPases are able to initiate specific signalling cascades[44,175]. DLC2 depletion resulted in increased levels of Cdc42, suggesting that a Cdc42 effector was kept activated and contributed to spindle deregulation. Therefore, I was interested in identifying next the responsible Cdc42 effector.

There are about 20 effectors reported for Cdc42[44,176]. Among all the known effectors, mDia3 was the one fitting best the criteria required to explain the mitotic phenotype. mDia3 is a still poorly characterized formin that is known to bind Cdc42. In 2004, Yasuda *et al.* showed that mDia3 and Cdc42 regulate chromosome alignment in HeLa cells[96]. Moreover, in the same paper endogenous mDia3 is reported to localize at the kinetochores.

A few years later, Mao's group presented mDia3 as a new target of Aurora B kinase[94]: mDia3 phosphorylation via Aurora B controls mDia3 activity and promotes formation of correct metaphase plates. These results led me thinking that mDia3 could be the effector I was looking for.

To test this hypothesis, I firstly blotted lysates from control, DLC2 and Kif1B KD HCE cells, non-synchronized or synchronized, for mDia3 expression. I observed that mDia3 expression was higher in non-dividing cells (non treated cells) and at the 90' in cells that had been depleted of either DLC2 or Kif1B. At 90', most of the control cells had completed metaphase whereas DLC2 and Kif1B KD cells were delayed, and at this time point the levels of mDia3 were still as high in depleted cells as those in controls after 45' (Figure 7.1).

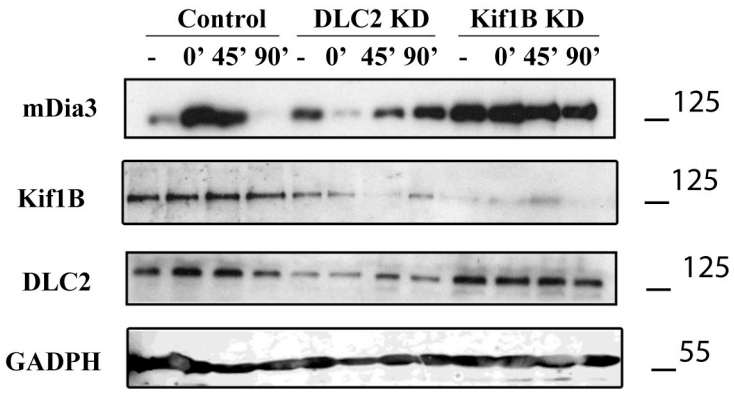

Figure 7.1 DLC2 and Kif1B KD leads to high levels of mDia3 in interphase and after 90′ of nocodazole washout.

Control, DLC2 and Kif1B KD HCE cells, treated or untreated with nocodazole, were analysed by WB as indicated. Expression of DLC2, Kif1B and mDia3 was detected. GADPH was used as an internal control.

By staining for endogenous mDia3 in HCE cells, I noticed that mDia3 was diffusely cytosolic under control conditions, but DLC2 of Kif1B depletion stimulated mDia3 recruitment to the cell cortex (Figure 7.2 A). These data suggest that increased Cdc42 signalling promotes cortical recruitment of mDia3. In reality, to further support this evidence I should have used a marker of cell-cell junctions or cell cortex to define that mDia3 is enriched specifically at the cell cortex. Perhaps also α-tubulin would have been important in this experiment, to show that mDia3 upon depletion of DLC2 and Kif1B is over recruited at the plus ends towards the ell cortex.

The mDia3 staining in DLC2 depleted cells was very similar to the one of Kif1B in control HCE cells. For this reason, I decided to check if mDia3, as Kif1B, could have been positioned at the kinetochores too. By staining for CREST, I was able to identify kinetochores in HCE cells. Figure 7.2 B shows that in control cells, no dots corresponding to kinetochores were detectable. However, mDia3-positive dots co-localazing with CREST were seen upon DLC2 and Kif1B depletion. Once again, I have to underline here the fact that this kinetochore staining is not sufficiently clear, and it would be nicer to use a mDia3 construct tagged of fused to a fluorescent protein, to monitor in live if it could localize at the kinetochores during cell division.

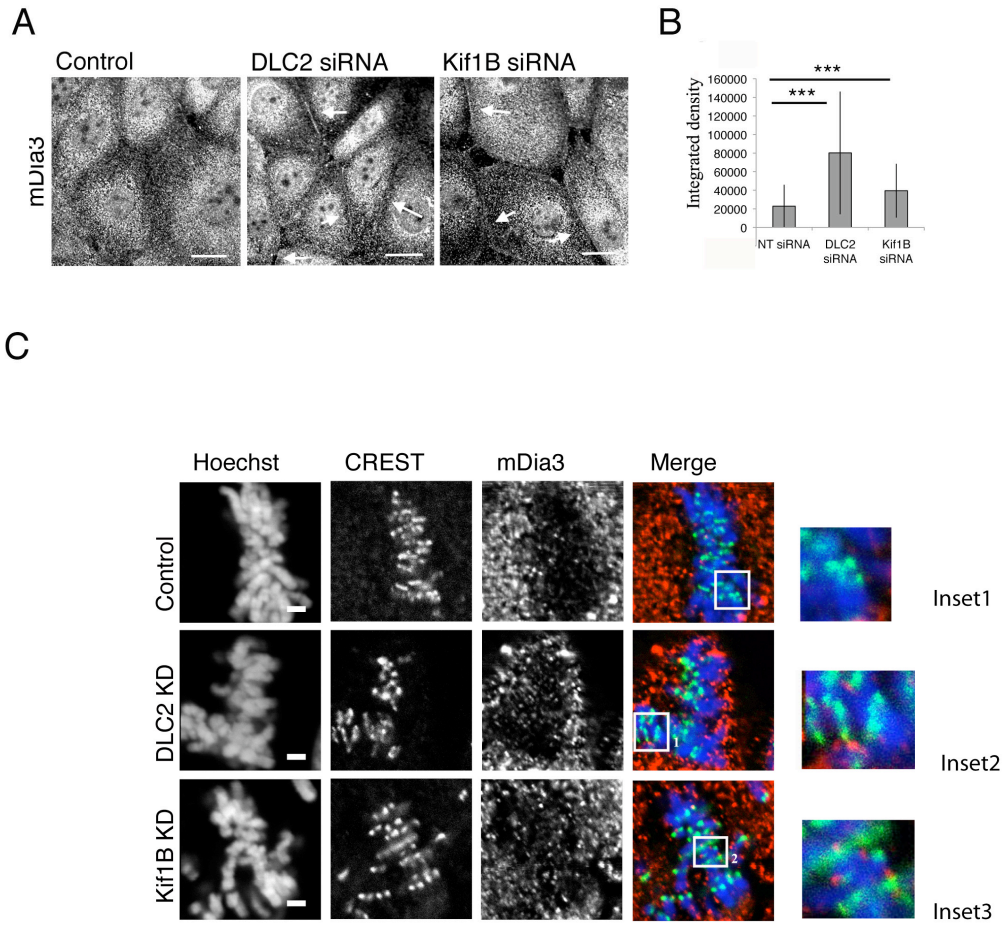

Figure 7.2 DLC2 and Kif1B KD cells have increased levels of mDia3 at the cell cortex and kinetochores.

(A) Confocal pictures showing mDia3 stained in Control, DLC2 KD and Kif1B KD HCE cells. (B) Chart showing the quantification for mDia3 intensity at the cell cortex. n=8 Bars represent mean of values. *** $p<0.001$

(C) Confocal pictures showing Control, DLC2 KD and Kif1B KD HCE cells stained for Hoechst (blue), CREST (green) and mDia3 (red). Bar represents 10μm (left panel) and 2μm (right panel).

7.2 mDia3 is recruited upon Cdc42 activation

To further investigate mDia3 recruitment, I tried to alter active/inactive Cdc42 levels within the cell and monitored the effect on mDia3 localization. Upon depletion of endogenous Cdc42, no mDia3 was detected either at the cell cortex or at the kinetochores (Figure 7.3 A and B). Moreover, depletion of Cdc42 blocked mDia3 recruitment triggered by DLC2 depletion (Figure 7.2 A and B). Similarly, transfection of DN Cdc42 in DLC2 KD cells (Figure 7.4) prevented recruitment, and overexpression of CA Cdc42 in control cells was sufficient to induce mDia3 recruitment to the cell cortex (Figure 7.4). As mentioned above, I should have used precise marker of cell cortex or kinetochores to define the enrichment or simply the staining localization of mDia3.

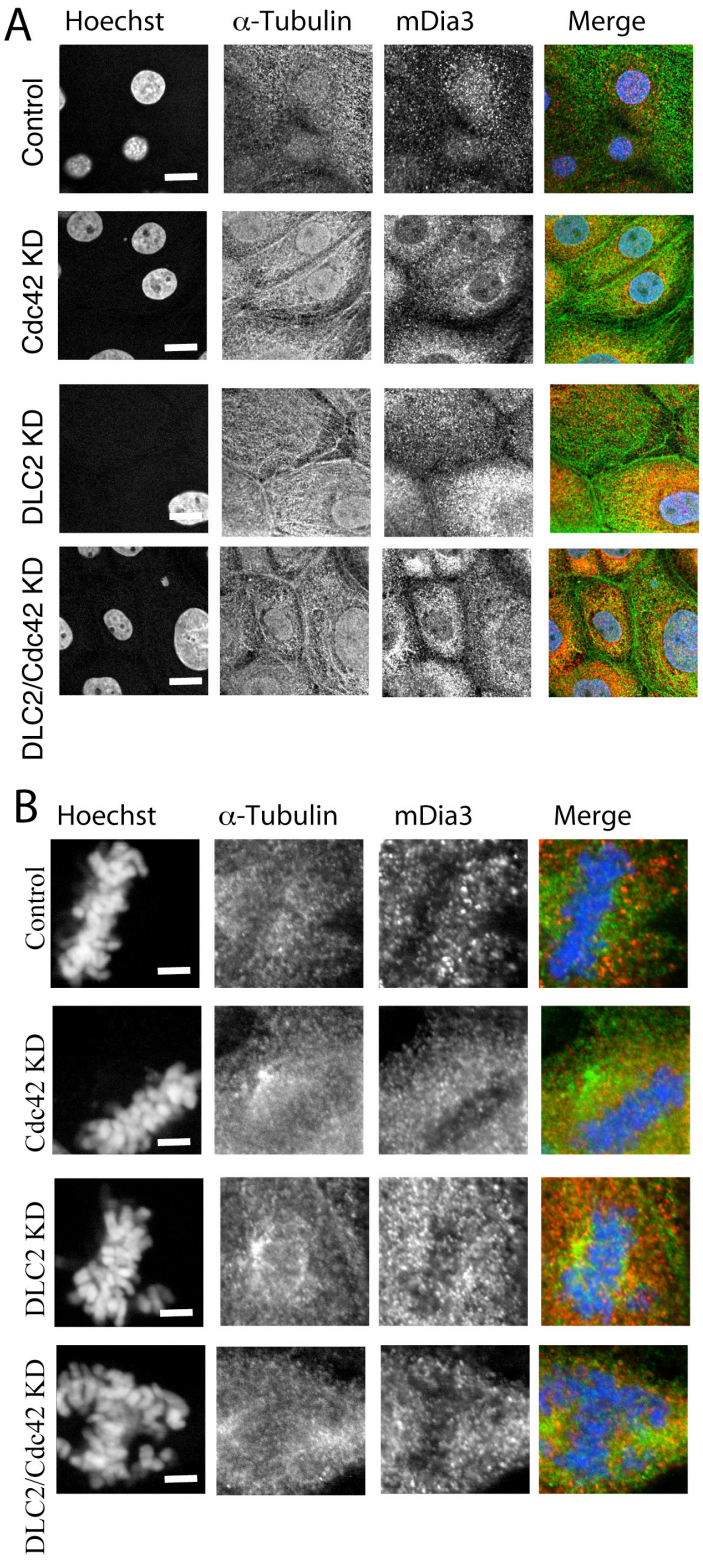

Figure 7.3 mDia3 is not recruited to kinetochores and cell cortex if Cdc42 is not active.
Confocal pictures showing Control, Cdc42 and DLC2 KD and Cdc42/DLC2 KD HCE cells stained in A for Hoechst and mDia3, and in B for mDia3 (red) red and α-tubulin (green) in B.
Bar represents 10μm (left panel) and 5μm (right panel).

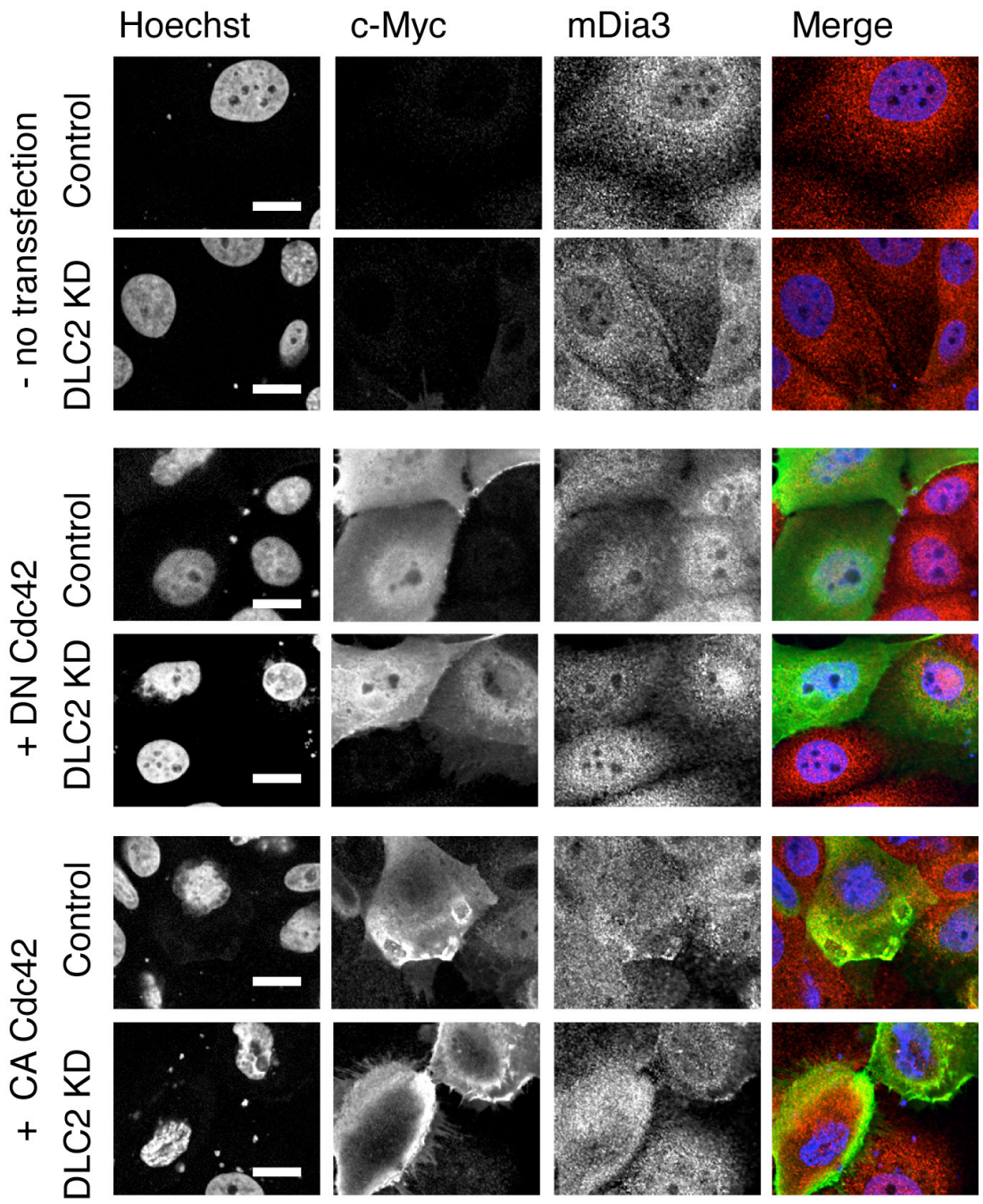

Figure 7.4 mDia3 is at the cell cortex when Cdc42 is active

Control and DLC2 KD HCE cells, untransfected or transfected with CA and DN form of Cdc42 were stained for mDia3 (in red), c-Myc (in green) and with Hoechst.

Bar represents 10μm.

7.3 mDia3 depletion induces chromosome misalignment

The results I presented in the first section of this chapter suggest that mDia3 acts downstream of DLC2. To better characterize its role, I performed mDia3 siRNA tranfection in HCE cells.

Firstly, I tested by WB the efficiency of the depletion (Figure 7.5). 4 siRNAs were used to deplete mDia3. All of them, but oligo4, were able to reduce mDia3 expression efficiently. Despite of the low efficiency of mDia3 oligo4, I chose to use a pool of all four to confirm the known role of mDia3 in metaphase.

Depletion of mDia3 in HCE cells resulted in chromosome misalignment as had done DLC2 and Kif1B depletion (Figure 7.6). Quantification of misaligned metaphase cells demonstrated that mDia3 depletion significantly increased chromosome misalignment and this could be rescued by double depletion DLC2 and mDia3 (Figure 7.7).

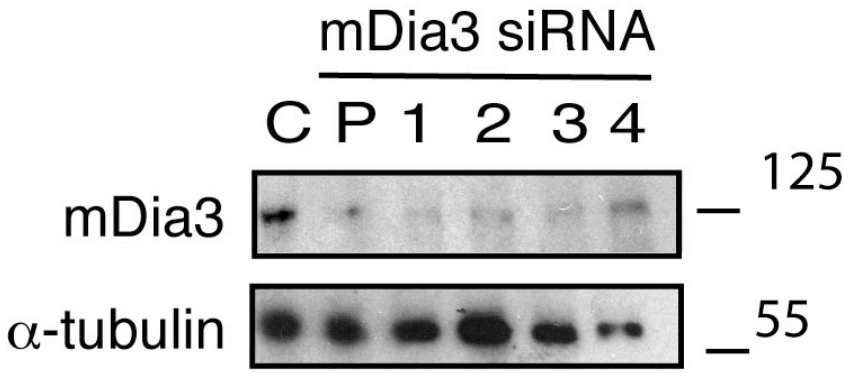

Figure 7.5 WB for validation of DLC2 KD in HCE cells
WB for mDia3 expression in HCE cells: C control, P pool of four siRNAs, 1 siRNA 1, siRNA 2, 3 siRNA 3, 4 siRNA 4. α-tubulin was used as an internal control.

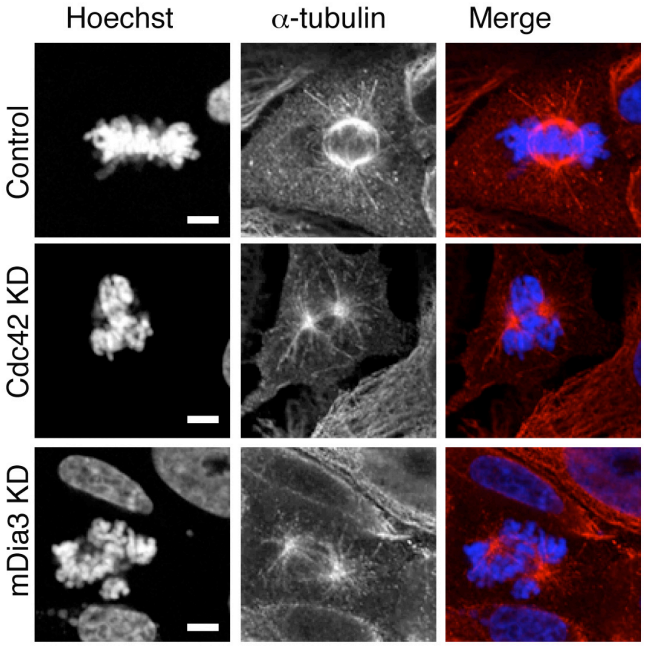

Figure 7.6 Cdc42 KD and mDia3 KD cells mitotic spindles are less dense in fibres
Confocal pictures of control, Cdc42 and mDia3 KD cells stained for DNA and MTs.
Bar represents 5μm.

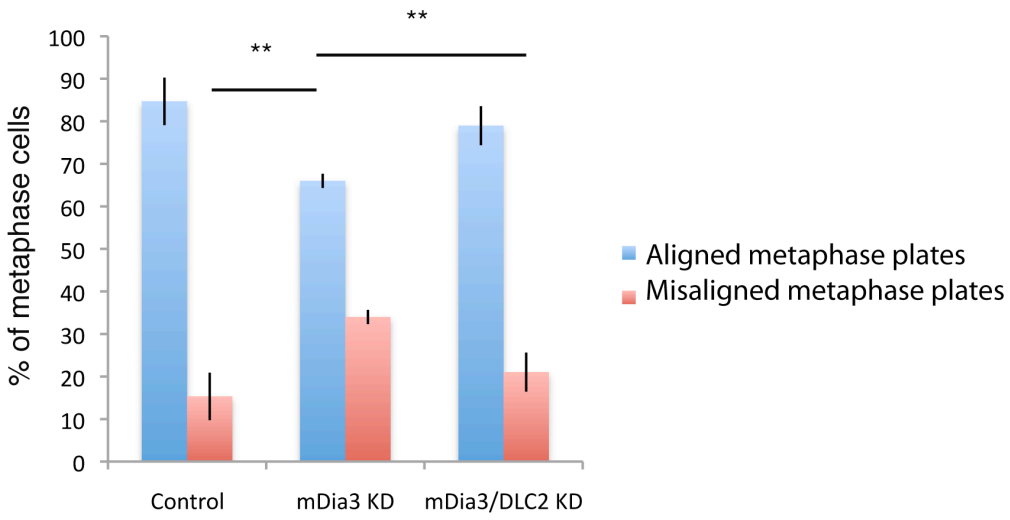

Figure 7.7 mDia3 KD results in increased chromosome misalignment
HCE cells were transfected with Control and mDia3 siRNAs.
Aligned and misaligned metaphase plates were counted and plotted. Over sixty cells were counted per conditions. This experiment was performed three times. Bars represent mean of values.
** $p<0.01$

7.4 mDia3 and Cdc42 depleted cells are delayed in metaphase

Due to the similarities to DLC2 KD cells, I was curious to follow up mitosis in Cdc42 and mDia3 KD cells and check the timing was affected.

By performing live imaging with HeLa cells stably transfected for mCherry-H2B (DNA marker) and α-tubulin-GFP to visualize the mitotic spindle structure, I could observe that similarly to DLC2 and Kif1B KD cells, mDia3 and Cdc42 KD mitotic spindles spun and rocked within the cell (Figure 7.8 A) (Watch Videos Chapter6-Control-atub-h2b, Video Chapter6-Cdc42kd-atub-h2b, Video Chapter6-mDia3kd-atub-h2b). The metaphase plate was not stable and showed chromosomes misaligned from the main axis of the metaphase plate. Depletion of Cdc42 and mDia3 caused significantly increased metaphase length (Figure 7.8 B).

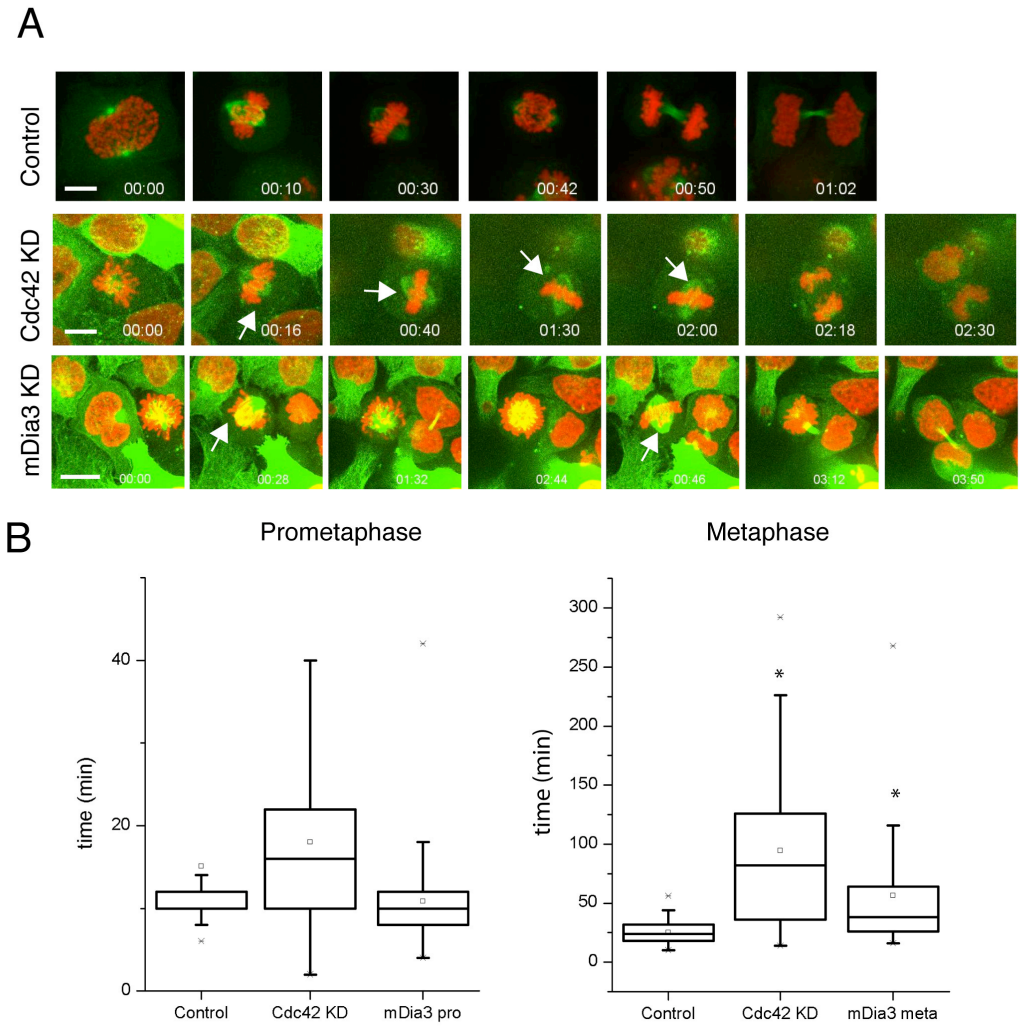

Figure 7.8 Live imaging of DLC2 and Kif1B KD HeLa cells

(A) HeLa cells stabely transfected with H2B-mCherry and α-tubulin-GFP and transfected with control, Cdc42 or mDia3 siRNAs were filmed throughout mitosis. Pictures were taken with a spinning Disc confocal every 2 minutes. White arrows are pointing at misaligned chromosomes. Watch Videos Chapter6-Control-atub-h2b, Video Chapter6-Cdc42kd-atub-h2b, Video Chapter6-mDia3kd-atub-h2b.

(B) Length of prometaphase and metaphase was calculated and plotted in a graph. . Over 30 cells per condition were counted. In charts where data are represented as box-whisker plots, the box size represents 75% of the population and the line inside the box represents the median of the sample. Maximum (in the upper quartile) and the minimum (in the lower quartile) values are represented by the size of the bars (whiskers).

7.5 DISCUSSION

My results indicate that mDia3 functions as an effector of Cdc42 downstream of DLC2. The fact that DLC2 and Kif1B depletion resulted in increased mDia3 protein expression and recruitment to the cell cortex and kinetochores indicates that mDia3 is involved in the DLC2 pathway.

mDia3 depletion caused chromosome misalignment and delays in metaphase. Similar results have been described in previous sections for Cdc42 KD. Thus, it must also be noticed that Ccd42 and mDia3 depleted cells result in misoriented spindles as well. This was in fact already reported for Cdc42[78,160], suggesting that depletion of Cdc42 impairs more mechanisms than the one of spindle positioning regulated by DLC2/Kif1B complex. Also mDia3 seems to be involved in more processes since its depletion causes chromosome misalignment, spindle positioning defect and misorientation too. This is an indication that mDia3 is involved in more pathways and most likely acts downstream other signal cascades, different from the one linked to DLC2. All together these data support the idea that controlled Cdc42 signalling within mitotic cells is important for correct chromosome segregation. In fact, both overactivation or deactivation of Cdc42 led to the same phenotype.

Strikingly, mDia3 was not detectable at the cell cortex or at the kinetochores in any conditions in which Kif1B was. Hence, mDia3 and Kif1B might compete for the same site. In this model, Kif1B would be the protein with highest affinity in normal cells. Activation of Cdc42 recruits mDia3 to the MT anchorage points (kinetochores and cell cortex) and here it triggers Kif1B mislocalization if Cdc42 is overactivated (see final discussion for more details).

I still have not discussed why chromosome attachment is affected by defective Cdc42 signalling. This will be the topic of the next chapter.

CHAPTER 8:
ANALYSIS OF MICROTUBULE DYNAMICS

CHAPTER 8: ANALYSIS OF MICROTUBULE DYNAMICS

8.1 Introduction to the dynamics of the mitotic spindle

The mitotic spindle is not a steady structure, but a dynamic one and under constant change. Its dynamics is due to the forces exerted on the spindle itself (Chapter 6) and the polymerization rate of MTs. Another important factor are also the forces originating outside the mitotic spindle, coming form the cell cortex (via cortical actin), and are transmitted via astral MTs.

I will present first the role of MT polymerization and, secondly, the impacting that cortical actin can have on the spindle stability.

8.1.1 Regulating MT polymerization/depolymerization

MTs undergo dynamic instability with constant transitioning between growing and shrinking states[177]. It has been shown that this mechanism depends on a cap at the tip of the fibre. Loss of this cap is thought to trigger the transition from growth to shrinkage, called catastrophe[178]. The transition depends on tubulin concentration, the time between tubulin dilution and catastrophe, and the induction of microtubule catastrophes by walking depolymerases. Also, the mechanism depends on binding of MT tips to specific anchoring proteins (as those at the kinetochores or at the cell cortex) that stabilize tips of growing microtubules.

There are three categories of MTs in the spindle: kinetochore MTs, nonkinetochore fibres and astral MTs. Kinetochore microtubules (K-MTs) have plus-ends anchored to the kinetochores and the minus-ends at the spindle poles. They pull on chromosomes at kinetochores and silence the spindle assembly checkpoint signal that is generated by unattached kinetochores. In mammalian cells, about 10–30 K-MTs bind each chromosome. At the same time, K-MTs bundle with each other and with nonkinetochore fibres. Since both ends are capped, K-MT turnover is much slower than the other microtubule classes, with a half-life of ~7 min in metaphase spindles and polymerization and depolymerization balanced at steady-state (data collected from analyses done in rat Kangaroo kidney epithelial cells, Ptk1)[152].

Nonkinetochore microtubules (nK-MTs) are represented by all microtubules that lie between spindle poles other than K-MTs (they are also known as interpolar microtubules). The nK-MTs comprise the majority of microtubules in mammalian spindles that have been studied by electron microscopy. They bundle in groups of 2–6, with anti-parallel interactions apparently preferred, during metaphase. Their function is poorly understood, but they are thought to help keeping the poles apart, support choromsome segregation during anaphase, and ensure its bipolarity. nK-MTs turnover is rapid, due to dynamic instability of plus-ends (sliding velocities measured in Xenopus extract has an average velocity of ~2 μm/min)[152].

Astral microtubules (a-MTs) are attached via minus-ends to the centrosome and they extend to the cell cortex. They position the spindle within the cell. a-MT turnover is comparable to nK-MTs, with growth and shrinkage rates of ~10–15 μm/min (data shown in pig kidney epithelial cell, LL-PK1)[152].

8.1.2 Actin polarity coordinates spindle dynamics

External forces are exerted not only inside the spindle but numerous forces generated outside of the cell and reflected on the cell cortex and subcortical actin influence the life of the mitotic spindle[151].

For example, it was shown that asymmetric meiotic divisions in mammalian oocytes depend on the acentric positioning of the spindle to format small polar bodies; this is ensured by cortical actin polarization, regulated by Cdc42 concentrated in restricted cortical regions, and the consequent recruitment of N-WASP, which regulates F-actin remodelling and accumulation[179].

8.2 Cortical actin is altered upon DLC2 and Kif1B depletion

Considering that DLC2 is a GAP for Cdc42 and Cdc42 has been reported as major player in controlling cortical actin behaviour, I wondered if the phenotype I observed in DLC2 depleted cells was due to an aberrant behaviour of cortical actin. If this was true, the spindle inside would read the wrong motion and, as a consequence, been altered in dynamics of MTs and chromosome attachment stability. To investigate this hypothesis, I took advantage of a recently developed tool: a fibronectin-coated micropatterned dish, where fibronectin was coated with a specific geometry (parallel lines)[180]. Although artificial, micropatterned substrates allow recreation of physiological conditions for controlled in vitro cell culture. It is possible to manipulate micropattern shapes and cells will adapt their cytoskeletal architecture according to the geometry of their microenvironment. This tool is used to study remodelling of actin and microtubule networks in the adaptation of cell polarity with respect to external constraints.

When plated on micropatterned dishes with parallel lines of fibronectin, Contol HeLa cells sit on the lines and spread along them. When they enter mitosis, retraction fibres form while the cells round up and the mitotic spindle senses their direction, and aligns along this line too. Subcortical actin polarizes along the direction of the retraction fibres. Retraction fibres exerted strong forces on the mitotic cell body, driving spindle positioning[151]. Moreover the geometry introduced with the pattern bias the behaviour of the subcortical actin network: the polarization in fact results from a side to side of the fibronectin line. Two additional types of actin behaviours can be seen: a non-polarized movement, with actin rotating along the cortex or an absence of polarization (Figure 8.1) (Watch videos Chapter8-absent polarization, Chapter8-polarized, Chapter8-circular actin).

DLC2 and Kif1B KD cells showed a significant increase in aberrant actin behaviour. The spindle was stable in its position and did not spin, and did not follow the actin behaviour anymore (Figure 8.2). Moreover, I looked at the positioning of the mitotic spindle compared to the retraction fibres. I did not measure the percentages of aberrant angles, but I annotated if the line crossing to through the spindle poles was parallel or not to the fibronecting line. Interestingly, I detected that the spindle aligned in an indepenent manner from the direction dictated by the fibronectin line in depleted cells (Figure 8.2). This data indicates that the actin behaviour was not read by the mitotic spindle in depleted cells. This

also suggested that astral MTs attaching to the cortex had become insensitive to changes in cortical actin.

I have shown in Chapter 3 that APC and p120catenin were impaired upon DLC2 depletion. This already indicated that astral MTs lost their anchoring point. The new set of data point toward the same conclusion and suggest that MTs were no longer anchored at the cell cortex.

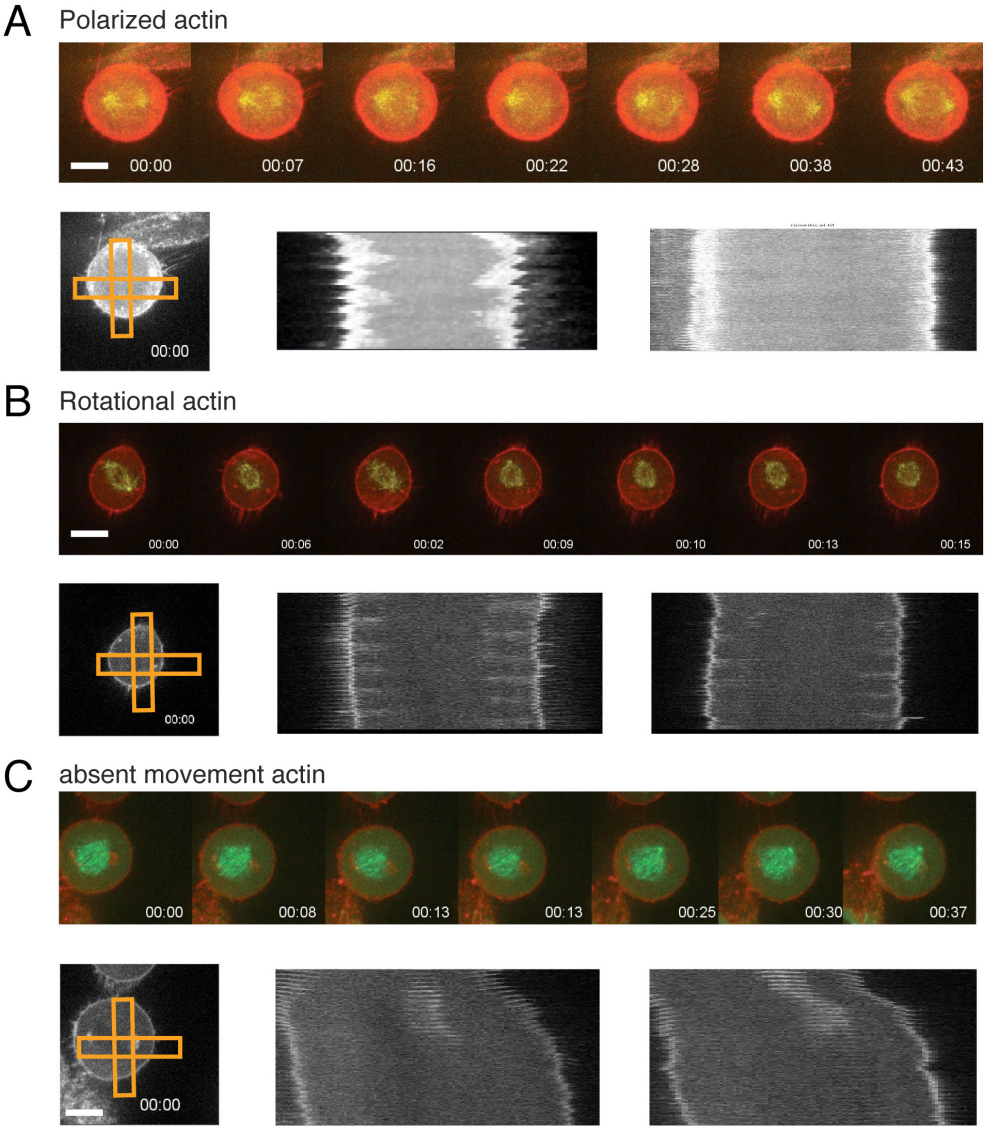

Figure 8.1 Categories of subcortical actin behaviour

HeLa cells stably transfected lifeact-EB3GFP were plated on micro-patterned dishes and filmed every 1′ from metaphase to follow actin behaviour in mitosis. Two major subgroups of behaviour were identified: polarized actin and non-polarized. Non polarized actin groups random polarization and absent polarization.

(A) Sequence of pictures for an example of polarized actin behaviour. To better show the actin movement from side to side two kymographs were drawn: one through the plane of the

polarization, and on perpendicular. The parallel one shows the alternate left-right shifting; the perperdicular one confirm that actin is excluded from this area.
(B) Sequence of pictures for an example of random polarized actin behaviour. The two kymographs show here that actin polarization is everywhere.
(C) Sequence of pictures for an example of absent polarization. The two kymographs drawn show that there is no polarization throughout the cell cortex.
Watch videos Chapter8-absent polarization, Chapter8-polarized, Chapter8-circular actin. Scale bars 10μm.

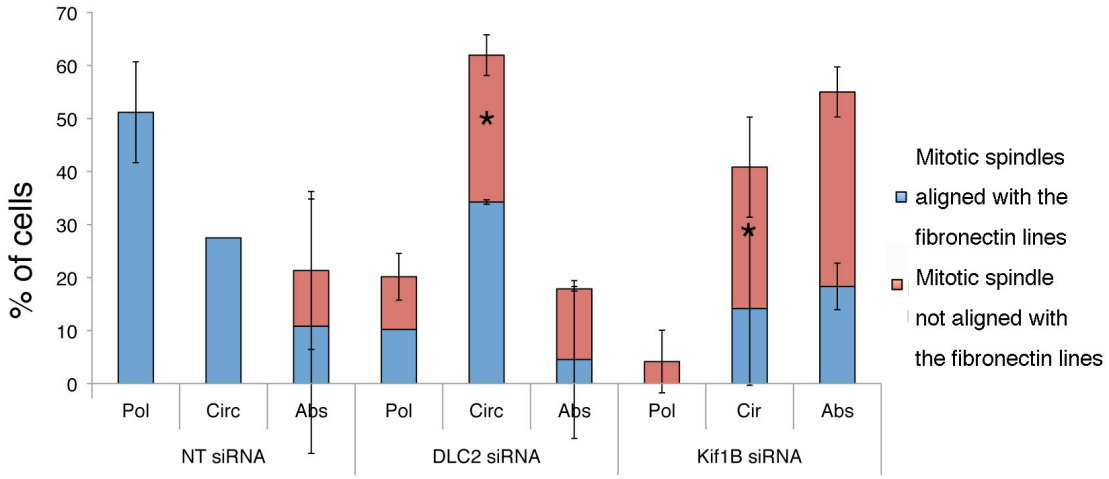

Figure 8.2 DLC2 and Kif1B depletion result in an increase in non-polarized actin behaviour and more misaligned mitotic spindles compared to the patterned lines.
HeLa cells stably transfected lifeact-EB3GFP were plated on micro-patterned dishes and filmed every 1' from metaphase to follow actin behaviour and spindle alignment in mitosis.
The chart shows percentages of cells with a specific actin behaviour on micropattern dish with parallel fibronectin lines (Pol:polarized action; Circ: circular movement; Abs: absent polarization). Blue bars represent cells with mitotic spindle aligned with the fibronectin line; red bars, misaligned spindle. Over 20 cells per condition were counted. Asterisks indicate significance of the particular sub group calculated in comparison with the corrispective control category (shown are means ± 1 SD; * $p<0.05$). Scale bars, 10 μm.

8.3 DLC2 and Kif1B KD cells have hyperstable MTs

Since my hypothesis was that there was a defect in MTs, I wondered if their dynamics was in fact affected upon depletion of DLC2 and Kif1B KD. I firstly thought perhaps fibres in DLC2 and Kif1B KD condition could have been unstable, which would have explained the chromosome instability as well as the loss of cortical anchorage. Therefore, I treated cells with Taxol to rescue a possible instability defect (taxol stabilizes MTs) and looked at the number of misaligned metaphase plates. However, Taxol treatment did not rescue the chromosome misalignment defect (Figure 8.3); it rather made control cells look worse. This suggested that hyperstabilization as well as destabilition can affect chromosome misalignment. If DLC2 and Kif1B KD cells were not rescued by taxol stabilization, it could be that the fibres were already too stable and therefore insensitive to further stabilization.

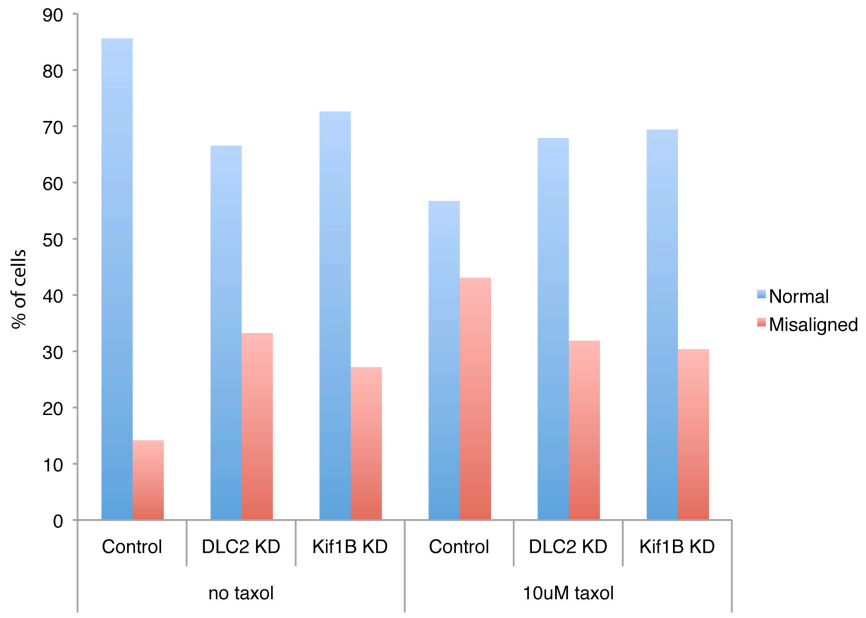

Figure 8.3 Taxol does not rescue DLC2 and Kif1B KD phenotype
Control, DLC2 KD and Kif1B KD HCE were treated with taxol to test the hypothesis if by stabilyzing microtubules, untreated and taxol treated cells. Over 60 cells with aligned or misaligned chromosomes were counted for each condition.

The hyperstability was also supported by the fact that astral MTs and spindle within the spindle (most likely interpolar fibres since they can expand also further than the methaphase plate itself and not kinetochore fibres since they are constrained by the fixed distance chromosome pole) were longer in DLC2 and Kif1B KD cells compared with control cells (Figure 8.4).

It was shown already that MT growth control cell shape and polarity[181]. Interestingly, it was also shown in Arabidopsis Thaliana that the MT stabilization can promote cell elongation on specific axes[182,183]. Since DLC2 and Kif1B depleted cell show hyperstable MTs, I wondered if also the cell shape could have been affected. Indeed, since astral MTs had more space to grow than the constrained KT-MT and non KT-MT, I have observed in DLC2 and Kif1B depleted cells an expansion of the longitudinal axis of the entire spindle (Figure 8.5). On the contrary the distance pole-to-pole and the vertical axis did no vary significantly from control.

To test whether the hyperstability defect was also detected inside the mitotic spindle, I performed a classic cold treatment assay. This technique tests the capability of MTs to depolymerize upon cold treatment. Since KT-MTs are more stable than the other MTs, they resist longer to cold, but after about 30' in control situation they become short too. Strikingly, cells depleted of DLC2 and Kif1B resisted the cold longer than control cells, and after 30' they still retained longer fibers (Figure 8.6). This phenotype does also correlates with the abnormalities in the metaphase plate compactness. In fact, the categories of cells that retain long MTs are classified for type of misalignment: category3 is mild chromosome scattering and category2 is excessive chromosome scattering. These two categories increased in comparison with cell that still have a normally aligned metaphase plate and that is sensitive to cold depolymerization, similarly to the control.

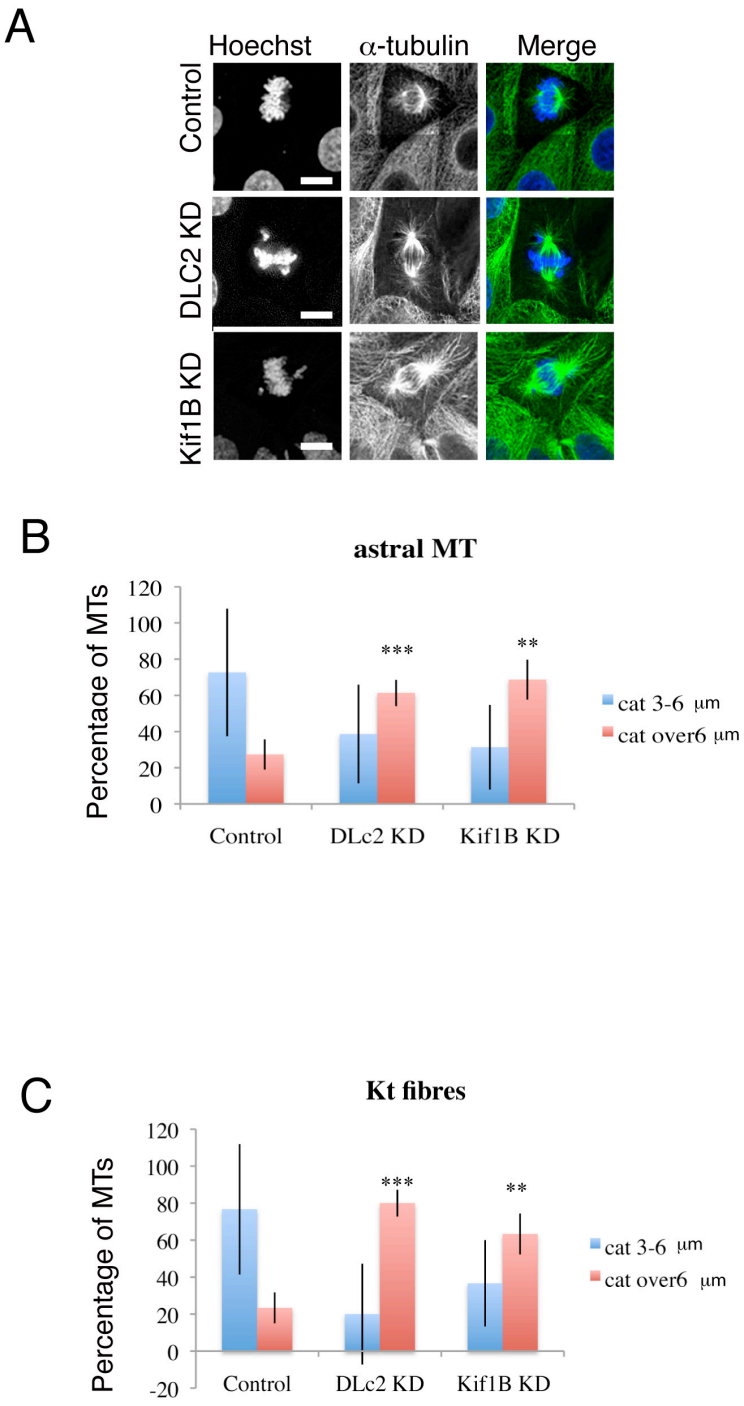

Figure 8.4 Astral and KTs fibers are longer in DLC2 and Kif1B KD cells

(A) Confocal pictures for control, DLC2 and Kif1B KD cells stained for Hoechst, EB1 (red) and α-Tubulin (green). Bar represents 10µm.

(B) Quantification of the KT MT length of Control, DLC2 and Kif1B KD HCE cell. Over 50 MTs per experiments were counted.

(C) Quantification of the astral MTs length of Control, DLC2 KD and Kif1B KD HCE cells. Over 50 MTs per experiments were counted

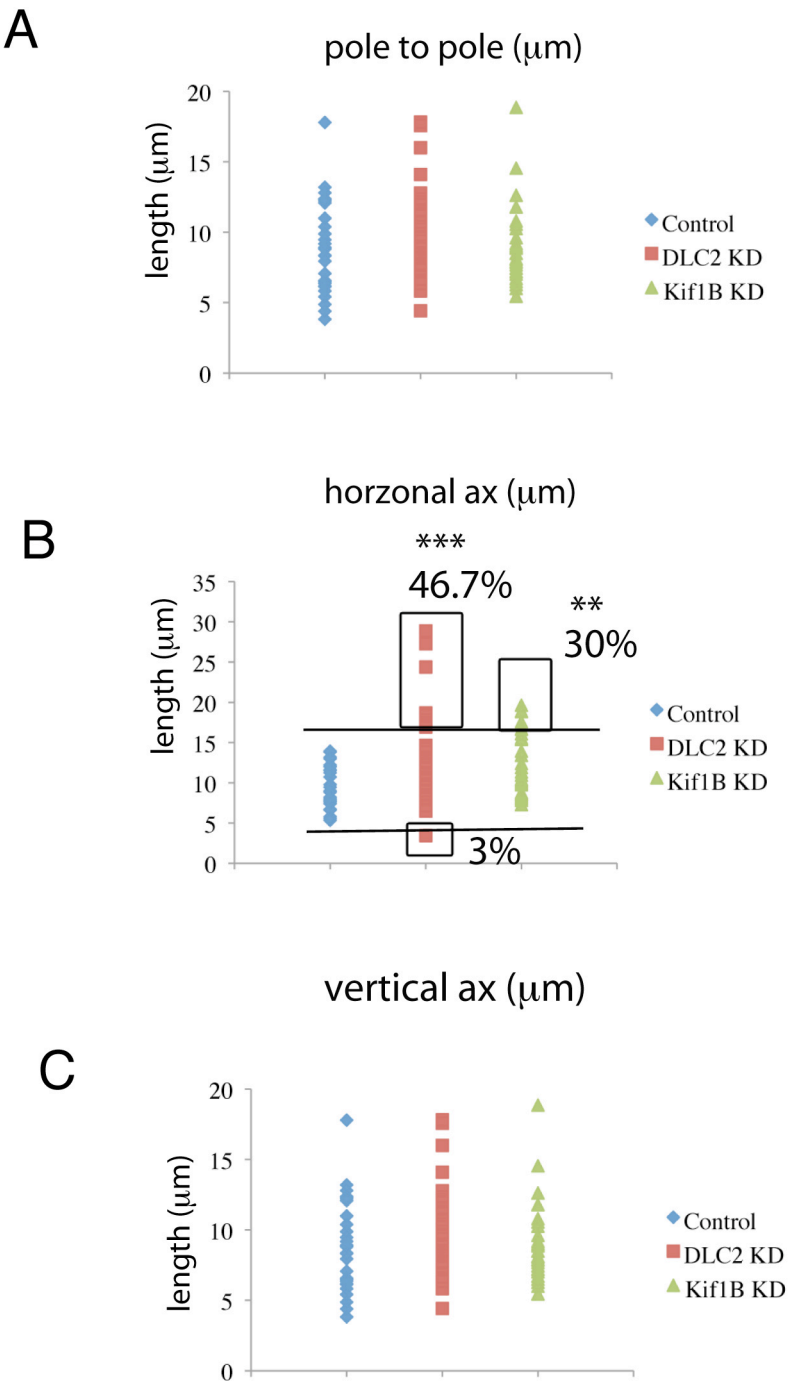

Figure 8.5 Mitotic DLC2 and Kif1B cells have a longer horizontal axis.

(A) Scatter plot of the pole-to-pole distance of Control, DLC2 and Kif1B KD HCE cells. Over 50 cells per experiments were counted.

(B) Scatter plot of the horizontal axis length (line from junction to junction passing through both spindle poles) of Control, DLC2 and Kif1B KD HCE cells. Over 50 cells per experiments were counted.

(C) Scatter plots of the vertical axis length of Control, DLC2 and Kif1B KD HCE cell. Over 50 cells per experiments were counted.

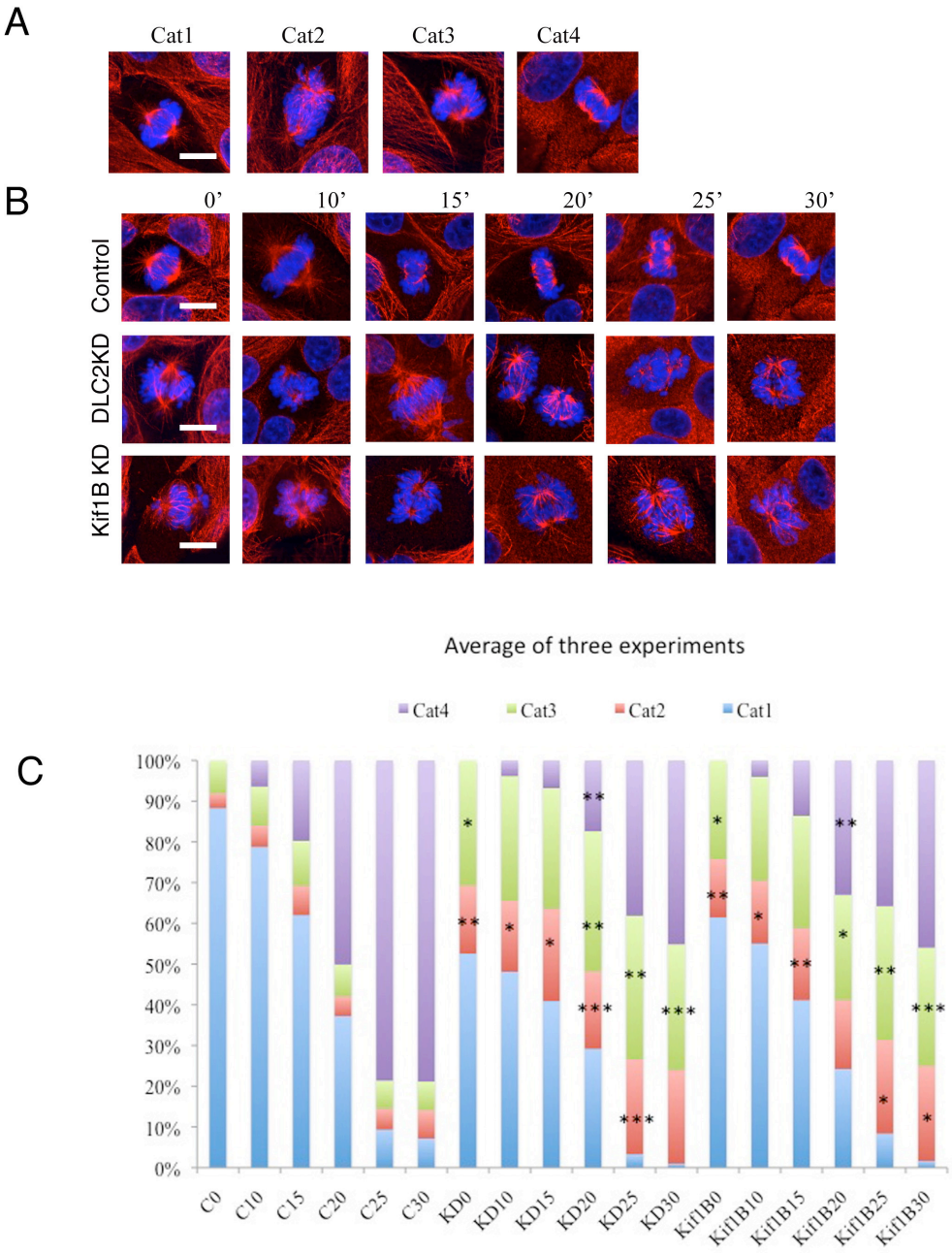

Figure 8.6 DLC2 and Kif1B KD cells have MTs with increased resistance to cold.

(A) Categories of cells counted in the chart in C. Bar represents 10μm.

(B) Examples of cells of Control, DLC2 and Kif1B KD cells treated with cold.

(C) Chart of percentages of the 4 categories through time for Control, DLC2 and Kif1B KD HCE cells. * $p<0.05$ ** $p<0.01$ *** $p<0.001$. Over 60 cells were counted per condition. This is an exemplar experiment, but the results were confirmed three times.

8.4 Cdc42 and mDia3 KD induce MTs instability

Taken into account that DLC2 and Kif1B depleted cells showed MT hyperstability and have increased levels of active Cdc42, I wondered if the two events were connected. To test this hypothesis, I decided to look at MT dynamics in cells depleted of Cdc42 and mDia3. Figure 8.7 shows the results of this assay: in contrast to the phenotype observed for DLC2 and Kif1B depletion, mDia3 and Cdc42 KD showed higher percentages of short fibres cells at early time-points. These data indicate that Cdc42 and mDia3 depletion induced instability of kinetochore microtubules. This phenotype does also correlates with the abnormalities in the metaphase plate compactness. In fact, the categories of cells that have shorter MTs are classified for type of misalignment: category3 is mild chromosome scattering and category2 is excessive chromosome scattering. These two categories increased in comparison with cell that still have a normally aligned metaphase plate and that is sensitive to cold depolymerization, similarly to the control.

To further analyse MT behaviour, I adopted the strategy of live imaging to follow EB3 behaviour. I used HeLa cells stably transfected with EB3-GFP and I imaged Control, mDia3 KD, Cdc42 KD, DLC2 KD and Kif1B KD cells every 10'. From the collected videos, speed, total time and total distance of EB3 comets were measured. Whereas speed was not affected in any condition, both total distance and total time were altered in all the KD conditions (Figure 8.8) (Watch videos Chapter8-Control-EB3, Chapter8-DLC2kd-EB3 Chapter8-Cdc42kd-EB3). For DLC2 KD and Kif1B KD cells, these parameters were higher than in controls; in Cdc42 KD and mDia3 KD situation they were lower (Figure 8.9 A and B) (Watch videos Chapter8-Control-EB3, Chapter8-DLC2kd-EB3 Chapter8-Cdc42kd-EB3).

As a last test for regulation of MT stability by DLC2 pathway, I used monastrol to measure MT length in monopolar spindles. In this condition, it becomes easier to measure MT length as MTs are not overlapping. Figure 8.10 and 8.11 show that both astral and Kinetochore microtubules were impaired in length. I have chosen HURP as a marker of kinetochore fibres, since it was reported to specifically localized along them and excluded from the interpolar fibres[184]; for astral MTs I have chosen PRC-1which was shown to stain interpolar fibres in mitosis and fibres in the midbody (which is consider rich in astral MT)[185]. DLC2 and Kif1B depletion caused hyperstability and resulted in longer fibres;

Cdc42 and mDia3 KD cells had unstable MTs that were significantly shorter than in controls.

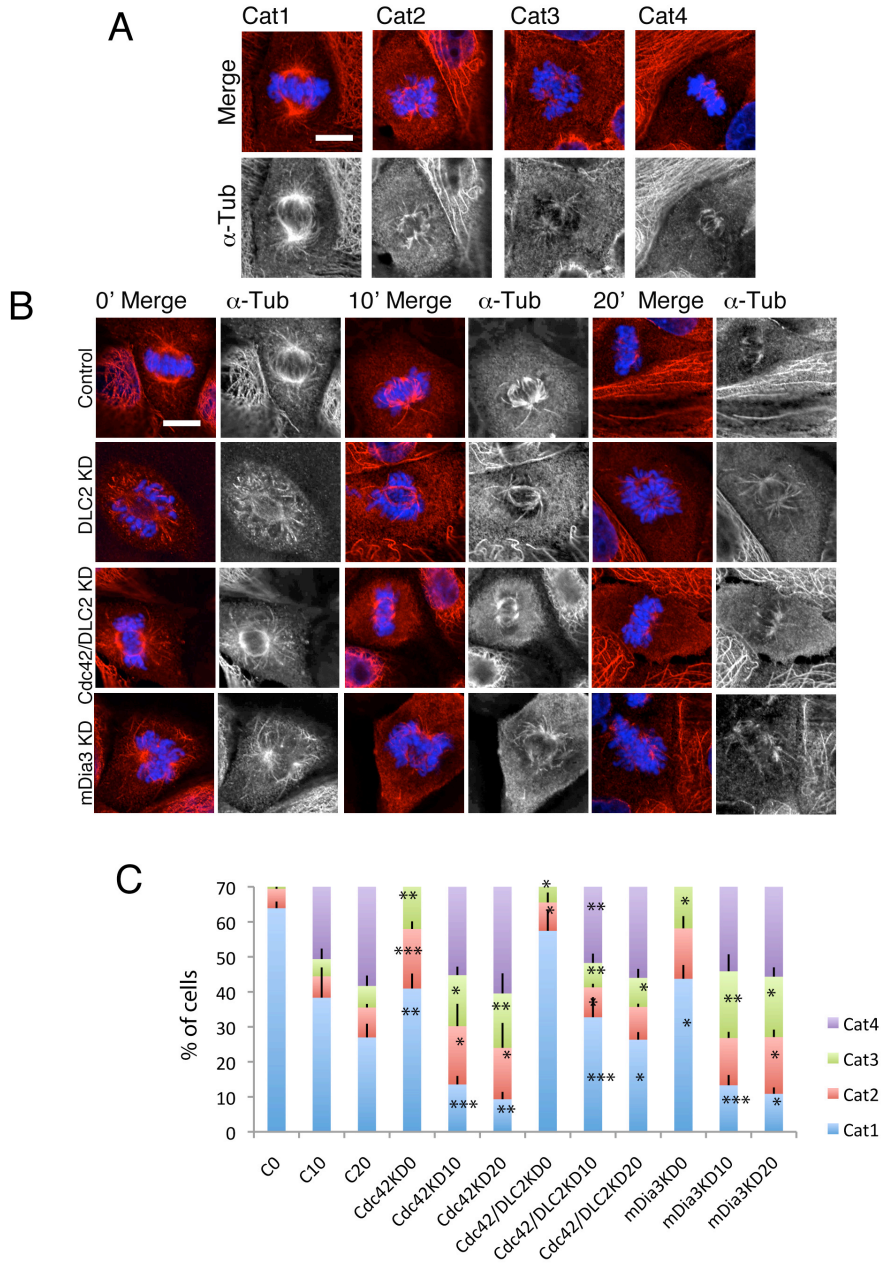

Figure 8.7 MTs in Cdc42 and mDia3 depleted cells depolymerize faster when exposed to cold.
(A) Categories of cells counted in the chart in C. Bar represents 10μm.
(B) Example panels of the response of Control, Cdc42 and mDia3 KD cells to cold.
(C) Chart of percentages of the 4 categories through time for Control, Cdc42 and mDia3 KD HCE cells. * $p<0.05$ ** $p<0.01$ *** $p<0.001$ Shown are mean of values of three experiments. Error bars represents standard deviations. Over 60 cells per condition were counted.

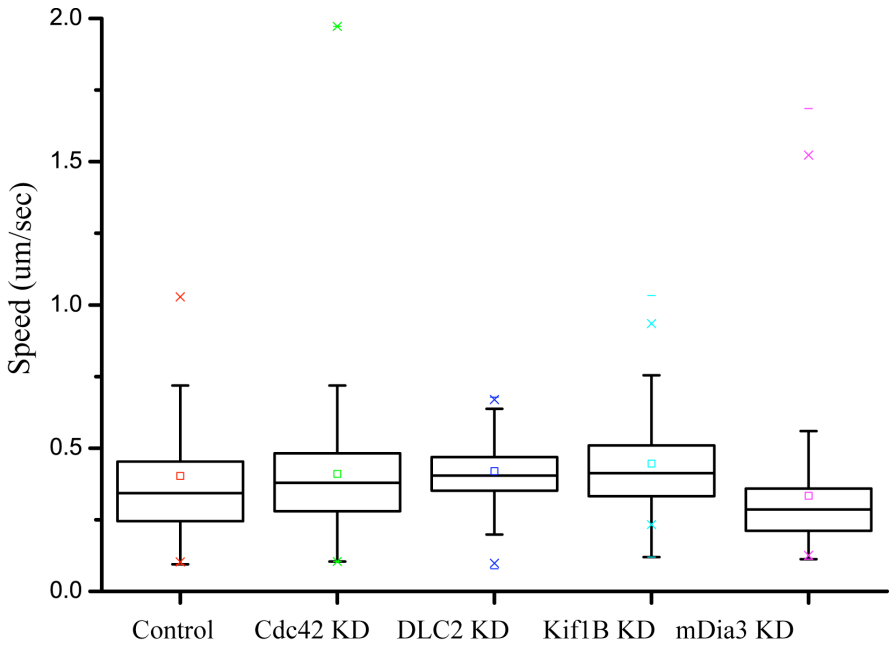

Figure 8.8 DLC2, Kif1B, Cdc42 and mDia3 depletion do not alter MT plus-end speed.

HeLa cells stably transfected with GFP-EB1 were filmed every 10''. From over 10 cells and 10 followed plus-ends per cell, speed of plus-ends was extracted and plotted in the chart. As shown, neither depletion of Cdc42 and mDia3 or DLC2 and Kif1B affected the overall speed of plus-end tips.

In charts where data are represented as box-whisker plots, the box size represents 75% of the population and the line inside the box represents the median of the sample. Maximum of the 75% (in the upper quartile) and the minimum of the 75% (in the lower quartile) values are represented by the size of the bars (whiskers). Over 100 plus ends were analyzed per condition. Watch videos Chapter8-Control-EB3, Chapter8-DLC2kd-EB3 Chapter8-Cdc42kd-EB3.

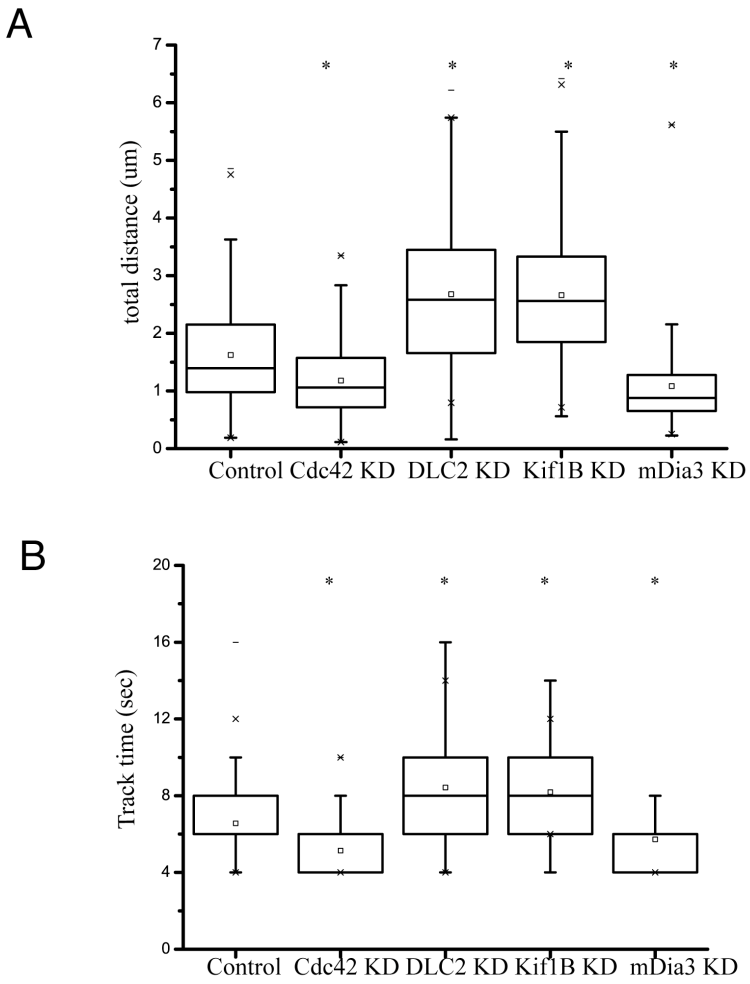

Figure 8.9 DLC2, Kif1B, Cdc42 and mDia3 depletion alter the track time and the distance MT plus-ends travel.

HeLa cells stably transfected with GFP-EB1 were filmed every 10''. From over 10 cells and 10 followed plus end per cell, total distance and total track time of plus-ends were extracted and plotted in the chart. As shown, Cdc42 and mDia3 depletion results in unstable plus-ends which underwent catastrophes after a shorter time compared with controls. On the contrary, DLC2 and Kif1B depletion result in longer growing plus end tips, able to travel for longer distances and times.

(A) Total distance chart

(B) Total track time

In charts where data are represented as box-whisker plots, the box size represents 75% of the population and the line inside the box represents the median of the sample. Maximum of the 75% (in the upper quartile) and the minimum of the 75% (in the lower quartile) values are represented by the size of the bars (whiskers). Over 100 plus ends were analyzed per condition.

Watch videos Chapter8-Control-EB3, Chapter8-DLC2kd-EB3 Chapter8-Cdc42kd-EB3.

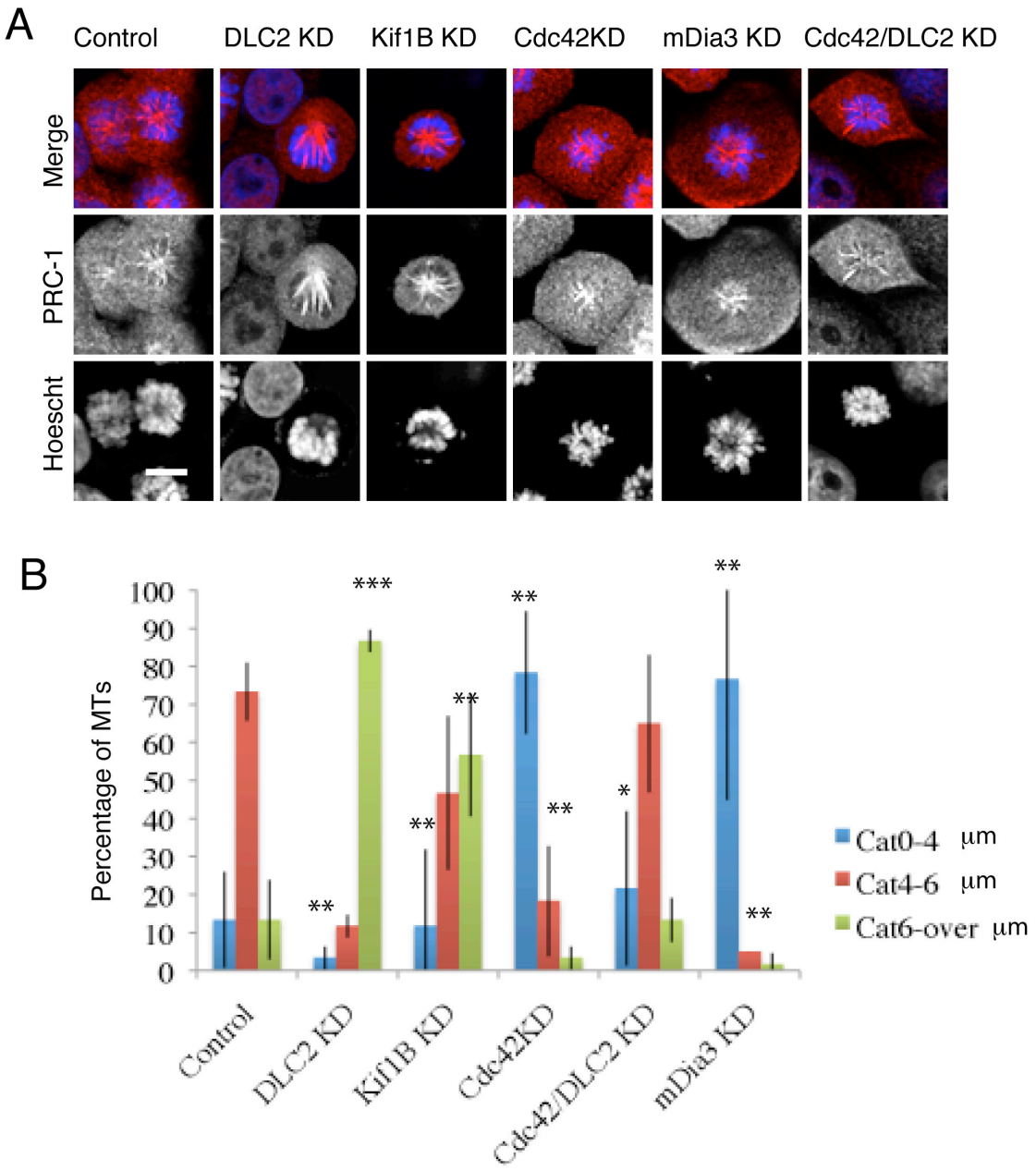

Figure 8.10 Astral MT length quantification

(A) Confocal pictures for monastrol treated control, DLC2, Kif1B, Cdc42, and mDia3 KD and Cdc42/DLC2 KD cells stained for Hoechst and PRC-1 (red). Bar represents 10µm

(B) Average chart for monastrol treated control, DLC2 KD and Kif1B KD, Cdc42 KD, mDia3 KD and Cdc42/DLC2 KD cells, showing the length of astral MTs.

* $p<0.05$ ** $p<0.01$ *** $p<0.001$ Shown are means and error bars represents standard deviations. Over 60 cells were counted per condition.

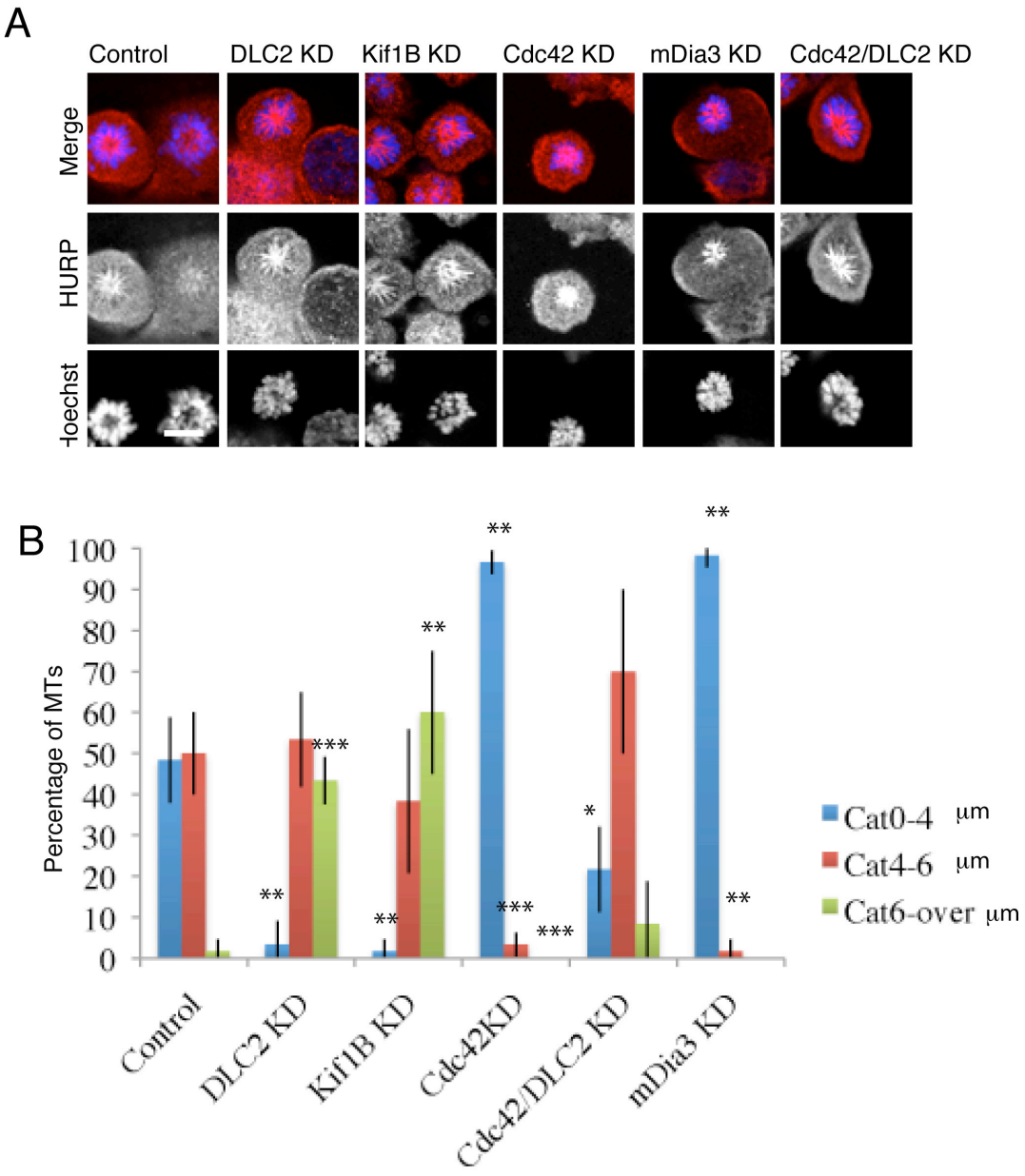

Figure 8.11 Kinetochore MTs length quantification

(A) Confocal pictures for monastrol treated control, DLC2, Kif1B, Cdc42, mDia3 and Cdc42/DLC2 KD cells stained for Hoechst and HURP (red). Bar represents 10μm

(B) Average chart for monastrol treated control, DLC2 KD and Kif1B KD, Cdc42 KD, mDia3 KD and Cdc42/DLC2 KD cells, showing the length of kinetochore MTs.

* $p<0.05$ ** $p<0.01$ *** $p<0.001$ Shown are means and error bars represents standard deviations. Over 60 cells were counted per condition.

8.5 DISCUSSION

I have shown in this chapter that unbalanced levels of active Cdc42 impairs MTs dynamics, resulting in the case of higher levels of active Cdc42 in hyperstability of MTs, and, in case of less active Cdc42, in MTs instability. It has been shown that growing/shrinking ratio is essential to ensure the proper kinetochore capture and alignment maintenance[186–188]. It seems that DLC2 pathway does not control the initial chromosome capture, but is essential for chromosome attachment maintenance in metaphase.

Depletion of DCL2 causes an increase in active Cdc42 and results in longer MTs. MT instability is intuitively connected to chromosome unattachment, as it is likely that short MTs cannot reach a kinetochore or stabilise a chromosome at the metaphase plate, also overgrowth triggers the same defect. However, MTs overgrowing also fail to attach and stabilse the metaphaseplate. This led to the formulation of a hypothesis that dictates a balance in MTs dynamics necessary for chromosome segregation efficiency[189]. This idea is discussed in details in Chapter 10, final discussion.

Considering that MT dynamics and chromosome capture is fundamental to ensure a correct chromosome distribution between the two daughter cells, I will discuss next the possibility that DLC2 depletion leads to aneuploidy. This idea was tested and will be presented in Chapter 9.

CHAPTER 9:
DLC2 AND KIF1B DEPLETION INDUCES ANEUPLOIDY

CHAPTER 9: DLC2 AND KIF1B DEPLETION INDUCES ANEUPLOIDY

9.1 Testing the aneuploidy hypothesis

Since its discovery and until today, DLC2 is known to act as a tumour suppressor, but no one has shown the molecular mechanism that explains why lack of DLC2 triggers tumour formation[104,136,190]. As I speculated in previous chapters (Chapter 6, discussion), one possibility could be onset of aneuploidy. Considering that DLC2 KD resulted in chromosome misattachment in metaphase because of MT overgrowth and taking into account that these cells are delayed in metaphase for almost the double of the time control cells take to progress to anaphase, induction of aneuploidy is possible and would explain how DLC2 might function as a tumour suppressor.

As DLC2 depleted cells spent more time in metaphase and failed in having all the chromosomes attached, these cells might finally escape from metaphase in a desperate attempt of surviving, without minding if chromosomes will be not parted equally.

To test this hypothesis, I performed an experiment to check aneuploidy in DLC2 and Kif1B KD cells versus control HCE cells. Taking advantage of the chromosome spread technique, I counted the number of chromosomes in mitotic cells and quantified them. As Figure 9.1 shows, the majority of DLC2 and Kif1B depletion cells contained less chromosomes than control cells, indicating that aneuploidy occurred upon depletion of DLC2 and Kif1B. Interestingly, not many cells with higher content of chromosomes were counted, suggesting that these cells most likely do not survive, or they loose chromosomes subsequently.

It is notorious that lack of DNA information is the cause of several neurological diseases, cardiac dysfunction, aging and cancer formation[191,192–194]. Here, I presented DLC2 as a major player in maintaining even chromosome number in cell division, which might underlie its pathological importance.

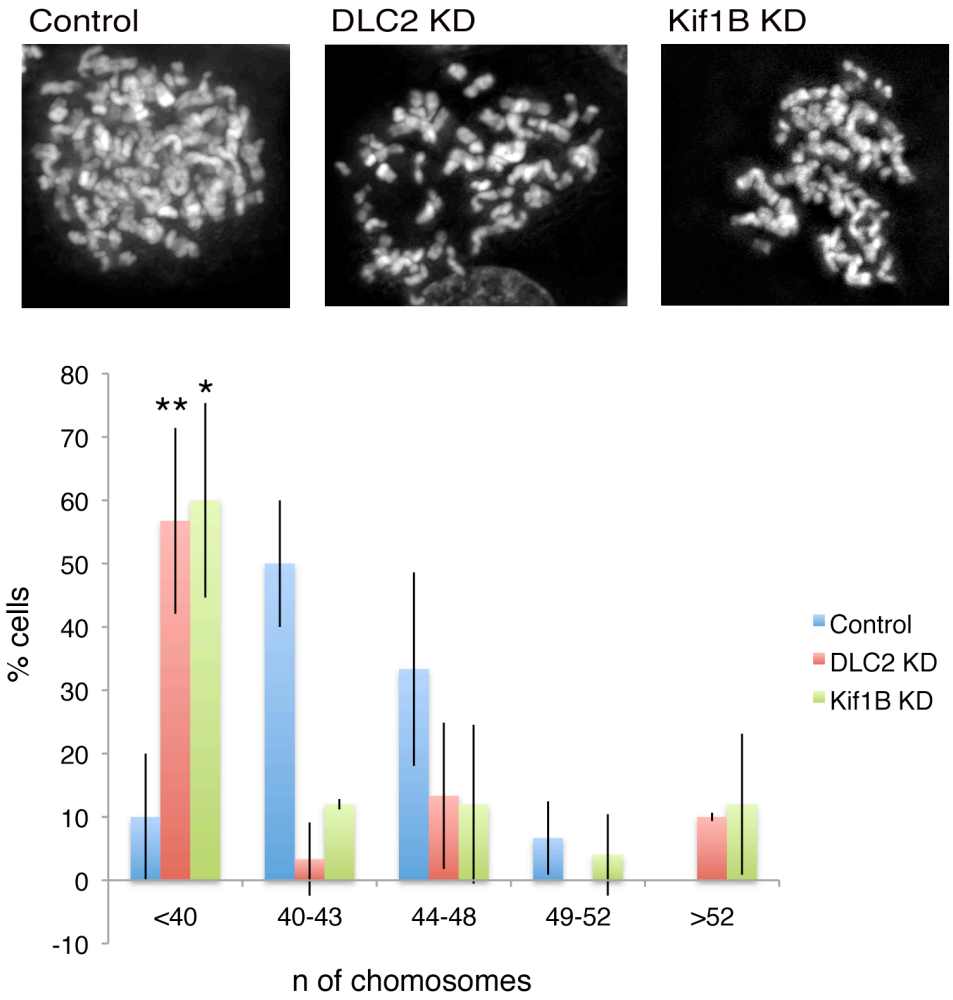

Figure 9.1 DLC2 and Kif1B depletion causes aneuploidy

Control and DLC2 or Kif1B KD HCE cells were analysed for chromosome numbers.

At the top are representative pictures of Control, DLC2 KD and Kif1B KD cells. The chart below represents percentage of cells with the indicated chromosome numbers.

Bars represent means +/- 1SD. * $p<0.05$ ** $p<0.01$. Over 20 cells per condition were counted. Experiment was repeated 3 times.

CHAPTER 10:
FINAL DISCUSSION

CHAPTER 10: FINAL DISCUSSION

10.1 Summary of data presented

In this thesis, I show data that shed light on the action of DLC2 as a tumour suppressor and its physiological role in epithelial cells. In the first three chapters of the results, I demonstrate that DLC2 is a Cdc42GAP involved in cell-cell junction and spindle stability and describe specific interactors of DLC2; in chapter 6, I describe in detail how DLC2 controls the length of mitosis and I introduced the concept that junction stability is a paramount factor for the satisfaction of the checkpoint in mitosis. Chapters 7 and 8 focus on Cdc42 and mDia3 as part of the DLC2 pathway in metapahse and how their regulation is important for correct cell division. Chapter 9 contains data that support the conclusion that the molecular mechanisms identified is potentially the one that underlying the tumour suppressor role of DLC2.

10.2 Epithelial integrity depends on both junction and spindle stability

In an epithelial sheet, mitosis and cell junction remodelling are two processes that must be orchestrated in parallel. In a simple epithelium, the main aim is to keep proliferating cells in the single layer. This can be achieved by the correct maintenance of cell-cell junctions that anchor the dividing cells to their neighbours; at the same time, junctions act as a platform that anchor astral microtubules, and stabilize orientation and positioning of the mitotic spindle. Only with the right balance of forces acting on the spindle can it split chromosomes equally into two daughters cells.

In animal cells, spindle position is fundamental because it determines the location of contractile ring assembly[195]. In fact, placing the spindle in the center of the cell will result in equal-size daughter cells, whereas positioning the spindle asymmetrically results in daughter cells of different sizes[196]. As an example, oocytes asymmetrically position the meiotic spindle to preserve most of the

cytoplasm in the egg in order to ensure all the specialized mRNA to be retained and support the initial stages of development.

The spindle positioning is controlled by astral microtubules by generating pulling forces at the cortex or pulling forces against the cytoplasm. Moreover, their attachment to the centrosomes is essential for the generation of pulling forces on the astral microtubules to move the spindle. During the years, some key molecules had been found controlling spindle positioning at the cell cortex: the most known one is dynein[197]. Dynein has been shown to captures astral MTs and pull them along the cell cortex. Later one it was discovered the NuMa-LGN-Giα complex that regulates dynein-dynactin pulling of the chromosomes in a polarized manner specifically in metaphase and in anaphase[198]. Another interesting player is F-actin. F-actin is required for cortical rigidity to prevent end-on microtubule contacts from pulling membrane tubules inward instead of moving the spindle pole outward[82,199].

Depletion of DLC2 affects both sides: junction stability and cortical actin behaviour on one hand, and spindle stability on the other. When I did the live imaging experiments, I could observe that more precisely DLC2 depletion affects the positioning of the mitotic spindle within the cell, which as a consequence, keeps spinning and rocking in the same planar plane. This is due to an aberrant behaviour of MT dynamics and their aberrant interaction with the cell cortex. As a result of this, actin polarity is perturbed and junctions are ripped off, destabilizing even more the whole system.

In accord with this observation, I have shown that DLC2 localizes along the MTs fibres (both astral and kinetochores MTs) and that it interacts with Kif1B and cell-cell junction components on the cortical side. In normal cells, Cdc42 can then be switched off by DLC2 and mitosis proceeds. The process is not stable, but highly dynamic and it is based on a fine equilibrium between levels of active and inactive Cdc42 (Figure 10.1). The correct balance of elements assures that MTs are attached at cell-cell junctions and at kinetochores, and that microtubules have the appropriate length.

When this mechanism is perturbed by DLC2 depletion, junctions are broken and MTs fibres have a different dynamic behaviour that leads to hyperstability and detachment from junctions and kinetochores. In this situation, Cdc42 is abnormally active (Figure 10.1). I described in the introduction the role of Cdc42 in junction stability and spindle orientation and the importance of its regulators. Although most papers mentioned discussed the effect of lack of active Cdc42 because of inactivation of specific GEFs or of KD of Cdc42 itself, here we

show that also the overactivation represents a danger for the cell and leads to destabilization of junctions and alters MTs dynamics. This is in agreement with previous work from our laboratory that demonstrated that the Cdc42 GAP SH3BP1, which forms a stable junction-associated complex, is required to contain junctional Cdc42 signalling and, thereby, maintain functional junctions in interphase cells (Elbediwy et al. 2012). As I will discuss in paragraph 10.4 in more detail, it is thus fundamental that not too high nor too low levels of active Cdc42 exist within a epithelial cell.

DLC2 is required for the maintenance of cell-cell junctions during mitosis and the stability of the metaphase plate. DLC2's main substrate during mitosis is Cdc42, which is supported by the observation that reduced expression of Cdc42 could rescue the DLC2 phenotype. A Cdc42 GAP that is selectively required during mitosis, but not in interphase cells, for junction maintenance had thus far not been identified. MgcRacGAP/CYK-4 had been shown to regulate Cdc42 during mitosis by expressing a dominant negative mutant that led to a prometaphase arrest[200]. However, unlike DLC2, depletion of MgcRacGAP/CYK-4 did not affect mitotic progression but caused a defect in cytokinesis[98]. The activity of Cdc42 peaks around metaphase and is then downregulated, which is required for mitotic progression[200]. Hence, DLC2 is required when Cdc42 activity starts to decline, further supporting its role as a major Cdc42 regulator during mitosis.

Interestingly, upon depletion of DLC2 Kif1B is mislocalized from the cell cortex, indicating that Kif1B plays a role downstream of DLC2. Such a downstream position in the pathway is also supported by the fact that upon depletion of Kif1B, DLC2 is not mislocalized.

For reasons that are still obscure, Kif1B helps stabilizing MT attachment and dynamics at the cell cortex and at the kinetochores. This is supported by the fact that depletion of Kif1B impairs MTs dynamics. How Kif1B does this, I can only speculate (10.6.)

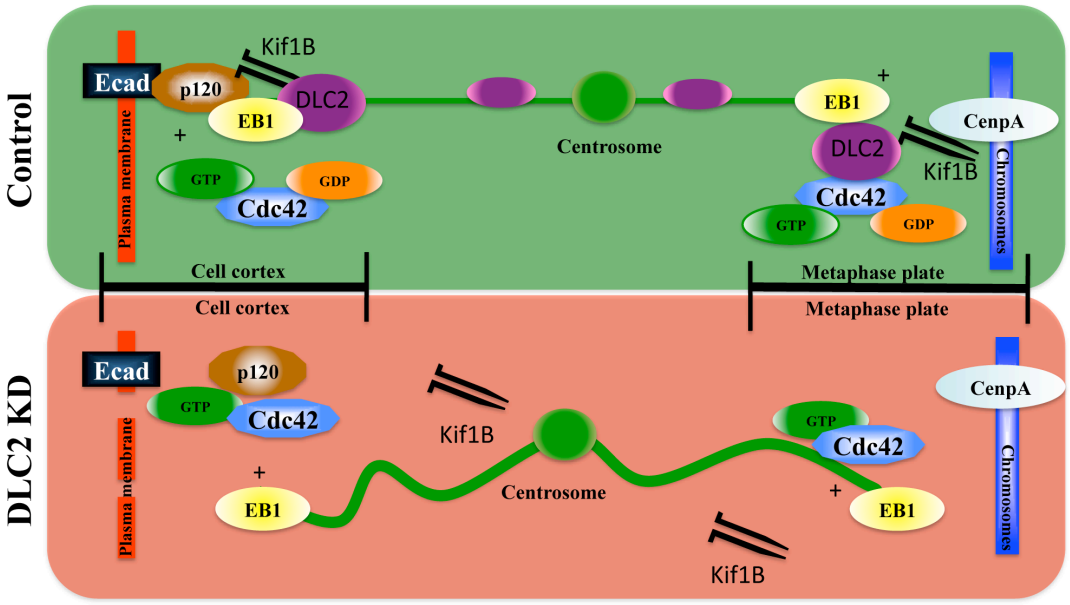

Figure 10.1 Model for DLC2 function

In normal cells, DLC2 specifically inactivates Cdc42 and regulates MT attachment at the cell cortex and at the kinetochores. Kif1B is recruited by DLC2 and helps MTs to be anchored at cell-cell junctions and at kinetochores. Upon depletion of DLC2, Kif1B is misplaced and MTs are not anchored on the junctional side (with broken junctions) and they are not properly attached at the kinetochore plate.

10.3 Are mDia3 and Kif1B mutually exclusive?

To complete the DLC2/Cdc42 pathway, I searched for an effector of Cdc42 that connects the aberrant MT behaviour and Cdc42. As I described in Chapter 7 of the results, mDia3 had been suggested to sit at the plus ends of MTs and stabilize them. Considering the hyperstable fibre phenotype I detected upon depletion of DLC2 and taking into account that DCL2 KD results in overactive Cdc42, mDia3 seemed the best candidate to fit into the picture.

Interestingly, mDia3 behaved in the opposite way of Kif1B: It localized to the cell cortex and kinetochores when Cdc42 was active. This let me think about the possibility that mDia3 and Kif1B could be mutually exclusive (Figure 10.2 A,B). A strong evidence that supports my idea is the result showing that in DLC2 KD cells, expression of an inactive form of Cdc42 rescues the cortical localisation of Kif1B and mDia3 is no longer recruited (Figure 10.3).

Since little is known about Kif1B, it is hard to speculate what the reason for this mutual exclusive localization is. It might be that they occupy the same site and

that this is dependent on Cdc42 activity. For instance, the activation of Cdc42 and its binding to mDia3 could lead to an increase of affinity of mDia3 for the site that Kif1B occupies. This would explain why Kif1B is mislocalized upon depletion of DLC2 and is brought back into place when Cdc42 DN is overexpressed in the cells.

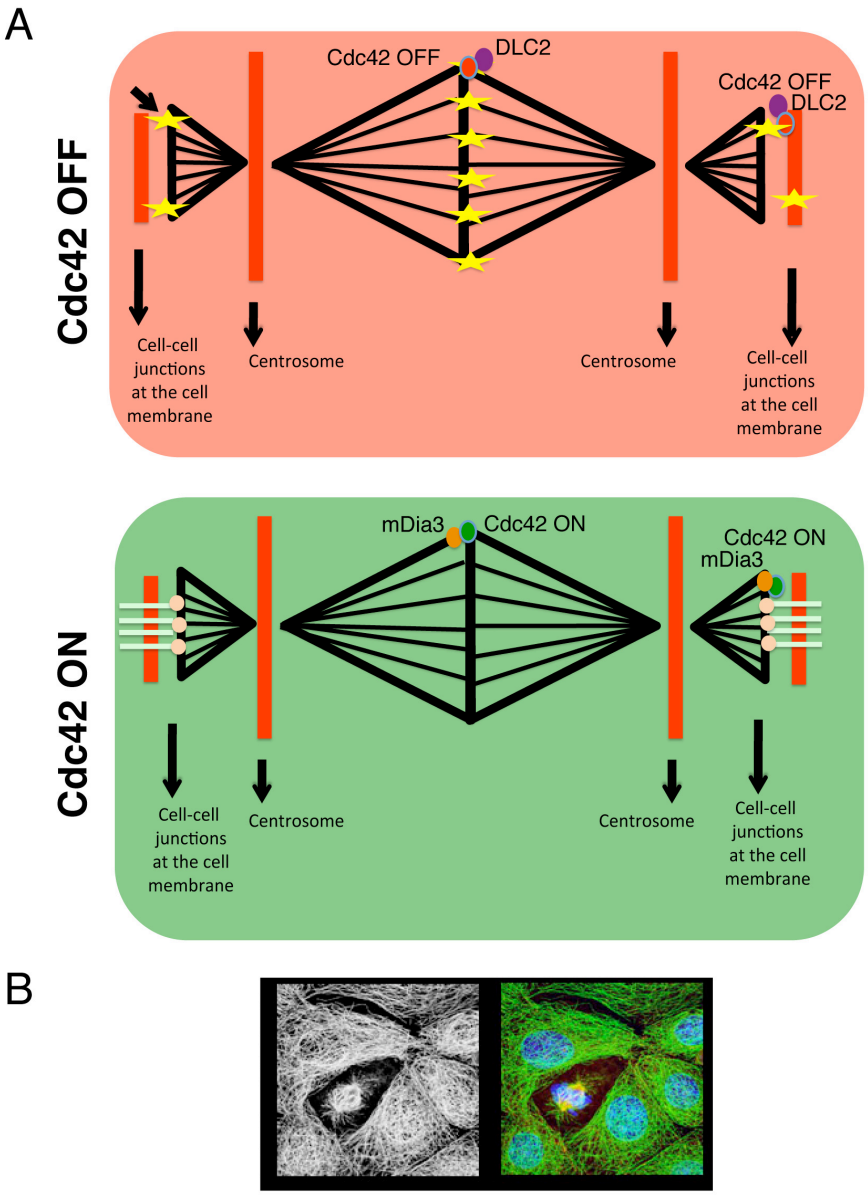

Figure 10.2 The alternation of mDia3 and Kif1B at sites that interact with the plus ends of MTs (control angle)

When the right balacance of Cdc42 is maintained, Cdc42 alternates between and active state (Cdc42 ON) and an inactive state (cdc42 OFF). Depending on the GTP-bound form, mDia3 is recruited at the cell cortex. In this situation, Kif1b is excluded from the plus ends of the MTs. Kif1B is represented by yellow stars.

(A) Schematic model of the Control situation

(B) Exemplar picture of Control HCE cell: in metaphase, the mitotic spindle (stained in green) is anchored at the cell-cell junctions and align all the chromosomes unto the metaphase plate.

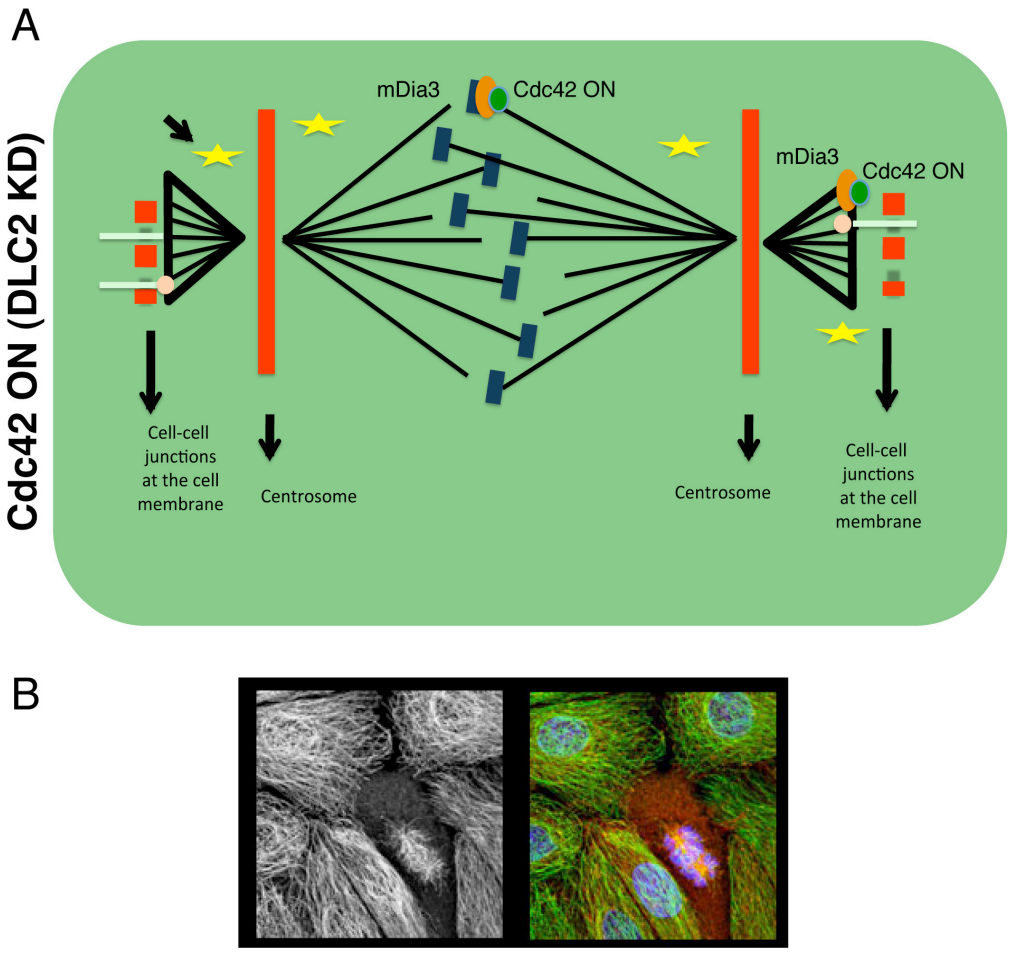

Figure 10.3 The alternation of mDia3 and Kif1B at the plus ends of MTs (DLC2 KD angle)
When DLC2 is depleted, mDia3 is recruited to sites that interact with the plus ends of MTs, due to the constant activation of Cdc42. Upon DLC2 depletion, Kif1b is mislocalized. Kif1B is represented by yellow stars.
(A) Schematic model of the DLC2 KD situation
(B) Example of DLC2 KD HCE cell: upon depletion of DLC2, the mitotic spindle (stained in green) is heavily distorted and unorganized, unable to align all the chromosomes unto the metaphase plate.

10.4 Too much or too less: it is always a matter of balance

In Chapter 8, I described how DLC2/Kif1B and Cdc42/mDia3 regulate in an opposing fashion the dynamics of MTs: depletion of DLC2 and Kif1B induces hyperstabylization of MTs, whereas Cdc42 and mDia3 KD leads to MT instability. Both situations alter the mitotic spindle so that the check-point for entry into anaphase is delayed, to ensure that chromosomes will be segregated correctly despite the abnormal MT dynamics,.

The mitotic spindle structure is not stiff, but dynamic and continuously evolving. Microtubules undergo phases of catastrophe and growth, which is at a particularly high-rate at the plus ends. Considering that the turnover is stable in the spindle (the half-life is ~7 min of k-MT), the growth and shrinkage rates of astral microtubules is about 10–15 μm/min[152]. Moreover a number of forces exerted at the membrane on astral microtubules must be taken into account: motor proteins such as dynein and some kinesins (kinesin 1 family members) catch astral microtubules and pull them at the cell cortex[201,202].

Comparing the mitotic apparatus to a suspension bridge for convenience, it is possible to elucidate this intricate mechanism of forces acting on the structure. As in a bridge, there is a platform part suspended (spindle and chromosomes), the anchoring part (astral MTs) coupled to a pair of pillars (cell-cell junctions and centrosome) on each edge (membrane). When forces are act on the bridge through, for example, motor proteins pulling or remodelling of junctions, the bridge oscillates and buffers this energy, unloading it onto the pillars (membrane and centrosomes)[148,203]. There is a tolerance threshold, a limit under which oscillations occur safely and beyond which the structure collapses. DLC2 regulation is responsible for junctional maintenance in metaphase through Cdc42 deactivation and localizes Kinesin 1B (Kif1B) at the cell cortex (Figure 10.4 A). If DLC2 is depleted, Kif1B is delocalized from the membrane, and mDia3 is recruited by active Cdc42, hyperstabilizes MTs, and, finally, junctions start to dissociate. All these uncontrolled movements at the cortex affect MTs within the spindle as well, leading to MT dissociation from kinetochores (Figure 10.4 B).

It is striking that the opposite phenotype caused by depletion of mDia3 and Cdc42 induces the same kind of delay in metaphase, but in this case the reason is instability of MTs (Figure 10.4 B). In a situation of unstable MTs, the astral MTs are not able to reach and be anchored properly at the cell cortex. This leads to

excessive spindle movements and, once again, defects in passing the mitotic check-point.

In 2012, Bakhoum and Compton proposed a model of MTs dynamics that sees both instability and hyperstability as important factors in the control of the mitotic timing and the success of cell division. Quoting, "*Hypostable kMT attachments fails to adequately satisfy the spindle assembly checkpoint leading to mitotic delay or arrest. Hyperstable kMT attachments lose efficient error correction with the consequence being the persistence of attachment errors in anaphase and an increase in chromosome mis-segregation leading to chromosomal instability (CIN)*"[189,204]. The importance of having correct MTs dynamics within a cell is also highlighted by the number of tumours caused by mutations that affect genes that hyperstabilize MTs, such as the overexpressed CenpH, Cyclin E, Hec1/Ndc80 complex, and MCT-1, or the mutated, deleted or underexpressed APC, β-catenin, pRB, and BRCA1[205–209].

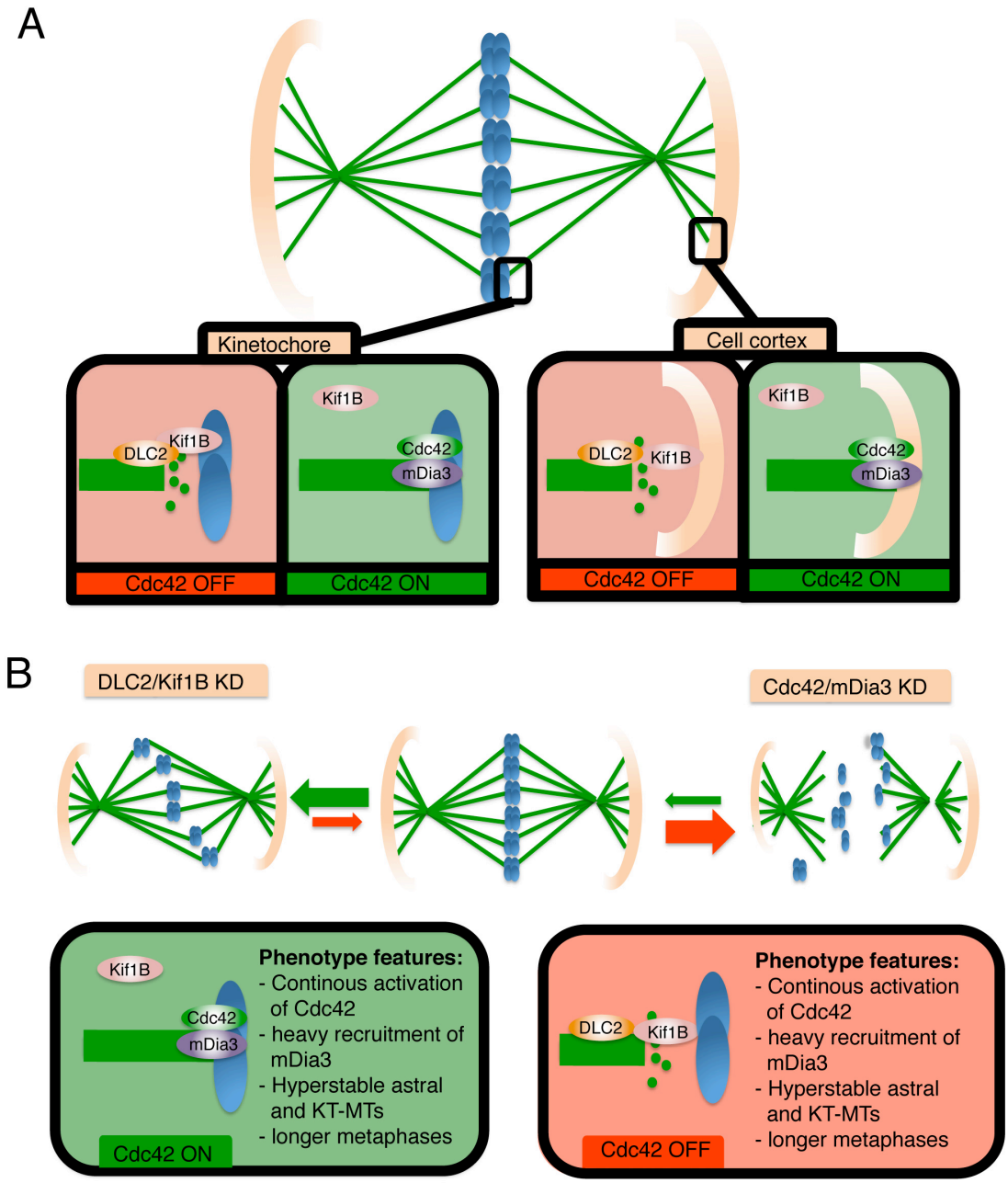

Figure 10.4 Balance is all that matters

(A) The proposed mechanism acts both at cell cortex and at the kinetochores. The cartoon shows that to keep epithelial integrity it is necessary to balance between negative regulation of Cdc42 and its activation and signalling via mDia3.

(B) Phenotype features of Cdc42 KD (right side of he picture) and DLC2 KD (left side).

10.5 The paradigm of focal adhesion

Several papers have shown previously that DLC2 as the other DLCs is localized at focal adhesions. I have never detected this in HCE or HeLa cells using immunofluorescence. It could be that this difference is caused by the difference in the system used. Most of my experiments were done with differentiated epithelial cells that had not previously been studied for DLC2. Many focal adhesion proteins associate with cell-cell junctions in differentiated epithelial cells, which may contribute to the difference in localisation.

Interestingly, in a Hepatocarcinoma cell line (HepG2 cells) it has been reported that expression of DLC2 leads to a block in in G1/S phase progression[135]. This evidence supports the idea of DLC2 as a tumour suppressor that acts directly on the length of the cell cycle and regulates its progression. Hence, DLC2 might regulate different steps along the cell cycle.

10.6 More can be done: open questions and future perspectives

One key element for a more complete comprehension of the role of DLC2 in physiological and abnormal conditions would be to understand how DLC2 is regulated. I showed that DLC2 is not regulated on the expression level during mitosis. Hence, it might be regulated by a posttranslational modification, such as phosphorylation. It has been described previously that Akt phosphorylates DLC2[210]. Phosphorylation of DLC1 by Akt has been shown to be essential for in activation of the tumour suppressor activity, since abrogation of the Akt specific-phospho site on DLC1 dramatically suppressed cell growth and anchorage-independent growth. Akt has been reported as a regulator of cell cycle. In particular, it positively regulates G1/S transition via inactivation of GSK3-β, which results in an increase in Cyclin-D1 expression[211]. In 2005, Lee et al advanced the hypothesis that Akt could also work as a regulator of G2/M. DLC2 phosphorylation by Akt has not been characterized in a context of mitosis, but it would be interesting to know if it is an activating or inactivating one, and to determine the effect on cell cycle progression.

Poorly characterized are also two of the domains within the protein: the START domain and the SAM domain. As previously mentioned, it was shown by Lee et al that DLC2 isoform γ induces arrest in cell cycle. Isoform γ lacks the N-

terminus part of the protein containing the SAM domain. I discussed in the introduction how the SAM domain is responsible for protein-protein interactions and if we connect this to the phenotype derived from the transfection of the truncated portion, we can speculate that the SAM domain is essential for the correct regulation of DCL2 in mitosis, since its lack causes an arrest in the cell cycle. I must point out, however, that the arrest discussed by Lee is in G1/S progression and not during mitosis. Nevertheless, taking all the information into count, it might be that a specific interaction via the SAM domain is required for Dlc2 function in mitosis

A captivating idea is that the START domain is involved in the regulation of DLC2 activity in a new way. I presented in the introduction the peculiarity of the DLC2 START domain: In contrast to other START domains, the one of DLC2 lacks what would be the third helix of a canonical, five helix motif. This is proposed to be important for the binding of bigger molecules in the pocket. In particular, it has been proposed that glucocorticoics could bind the DLC2 START domain. It is remarkable that the START domain is contained exclusively in the DLC proteins and not in any other GAPs identified in the human genome. This could suggest a unique modulation of DLC protein activity through the START domain. It would be intriguing to test the hypothesis that an external signal, such as glucocorticoids, could actually act directly on DLC2 and regulate its activity and its effect on the cell cycle.

Although this study depicted the mechanism of action of DLC2, I still have not explained what the exact role of Kif1B is. Kif1B is a poorly investigated kinesin, belonging to the family 3. Despite none of the family 3 members having been associated with depolymerising activity, there are no reasons to exclude that Kif1B has a depolymerising activity[212]. An alternative possibility would be that Kif1B orchestrates indirectly depolymerization. This idea is supported by the evidence that depletion of Kif1B results in longer MTs.

Bibliography

1. Coradini, D., Casarsa, C. & Oriana, S. Epithelial cell polarity and tumorigenesis: new perspectives for cancer detection and treatment. *Acta Pharmacol. Sin.* **32,** 552–64 (2011).
2. Royer, C. & Lu, X. Epithelial cell polarity: a major gatekeeper against cancer? *Cell Death Differ.* **18,** 1470–7 (2011).
3. McCaffrey, L. M. & Macara, I. G. Epithelial organization, cell polarity and tumorigenesis. *Trends Cell Biol.* **21,** 727–35 (2011).
4. Matter, K. & Balda, M. S. Signalling to and from tight junctions. *Nat. Rev. Mol. Cell Biol.* **4,** 225–36 (2003).
5. Farquhar, M. G. & Palade, G. E. Junctional complexes in various epithelia. *J. Cell Biol.* **17,** 375–412 (1963).
6. Aijaz, S., Balda, M. S. & Matter, K. Tight junctions: molecular architecture and function. *Int. Rev. Cytol.* **248,** 261–298 (2006).
7. Tsukita, S. & Furuse, M. Occludin and claudins in strands : leading or supporting players ? **9,** 87–92 (1999).
8. Van Itallie, C. M. & Anderson, J. M. Claudins and epithelial paracellular transport. *Annu. Rev. Physiol.* **68,** 403–29 (2006).
9. Balda, M. S. & Matter, K. Tight junctions at a glance. *J. Cell Sci.* **121,** 3677–82 (2008).
10. Matter, K., Aijaz, S., Tsapara, A. & Balda, M. S. Mammalian tight junctions in the regulation of epithelial differentiation and proliferation. *Curr. Opin. Cell Biol.* **17,** 453–8 (2005).
11. Balda, M. Epithelial cell adhesion and the regulation of gene expression. *Trends Cell Biol.* **13,** 310–318 (2003).
12. Dhawan, P. *et al.* Claudin-1 regulates cellular transformation and metastatic behavior in colon cancer. *J. Clin. Invest.* **115,** 1765–1776 (2005).
13. Tiwari-Woodruff, S. K. *et al.* OSP/claudin-11 forms a complex with a novel member of the tetraspanin super family and beta1 integrin and regulates proliferation and migration of oligodendrocytes. *J. Cell Biol.* **153,** 295–305 (2001).
14. Martin, T. A., Watkins, G., Mansel, R. E. & Jiang, W. G. Loss of tight junction plaque molecules in breast cancer tissues is associated with a poor prognosis in patients with breast cancer. *Eur. J. Cancer* **40,** 2717–2725 (2004).
15. Arakawa, Y. Y. *et al.* Transcription of dbpA, a Y box binding protein, is positively regulated by E2F1: implications in hepatocarcinogenesis. *Biochem. Biophys. Res. Commun.* **322,** 297–302 (2004).
16. Jamora, C. & Fuchs, E. Intercellular adhesion, signalling and the cytoskeleton. *Nat. Cell Biol.* **4,** E101–8 (2002).
17. Hartsock, A. & Nelson, W. J. Adherens and Tight Junctions: Structure, Function and Connections to the Actin Cytoskeleton. *Biochim Biophys Acta* **1778,** 660–669 (2009).
18. Drees, F., Pokutta, S., Yamada, S., Nelson, W. J. & Weis, W. I. α-Catenin Is a Molecular Switch that Binds E-Cadherin-β-Catenin and Regulates Actin-Filament Assembly. *Cell* **123,** 903–915 (2005).
19. Drees, F., Pokutta, S., Yamada, S., Nelson, W. J. & William, I. Catenin Is a Molecular Switch that Binds E-Cadherin-β-Catenin and Regulates Actin-Filament Assembly. *Cell* **123,** 903–915 (2005).
20. Brembeck, F. H. *et al.* Essential role of BCL9-2 in the switch between β-catenin's adhesive and transcriptional functions. *Genes Dev.* **18,** 2225–2230 (2004).
21. Berx, G. & Van Roy, F. The E-cadherin/catenin complex: an important gatekeeper in breast cancer tumorigenesis and malignant progression. *Breast Cancer Res.* **3,** 289–93 (2001).
22. Ichii, T. & Takeichi, M. P120-Catenin Regulates Microtubule Dynamics and Cell Migration in a Cadherin-Independent Manner. *Genes Cells* **12,** 827–39 (2007).
23. Rikitake, Y., Mandai, K. & Takai, Y. The role of nectins in different types of cell-cell adhesion. *J. Cell Sci.* **125,** 3713–22 (2012).
24. Brooke, M. a, Nitoiu, D. & Kelsell, D. P. Cell-cell connectivity: desmosomes and disease. *J. Pathol.* **226,** 158–71 (2012).
25. Thomason, H. a, Scothern, A., McHarg, S. & Garrod, D. R. Desmosomes: adhesive strength and signalling in health and disease. *Biochem. J.* **429,** 419–33 (2010).
26. Garrod, D. R., Berika, M. Y., Bardsley, W. F., Holmes, D. & Tabernero, L. Hyper-adhesion in desmosomes: its regulation in wound healing and possible relationship to cadherin crystal structure. *J. Cell Sci.* **118,** 5743–54 (2005).
27. Dusek, R. L. & Attardi, L. D. Desmosomes: new perpetrators in tumour suppression. *Nat. Rev. Cancer* **11,** 317–23 (2011).
28. Martin-Belmonte, F. & Perez-Moreno, M. Epithelial cell polarity, stem cells and cancer. *Nat. Rev. Cancer* **12,** 23–38 (2012).
29. Baum, B. & Georgiou, M. Dynamics of adherens junctions in epithelial establishment, maintenance, and remodeling. *J. Cell Biol.* **192,** 907–17 (2011).

30. Ladoux, B. *et al*. Strength dependence of cadherin-mediated adhesions. *Biophys. J.* **98,** 534–42 (2010).
31. Shewan, A. M. *et al*. Myosin 2 is a key Rho kinase target necessary for the local concentration of E-cadherin at cell-cell contacts. *Mol. Biol. Cell* **16,** 4531–42 (2005).
32. Yamada, S. & Nelson, W. J. Localized zones of Rho and Rac activities drive initiation and expansion of epithelial cell-cell adhesion. *J. Cell Biol.* **178,** 517–27 (2007).
33. Liu, Z. *et al*. Mechanical tugging force regulates the size of cell-cell junctions. *Proc. Natl. Acad. Sci. U. S. A.* **107,** 9944–9 (2010).
34. Sawyer, J. K. *et al*. A contractile actomyosin network linked to adherens junctions by Canoe/afadin helps drive convergent extension. *Mol. Biol. Cell* **22,** 2491–508 (2011).
35. Harris, T. J. C., Sawyer, J. K. & Peifer, M. How the cytoskeleton helps build the embryonic body plan: models of morphogenesis from Drosophila. *Curr. Top. Dev. Biol.* **89,** 55–85 (2009).
36. Martin, A. C., Kaschube, M. & Wieschaus, E. F. Pulsed contractions of an actin-myosin network drive apical constriction. *Nature* **457,** 495–9 (2009).
37. Dawes-Hoang, R. E. *et al*. folded gastrulation, cell shape change and the control of myosin localization. *Development* **132,** 4165–78 (2005).
38. Solon, J., Kaya-Copur, A., Colombelli, J. & Brunner, D. Pulsed forces timed by a ratchet-like mechanism drive directed tissue movement during dorsal closure. *Cell* **137,** 1331–42 (2009).
39. Jaffe, A. B. & Hall, A. Rho GTPases: biochemistry and biology. *Annu. Rev. Cell Dev. Biol.* **21,** 247–69 (2005).
40. Boguski, M. S. & McCormick, F. Proteins regulating Ras and its relatives. *Nature* **366,** 643–654 (1993).
41. Samarin, S. & Nusdrat, A. Regulation of epithelial apical junctional complex by Rho family GTPases. *Front. Biosci.* **14,** 1129–1142 (2009).
42. Cherfils, J. & Chardin, P. GEFs: structural basis for their activation of small GTP-binding proteins. *Trends Biochem. Sci.* **24,** 306–11 (1999).
43. Lamarche, N. & Hall, A. GAPs for rho-related GTPases. *Trends Genet.* **10,** 436–440 (1994).
44. Bishop, a L. & Hall, a. Rho GTPases and their effector proteins. *Biochem. J.* **348 Pt 2,** 241–55 (2000).
45. Etienne-Manneville, S. & Hall, A. Rho GTPases in cell biology. *Nature* **420,** 629–35 (2002).
46. Balda, M. S. *et al*. Assembly and sealing of tight junctions: possible participation of G-proteins, phospholipase C, protein kinase C and calmodulin. *J. Membr. Biol.* **122,** 193–202 (1991).
47. Otani, T., Ichii, T., Aono, S. & Takeichi, M. Cdc42 GEF Tuba regulates the junctional configuration of simple epithelial cells. *J. Cell Biol.* **175,** 135–146 (2006).
48. Benais-Pont, G. *et al*. Identification of a tight junction-associated guanine nucleotide exchange factor that activates Rho and regulates paracellular permeability. *J. Cell Biol.* **160,** 729–740 (2003).
49. Aijaz, S., D'Atri, F., Citi, S., Balda, M. S. & Matter, K. Binding of GEF-H1 to the tight junction-associated adaptor cingulin results in inhibition of Rho signaling and G1/S phase transition. *Dev. Cell* **8,** 777–86 (2005).
50. Guillemot, L., Paschoud, S., Jond, L., Foglia, A. & Citi, S. Paracingulin regulates the activity of Rac1 and RhoA GTPases by recruiting Tiam1 and GEF-H1 to epithelial junctions. *Mol. Biol. Cell* **19,** 4442–4453 (2008).
51. Krendel, M., Zenke, F. T. & Bokoch, G. M. Nucleotide exchange factor GEF-H1 mediates cross-talk between microtubules and the actin cytoskeleton. *Nat. Cell Biol.* **4,** 294–301 (2002).
52. Ren, Y. Cloning and Characterization of GEF-H1, a Microtubule-associated Guanine Nucleotide Exchange Factor for Rac and Rho GTPases. *J. Biol. Chem.* **273,** 34954–34960 (1998).
53. Terry, S. J. *et al*. Spatially restricted activation of RhoA signalling at epithelial junctions by p114RhoGEF drives junction formation and morphogenesis. *Nat. Cell Biol.* **13,** 159–166 (2011).
54. Elbediwy, A. *et al*. Epithelial junction formation requires confinement of Cdc42 activity by a novel SH3BP1 complex. *J. Cell Biol.* **198,** 677–93 (2012).
55. Yano, T. *et al*. Tara up-regulates E-cadherin transcription by binding to the Trio RhoGEF and inhibiting Rac signaling. *J. Cell Biol.* **193,** 319–32 (2011).
56. Kashef, J. *et al*. Cadherin-11 regulates protrusive activity in Xenopus cranial neural crest cells upstream of Trio and the small GTPases. *Genes Dev.* **23,** 1393–8 (2009).
57. Wallace, S. W., Durgan, J., Jin, D. & Hall, A. Cdc42 Regulates Apical Junction Formation in Human Bronchial Epithelial Cells through PAK4 and Par6B. *Mol. Biol. Cell* **21,** 2996–3006 (2010).
58. Vega, F. M. & Ridley, A. J. Rho GTPases in cancer cell biology. *FEBS Lett.* **582,** 2093–101 (2008).
59. Perona, R. *et al*. Tumorigenic activity of rho genes from Aplysia californica. *Oncogene* **8,** 1285–1292 (1993).
60. Del Peso, L. *et al*. Rho proteins induce metastatic properties in vivo. *Oncogene* **15,** 3047–3057 (1997).

61. Hoffman, G. R. & Cerione, R. A. Signaling to the Rho GTPases: networking with the DH domain. *FEBS Lett*. **513,** 85–91 (2002).
62. Yuan, B. Z. *et al*. Cloning, characterization, and chromosomal localization of a gene frequently deleted in human liver cancer (DLC-1) homologous to rat RhoGAP. *Cancer Res*. **58,** 2196–2199 (1998).
63. Fritz, G., Just, I. & Kaina, B. Rho GTPases are over-expressed in human tumors. *Int. J. cancer J. Int. du cancer* **81,** 682–687 (1999).
64. Van Hengel, J. *et al*. Continuous cell injury promotes hepatic tumorigenesis in cdc42-deficient mouse liver. *Gastroenterology* **134,** 781–792 (2008).
65. Cunliffe, H. E., Jiang, Y., Fornace, K. M., Yang, F. & Meltzer, P. S. PAR6B is required for tight junction formation and activated PKCz localization in breast cancer. *Am J Cancer Res* **2,** 478–491 (2012).
66. Fields, A. P. & Regala, R. P. Protein kinase C iota: human oncogene, prognostic marker and therapeutic target. *Pharmacol. Res. Off. J. Ital. Pharmacol. Soc*. **55,** 487–497 (2007).
67. Zen, K. *et al*. Defective expression of polarity protein PAR-3 gene (PARD3) in esophageal squamous cell carcinoma. *Oncogene* **28,** 2910–2918 (2009).
68. Sugihara, K. *et al*. Rac1 is required for the formation of three germ layers during gastrulation. *Oncogene* **17,** 3427–3433 (1998).
69. Kissil, J. L. *et al*. Requirement for Rac1 in a K-ras induced lung cancer in the mouse. *Cancer Res*. **67,** 8089–8094 (2007).
70. Malliri, A. *et al*. Mice deficient in the Rac activator Tiam1 are resistant to Ras-induced skin tumours. *Nature* **417,** 867–871 (2002).
71. Blanpain, C., Horsley, V. & Fuchs, E. Epithelial Stem Cells: Turning over New Leaves. *Cell* **128,** 445–458 (2007).
72. Huttner, W. B. & Brand, M. Asymmetric division and polarity of neuroepithelial cells. *Curr. Opin. Neurobiol*. **7,** 29–39 (1997).
73. Bolhy, S. *et al*. A Nup133-dependent NPC-anchored network tethers centrosomes to the nuclear envelope in prophase. *J. Cell Biol*. **192,** 855–71 (2011).
74. Lénárt, P. *et al*. A contractile nuclear actin network drives chromosome congression in oocytes. *Nature* **436,** 812–8 (2005).
75. Foley, E. a & Kapoor, T. M. Microtubule attachment and spindle assembly checkpoint signalling at the kinetochore. *Nat. Rev. Mol. Cell Biol*. **14,** 25–37 (2013).
76. Elzen, N. Den, Buttery, C. V, Maddugoda, M. P., Ren, G. & Yap, A. S. Cadherin Adhesion Receptors Orient the Mitotic Spindle during Symmetric Cell Division in Mammalian Epithelia. *Mol Biol Cell* **20,** 3740–3750 (2009).
77. Durgan, J., Kaji, N., Jin, D. & Hall, A. Par6B and atypical PKC regulate mitotic spindle orientation during epithelial morphogenesis. *J. Biol. Chem*. **286,** 12461–74 (2011).
78. Hao, Y. *et al*. Par3 controls epithelial spindle orientation by aPKC-mediated phosphorylation of apical Pins. *Curr. Biol*. **20,** 1809–1818 (2010).
79. McCartney, B. M. *et al*. Drosophila APC2 and Armadillo participate in tethering mitotic spindles to cortical actin. *Nat. Cell Biol*. **3,** 933–938 (2001).
80. Caldwell, C. M. & Kaplan, K. B. The role of APC in mitosis and in chromosome instability. *Adv. Exp. Med. Biol*. **656,** 51–64 (2009).
81. Baker, J. & Garrod, D. Epithelial cells retain junctions during mitosis. *J. Cell Sci*. **104,** 415–25 (1993).
82. Kunda, P. & Baum, B. The actin cytoskeleton in spindle assembly and positioning. *Trends Cell Biol*. **19,** 174–9 (2009).
83. Legoff, L., Rouault, H. & Lecuit, T. A global pattern of mechanical stress polarizes cell divisions and cell shape in the growing Drosophila wing disc. *Development* **140,** 4051–9 (2013).
84. Guillot, C. & Lecuit, T. Adhesion disengagement uncouples intrinsic and extrinsic forces to drive cytokinesis in epithelial tissues. *Dev. Cell* **24,** 227–41 (2013).
85. Levayer, R. & Lecuit, T. Oscillation and polarity of E-cadherin asymmetries control actomyosin flow patterns during morphogenesis. *Dev. Cell* **26,** 162–75 (2013).
86. Herszterg, S., Leibfried, A., Bosveld, F., Martin, C. & Bellaiche, Y. Interplay between the dividing cell and its neighbors regulates adherens junction formation during cytokinesis in epithelial tissue. *Dev. Cell* **24,** 256–70 (2013).
87. Jauffred, B. *et al*. Regulation of centrosome movements by numb and the collapsin response mediator protein during Drosophila sensory progenitor asymmetric division. *Development* **140,** 2657–68 (2013).
88. Villalonga, P. & Ridley, A. J. Rho GTPases and cell cycle control. *Growth factors Chur Switz*. **24,** 159–164 (2006).

89. Hanashiro, K., Brancaccio, M. & Fukasawa, K. Activated ROCK II by-passes the requirement of the CDK2 activity for centrosome duplication and amplification. *Oncogene* **30,** 2188–2197 (2011).
90. Kanai, M., Crowe, M. S., Zheng, Y., Vande Woude, G. F. & Fukasawa, K. RhoA and RhoC are both required for the ROCK II-dependent promotion of centrosome duplication. *Oncogene* **29,** 6040–6050 (2010).
91. Maddox, A. S. & Burridge, K. RhoA is required for cortical retraction and rigidity during mitotic cell rounding. *J. Cell Biol.* **160,** 255–265 (2003).
92. Vasiliev, J. M., Omelchenko, T., Gelfand, I. M., Feder, H. H. & Bonder, E. M. Rho overexpression leads to mitosis-associated detachment of cells from epithelial sheets: a link to the mechanism of cancer dissemination. *Proc. Natl. Acad. Sci. U. S. A.* **101,** 12526–12530 (2004).
93. Bakal, C. J. *et al.* The Rho GTP exchange factor Lfc promotes spindle assembly in early mitosis. *Proc. Natl. Acad. Sci. U. S. A.* **102,** 9529–9534 (2005).
94. Guo, Y., Cheng, L., Ahmad, S. & Mao, Y. Formin mDia3: A novel target for Aurora B kinase. *Bioarchitecture* **1,** 88–90 (2011).
95. Cheng, L. & Mao, Y. mDia3-EB1-APC: A connection between kinetochores and microtubule plus ends. *Commun. Integr. Biol.* **4,** 480–2 (2011).
96. Yasuda, S. *et al.* Cdc42 and mDia3 regulate microtubule attachment to kinetochores. *Nature* **428,** 767–771 (2004).
97. Ban, R., Irino, Y., Fukami, K. & Tanaka, H. Human mitotic spindle-associated protein PRC1 inhibits MgcRacGAP activity toward Cdc42 during the metaphase. *J. Biol. Chem.* **279,** 16394–16402 (2004).
98. Yüce, Ö., Piekny, A. & Glotzer, M. An ECT2–centralspindlin complex regulates the localization and function of RhoA. *J. Cell Biol.* **170,** 571–582 (2005).
99. Nishimura, Y. & Yonemura, S. Centralspindlin regulates ECT2 and RhoA accumulation at the equatorial cortex during cytokinesis. *J. Cell Sci.* **119,** 104–114 (2006).
100. Petronczki, M., Glotzer, M., Kraut, N. & Peters, J.-M. Polo-like kinase 1 triggers the initiation of cytokinesis in human cells by promoting recruitment of the RhoGEF Ect2 to the central spindle. *Dev. Cell* **12,** 713–25 (2007).
101. Wolfe, B. A., Takaki, T., Petronczki, M. & Glotzer, M. Polo-Like Kinase 1 Directs Assembly of the HsCyk-4 RhoGAP/Ect2 RhoGEF Complex to Initiate Cleavage Furrow Formation. *PLoS Biol.* **7,** 15 (2009).
102. Hirose, K., Kawashima, T., Iwamoto, I., Nosaka, T. & Kitamura, T. MgcRacGAP is involved in cytokinesis through associating with mitotic spindle and midbody. *J. Biol. Chem.* **276,** 5821–5828 (2001).
103. Homma, Y. & Emori, Y. A dual functional signal mediator showing RhoGAP and phospholipase C-delta stimulating activities. *Eur. Mol. Biol. Organ. J.* **14,** 286–291 (1995).
104. Ching, Y.-P. *et al.* Deleted in liver cancer (DLC) 2 encodes a RhoGAP protein with growth suppressor function and is underexpressed in hepatocellular carcinoma. *J. Biol. Chem.* **278,** 10824–10830 (2003).
105. Durkin, M. E., Ullmannova, V., Guan, M. & Popescu, N. C. Deleted in liver cancer 3 (DLC-3), a novel Rho GTPase-activating protein, is downregulated in cancer and inhibits tumor cell growth. *Oncogene* **26,** 4580–4589 (2007).
106. Kim, C. A. & Bowie, J. U. SAM domains: uniform structure, diversity of function. *Trends Biochem. Sci.* **28,** 625–628 (2003).
107. Kwan, J. J. & Donaldson, L. W. The NMR structure of the murine DLC2 SAM domain reveals a variant fold that is similar to a four-helix bundle. *BMC Struct. Biol.* **7,** 34 (2007).
108. Li, H. *et al.* Solution structures, dynamics, and lipid-binding of the sterile alpha-motif domain of the deleted in liver cancer 2. *Proteins* **67,** 1154–1166 (2007).
109. De Kreuk, B.-J. *et al.* The SAM domain of the RhoGAP DLC1 binds EF1A1 to regulate cell migration. *J. Cell Sci.* **122,** 2375–2388 (2011).
110. Thornton, S., Anand, N., Purcell, D. & Lee, J. Not just for housekeeping: protein initiation and elongation factors in cell growth and tumorigenesis. *J. Mol. Med. Berlin Ger.* **81,** 536–48 (2003).
111. Hoffert, J. D., Pisitkun, T., Wang, G., Shen, R.-F. & Knepper, M. A. Quantitative phosphoproteomics of vasopressin-sensitive renal cells: Regulation of aquaporin-2 phosphorylation at two sites. *Proc. Natl. Acad. Sci. U. S. A.* **103,** 7159–7164 (2006).
112. Songyang, Z. *et al.* Use of an oriented peptide library to determine the optimal substrates of protein kinases. *Curr. Biol.* **4,** 973–982 (1994).
113. Li, S. S. C. Specificity and versatility of SH3 and other proline-recognition domains: structural basis and implications for cellular signal transduction. *Biochem. J.* **390,** 641–653 (2005).
114. Bos, J. L., Rehmann, H. & Wittinghofer, A. GEFs and GAPs: critical elements in the control of small G proteins. *Cell* **129,** 865–877 (2007).
115. Li, G. & Zhang, X. C. GTP hydrolysis mechanism of Ras-like GTPases. *J. Mol. Biol.* **340,** 921–932 (2004).

116. Sekimata, M., Kabuyama, Y., Emori, Y. & Homma, Y. Morphological changes and detachment of adherent cells induced by p122, a GTPase-activating protein for Rho. *J. Biol. Chem.* **274,** 17757–17762 (1999).
117. Alpy, F. & Tomasetto, C. Give lipids a START: the StAR-related lipid transfer (START) domain in mammals. *J. Cell Sci.* **118,** 2791–2801 (2005).
118. Alpy, F., Legueux, F., Bianchetti, L. & Tomasetto, C. START domain-containing proteins: a review of their role in lipid transport and exchange. *Med. Sci. MS* **25,** 181–191 (2009).
119. Bernards, A. & Settleman, J. GAP control: regulating the regulators of small GTPases. *Trends Cell Biol.* **14,** 377–385 (2004).
120. Durkin, M. E., Yuan, B.-Z., Thorgeirsson, S. S. & Popescu, N. C. Gene structure, tissue expression, and linkage mapping of the mouse DLC-1 gene (Arhgap7). *Gene* **288,** 119–127 (2002).
121. Chan, T. *et al.* DLC-1, a Rho GTPase-activating protein with tumor suppressor function, is essential for embryonic development. *FEBS Lett.* **581,** 2691–2696 (2007).
122. Wong, C. C.-L. *et al.* Deleted in Liver Cancer 1 (DLC1) Negatively Regulates Rho/ROCK/MLC Pathway in Hepatocellular Carcinoma. *PLoS One* **3,** 10 (2008).
123. Ferrell, J. E. What do scaffold proteins really do? *Sci. STKE signal Transduct. Knowl. Environ.* **2000,** pe1 (2000).
124. Lin, Y. *et al.* DLC2 modulates angiogenic responses in vascular endothelial cells by regulating cell attachment and migration. *Oncogene* **29,** 3010–3016 (2010).
125. Bernards, A. GAPs galore! A survey of putative Ras superfamily GTPase activating proteins in man and Drosophila. *Biochim. Biophys. Acta BBA Rev. Cancer* **1603,** 47–82 (2003).
126. Denholm, B. *et al.* Crossveinless-c is a RhoGAP required for actin reorganisation during morphogenesis. *Dev. Cambridge Engl.* **132,** 2389–2400 (2005).
127. Billuart, P., Winter, C. G., Maresh, A., Zhao, X. & Luo, L. Regulating axon branch stability: the role of p190 RhoGAP in repressing a retraction signaling pathway. *Cell* **107,** 195–207 (2001).
128. Goodison, S. *et al.* The RhoGAP protein DLC-1 functions as a metastasis suppressor in breast cancer cells. *Cancer Res.* **65,** 6042–6053 (2005).
129. Peng, D. *et al.* Genetic and epigenetic alterations of DLC-1, a candidate tumor suppressor gene, in nasopharyngeal carcinoma. *Acta Biochim. Biophys. Sin. (Shanghai).* **38,** 349–355 (2006).
130. Ullmannova, V. & Popescu, N. C. Expression profile of the tumor suppressor genes DLC-1 and DLC-2 in solid tumors. *Int. J. Oncol.* **29,** 1127–1132 (2006).
131. Yuan, B.-Z. *et al.* DLC-1 gene inhibits human breast cancer cell growth and in vivo tumorigenicity. *Oncogene* **22,** 445–450 (2003).
132. Song, Y. *et al.* High-frequency promoter hypermethylation of the deleted in liver cancer-1 gene in multiple myeloma. *J. Clin. Pathol.* **59,** 947–951 (2006).
133. Teramoto, A. *et al.* Less frequent promoter hypermethylation of DLC-1 gene in primary breast cancers. *Oncol. Rep.* **12,** 141–144 (2004).
134. Yuan, B.-Z., Durkin, M. E. & Popescu, N. C. Promoter hypermethylation of DLC-1, a candidate tumor suppressor gene, in several common human cancers. *Cancer Genet. Cytogenet.* **140,** 113–117 (2003).
135. Leung, T. H.-Y., Yam, J. W.-P., Chan, L. K., Ching, Y.-P. & Ng, I. O.-L. Deleted in liver cancer 2 suppresses cell growth via the regulation of the Raf-1-ERK1/2-p70S6K signalling pathway. *Liver Int. Off. J. Int. Assoc. Study Liver* **30,** 1315–1323 (2010).
136. Leung, T. H.-Y. *et al.* Deleted in liver cancer 2 (DLC2) suppresses cell transformation by means of inhibition of RhoA activity. *Proc. Natl. Acad. Sci. U. S. A.* **102,** 15207–12 (2005).
137. Xiaorong, L., Wei, W., Liyuan, Q. & Kaiyan, Y. Underexpression of Deleted in liver cancer 2 (DLC2) is associated with overexpression of RhoA and poor prognosis in hepatocellular carcinoma. *BMC Cancer* **8,** 205 (2008).
138. Qian, X. *et al.* Oncogenic inhibition by a deleted in liver cancer gene requires cooperation between tensin binding and Rho-specific GTPase-activating protein activities. *Proc. Natl. Acad. Sci. U. S. A.* **104,** 9012–9017 (2007).
139. Nagaraja, G. M. & Kandpal, R. P. Chromosome 13q12 encoded Rho GTPase activating protein suppresses growth of breast carcinoma cells, and yeast two-hybrid screen shows its interaction with several proteins. *Biochem. Biophys. Res. Commun.* **313,** 654–665 (2004).
140. Holeiter, G. *et al.* The RhoGAP protein Deleted in Liver Cancer 3 (DLC3) is essential for adherens junctions integrity. *Oncogenesis* **1,** e13 (2012).
141. Kimura, K., Tsuji, T., Takada, Y., Miki, T. & Narumiya, S. Accumulation of GTP-bound RhoA during Cytokinesis and a Critical Role of ECT2 in This Accumulation. *J. Biol. Chem.* **275,** 17233–17236 (2000).
142. Bomont, P., Maddox, P., Shah, J. V, Desai, A. B. & Cleveland, D. W. Unstable microtubule capture at kinetochores depleted of the centromere-associated protein CENP-F. *Eur. Mol. Biol. Organ. J.* **24,** 3927–3939 (2005).

143. Logarinho, E. *et al*. CLASPs prevent irreversible multipolarity by ensuring spindle-pole resistance to traction forces during chromosome alignment. *Nat. Cell Biol.* **14,** 1–10 (2012).
144. Vader, G. *et al*. The chromosomal passenger complex controls spindle checkpoint function independent from its role in correcting microtubule kinetochore interactions. *Mol. Biol. Cell* **18,** 4553–64 (2007).
145. DeLuca, K. F., Lens, S. M. A. & DeLuca, J. G. Temporal changes in Hec1 phosphorylation control kinetochore-microtubule attachment stability during mitosis. *J. Cell Sci.* **124,** 622–34 (2011).
146. Ferreira, J. G., Pereira, A. J., Akhmanova, A. & Maiato, H. Aurora B spatially regulates EB3 phosphorylation to coordinate daughter cell adhesion with cytokinesis. *J. Cell Biol.* **201,** 709–724 (2013).
147. Sugiyama, K. *et al*. Aurora-B associated protein phosphatases as negative regulators of kinase activation. *Oncogene* **21,** 3103–11 (2002).
148. Amaro, A. C. *et al*. Molecular control of kinetochore-microtubule dynamics and chromosome oscillations. *Nat. Cell Biol.* **12,** 319–329 (2010).
149. Astuti, D. *et al*. Germline mutations in DIS3L2 cause the Perlman syndrome of overgrowth and Wilms tumor susceptibility. *Nat. Genet.* **44,** 277–84 (2012).
150. Tighe, A., Ray-Sinha, A., Staples, O. D. & Taylor, S. S. GSK-3 inhibitors induce chromosome instability. *BMC Cell Biol.* **8,** 34 (2007).
151. Fink, J. *et al*. External forces control mitotic spindle positioning. *Nat. Cell Biol.* **13,** 771–8 (2011).
152. Dumont, S. & Mitchison, T. J. Force and length in the mitotic spindle. *Curr. Biol.* **19,** R749–R761 (2009).
153. Zhao, C. *et al*. Charcot-Marie-Tooth Disease Type 2A Caused by Mutation in a Microtubule Motor KIF1Bβ. *Cell* **105,** 587–597 (2001).
154. Wang, Z.-C. *et al*. Genetic Polymorphism of the Kinesin-Like Protein KIF1B Gene and the Risk of Hepatocellular Carcinoma. *PLoS One* **8,** e62571 (2013).
155. Chen, Y. Y. *et al*. Genomic structure and mutational analysis of the human KIF1Balpha gene located at 1p36.2 in neuroblastoma. *Int. J. Oncol.* **23,** 737–744 (2003).
156. Nangaku, M. *et al*. KIF1B, a novel microtubule plus end-directed monomeric motor protein for transport of mitochondria. *Cell* **79,** 1209–1220 (1994).
157. Niwa, S., Tanaka, Y. & Hirokawa, N. KIF1B-and KIF1A-mediated axonal transport of presynaptic regulator Rab3 occurs in a GTP-dependent manner through DENN/MADD. *Nat. Cell Biol.* **10,** 1269–1279 (2008).
158. Jaffe, A. B., Kaji, N., Durgan, J. & Hall, A. Cdc42 controls spindle orientation to position the apical surface during epithelial morphogenesis. *J. Cell Biol.* **183,** 625–33 (2008).
159. Kovacs, E. M., Verma, S., Thomas, S. G. & Yap, A. S. Tuba and N-WASP function cooperatively to position the central lumen during epithelial cyst morphogenesis. *Cell Adh. Migr.* **5,** 344–50
160. Mitsushima, M., Toyoshima, F. & Nishida, E. Dual role of Cdc42 in spindle orientation control of adherent cells. *Mol. Cell. Biol.* **29,** 2816–27 (2009).
161. Rodriguez-Fraticelli, A. E. *et al*. The Cdc42 GEF Intersectin 2 controls mitotic spindle orientation to form the lumen during epithelial morphogenesis. *J. Cell Biol.* **189,** 725–38 (2010).
162. Carmena, M., Wheelock, M., Funabiki, H. & Earnshaw, W. C. The chromosomal passenger complex (CPC): from easy rider to the godfather of mitosis. *Nat. Rev. Mol. Cell Biol.* **13,** 789–803 (2012).
163. Bakhoum, S. F. & Compton, D. A. Chromosomal instability and cancer: a complex relationship with therapeutic potential. *J. Clin. Invest.* **122,** 1138–43 (2012).
164. Nezi, L. & Musacchio, A. Sister chromatid tension and the spindle assembly checkpoint. *Curr. Opin. Cell Biol.* **21,** 785–95 (2009).
165. Mantel, C. & Broxmeyer, H. E. A new connection between the spindle checkpoint, asymmetric cell division and cytokine signaling. *Cell Cycle* **6,** 144–6 (2007).
166. Mapelli, M. & Musacchio, A. MAD contortions: conformational dimerization boosts spindle checkpoint signaling. *Curr. Opin. Struct. Biol.* **17,** 716–25 (2007).
167. Sczaniecka, M. M. & Hardwick, K. G. The spindle checkpoint: how do cells delay anaphase onset? *SEB Exp. Biol. Ser.* **59,** 243–56 (2008).
168. Suijkerbuijk, S. J. E. & Kops, G. J. P. L. Preventing aneuploidy: the contribution of mitotic checkpoint proteins. *Biochim. Biophys. Acta* **1786,** 24–31 (2008).
169. Sun, S.-C. & Kim, N.-H. Spindle assembly checkpoint and its regulators in meiosis. *Hum. Reprod. Update* **18,** 60–72
170. Schuyler, S. C., Wu, Y.-F. & Kuan, V. J.-W. The Mad1-Mad2 balancing act - a damaged spindle checkpoint in chromosome instability and cancer. *J. Cell Sci.* **125,** 4197–206 (2012).
171. Hewitt, L. *et al*. Sustained Mps1 activity is required in mitosis to recruit O-Mad2 to the Mad1-C-Mad2 core complex. *J. Cell Biol.* **190,** 25–34 (2010).
172. Daum, J. R. *et al*. Cohesion fatigue induces chromatid separation in cells delayed at metaphase. *Curr. Biol.* **21,** 1018–24 (2011).

173. McGranahan, N., Burrell, R. A., Endesfelder, D., Novelli, M. R. & Swanton, C. Cancer chromosomal instability: therapeutic and diagnostic challenges. *EMBO Rep*. **13,** 528–38 (2012).
174. Pfau, S. J. & Amon, A. Chromosomal instability and aneuploidy in cancer: from yeast to man. *EMBO Rep*. **13,** 515–27 (2012).
175. Van Aelst, L. & D'Souza-Schorey, C. Rho GTPases and signaling networks. *Genes Dev*. **11,** 2295–2322 (1997).
176. Cotteret, S. & Chernoff, J. The evolutionary history of effectors downstream of Cdc42 and Rac. *Genome Biol*. **3,** REVIEWS0002 (2002).
177. Flink, C. & Odde, D. J. Science + dance = bodystorming. *Trends Cell Biol*. **22,** 613–6 (2012).
178. Brun, L., Rupp, B., Ward, J. J. & Nédélec, F. A theory of microtubule catastrophes and their regulation. *Proc. Natl. Acad. Sci. U. S. A.* **106,** 21173–8 (2009).
179. Dehapiot, B., Carrière, V., Carroll, J. & Halet, G. Polarized Cdc42 activation promotes polar body protrusion and asymmetric division in mouse oocytes. *Dev. Biol*. **377,** 202–12 (2013).
180. Théry, M. Micropatterning as a tool to decipher cell morphogenesis and functions. *J. Cell Sci*. **123,** 4201–13 (2010).
181. Siegrist, S. E. & Doe, C. Q. Microtubule-induced cortical cell polarity .
182. Mathur, J. Microtubule Stabilization Leads to Growth Reorientation in Arabidopsis Trichomes. *PLANT CELL ONLINE* **12,** 465–478 (2000).
183. Bonetta, L. Microtubules shape the cell. *J. Cell Biol*. **169,** 553–553 (2005).
184. Wong, J. & Fang, G. HURP controls spindle dynamics to promote proper interkinetochore tension and efficient kinetochore capture. *J. Cell Biol*. **173,** 879–91 (2006).
185. Liu, J. *et al*. PRC1 cooperates with CLASP1 to organize central spindle plasticity in mitosis. *J. Biol. Chem*. **284,** 23059–71 (2009).
186. Civelekoglu-Scholey, G. & Scholey, J. M. Mitotic force generators and chromosome segregation. *Cell. Mol. Life Sci*. **67,** 2231–50 (2010).
187. Paul, R. *et al*. Computer simulations predict that chromosome movements and rotations accelerate mitotic spindle assembly without compromising accuracy. *Proc. Natl. Acad. Sci. U. S. A.* **106,** 15708–13 (2009).
188. Wollman, R. *et al*. Efficient chromosome capture requires a bias in the "search-and-capture" process during mitotic-spindle assembly. *Curr. Biol*. **15,** 828–32 (2005).
189. Bakhoum, S. F. & Compton, D. A. Kinetochores and disease: keeping microtubule dynamics in check! *Curr. Opin. Cell Biol*. **24,** 64–70 (2012).
190. Wong, C.-M. *et al*. Rho GTPase-activating protein deleted in liver cancer suppresses cell proliferation and invasion in hepatocellular carcinoma. *Cancer Res*. **65,** 8861–8 (2005).
191. Stephens, D. M. & Byrd, J. C. Chronic lymphocytic leukemia with del(17p13.1): a distinct clinical subtype requiring novel treatment approaches. *Oncology (Williston Park)*. **26,** 1044–54 (2012).
192. Ricke, R. M. & van Deursen, J. M. Aneuploidy in health, disease, and aging. *J. Cell Biol*. **201,** 11–21 (2013).
193. Biesecker, L. G. & Spinner, N. B. A genomic view of mosaicism and human disease. *Nat. Rev. Genet*. **14,** 307–20 (2013).
194. Fahed, A. C., Gelb, B. D., Seidman, J. G. & Seidman, C. E. Genetics of congenital heart disease: the glass half empty. *Circ. Res*. **112,** 707–20 (2013).
195. McNally, F. J. Mechanisms of spindle positioning. *J. Cell Biol*. **200,** 131–40 (2013).
196. Green, R. A., Paluch, E. & Oegema, K. Cytokinesis in animal cells. *Annu. Rev. Cell Dev. Biol*. **28,** 29–58 (2012).
197. Gusnowski, E. M. & Srayko, M. Visualization of dynein-dependent microtubule gliding at the cell cortex: implications for spindle positioning. *J. Cell Biol*. **194,** 377–86 (2011).
198. Kiyomitsu, T. & Cheeseman, I. M. Chromosome- and spindle-pole-derived signals generate an intrinsic code for spindle position and orientation. *Nat. Cell Biol*. **14,** 311–7 (2012).
199. Redemann, S. *et al*. Membrane invaginations reveal cortical sites that pull on mitotic spindles in one-cell C. elegans embryos. *PLoS One* **5,** e12301 (2010).
200. Oceguera-Yanez, F. *et al*. Ect2 and MgcRacGAP regulate the activation and function of Cdc42 in mitosis. *J. Cell Biol*. **168,** 221–32 (2005).
201. Wittmann, T., Hyman, A. & Desai, A. The spindle: a dynamic assembly of microtubules and motors. *Nat. Cell Biol*. **3,** E28–E34 (2001).
202. Gatlin, J. C. & Bloom, K. Microtubule motors in eukaryotic spindle assembly and maintenance. *Semin. cell Dev. Biol*. **21,** 248–254 (2010).
203. Shimamoto, Y., Maeda, Y. T., Ishiwata, S., Libchaber, A. J. & Kapoor, T. M. Insights into the micromechanical properties of the metaphase spindle. *Cell* **145,** 1062–1074 (2011).
204. Thompson, S. L., Bakhoum, S. F. & Compton, D. a. Mechanisms of chromosomal instability. *Curr. Biol*. **20,** R285–95 (2010).

205. Dikovskaya, D. *et al*. Loss of APC induces polyploidy as a result of a combination of defects in mitosis and apoptosis. *J. Cell Biol*. **176,** 183–95 (2007).
206. Fodde, R. *et al*. Mutations in the APC tumour suppressor gene cause chromosomal instability. *Nat. Cell Biol*. **3,** 433–8 (2001).
207. Aoki, K. *et al*. Chromosomal instability by beta-catenin/TCF transcription in APC or beta-catenin mutant cells. *Oncogene* **26,** 3511–20 (2007).
208. Joukov, V. *et al*. The BRCA1/BARD1 heterodimer modulates ran-dependent mitotic spindle assembly. *Cell* **127,** 539–52 (2006).
209. Manning, A. L., Longworth, M. S. & Dyson, N. J. Loss of pRB causes centromere dysfunction and chromosomal instability. *Genes Dev*. **24,** 1364–76 (2010).
210. Ko, F. C. F. *et al*. Akt phosphorylation of deleted in liver cancer 1 abrogates its suppression of liver cancer tumorigenesis and metastasis. *Gastroenterology* **139,** 1397–1407 (2010).
211. Lee, S., Park, J. & Park, E. Akt-induced promotion of cell-cycle progression at G2/M phase involves upregulation of NF-Y binding activity in PC12 cells. *J. Cell*. **205,** 270–277 (2005).
212. Wordeman, L. Microtubule-depolymerizing kinesins. *Curr. Opin. Cell Biol*. **17,** 82–8 (2005).

ACKNOWLEDGEMENTS

Choosing the right words is always arduous. I would like to state at best my gratitude to all the people that have accompanied me in this magic journey called the PhD. Four years ago, I decided to undertake this adventure in London, a city where I had never been before. I did not know anyone, but I came with a dream. My dream was to learn how to investigate one of the many mysteries in science and to learn the scientific method. Eleanor Roosevelt once said *"The future belongs to those who believe in the beauty of their* dreams." On the wave of this enthusiasm, I packed my things and moved to London.

Looking at this bound thesis, I feel as though a dream has become true. In sooth, a dream never becomes true if only the dreamer believes in it. It requires other people equally believing, and besides this, supporting. As a matter of fact, this work would not have been possible without those who had faith in me and encouraged me along the way.

Many are the special souls I have met during these four years in London and many are those I would like to thank for the great support served. First and foremost, I would like to thank my PI, Prof Karl Matter for accepting me in the lab after a three month rotation. He did not know me well, nor my way of working and neither my personality, but he took a gamble and decided that we would draw up a project together. That is how this thesis started. Along the way, he has always supported me, believed in my ideas and corrected me when the mistakes of a learning mind led the project astray. He has been a brilliant teacher and what I have achieved I owe principally to him.

Alongside Karl, I would like to mention how important the contributions of a group of inspiring scientists were. Through their talks and under their guidance I orientated this project toward the fascinating field of cell division. I still remember the first time I detected a mitotic spindle in the lab of Prof Buzz Baum, and when I learnt how to study it afterwards in the labs of Prof Ronald Vale and Helder Maiato. Muito Obrigada, Helder, por me ter recebido e permitido desenvolver uma parte fundamental do meu projecto, no seu laboratório. Sem a sua ajuda, muitas questões importantes permaneceriam sem solução.

A factor that cannot be neglected is the comfortable work environment created by wonderful colleagues/friends in the Institute of Ophthalmology. Firstly, Kasia, determined scientist and my model of logic, and nevertheless my

dear friend; Ahmed, listener to my continuous complaining; Clare, example of genuine will of learning, strong and never giving up; Barbara, for the long de-stressful chats in Italian; Ceniz for his jokes; Maria for her support and care; and Elena. Many people that are currently or were in the Institute of Ophthalmology deserve special thanks: Zanetta, Tom, Simon, Jenny, Katherina, Joana and…of course Jack for believing in my presenting skills and reminding me all the time that a bad day was never a good reason to give up, rather to roll up one's sleeves and work harder.

Achas que eu esqueci de você, Ingrid? Não há palavras para descrever a minha gratidão. Tu és a minha família em Londres, e o meu modelo de comportamento. A sua força e tenacidade, sua amizade e lealdade me ensinaram lições de vida que eu nunca vou esquecer. Continuando a escrever português, deveria agradecer tuda a gente no Instituto de Biologia Molecular e Celular (IBMC) no Porto: Danica pelas corridas perto do rio Douro, Zaira para estar sempre contente e de bom humor, Martina por organizar a minha chegada, Jorge para ser uma magnifica chefia, sempre activa, curiosa de saber, e criadora de alternativas quando havia problemas.

Vorrei infine ringraziare la mia cara famiglia. Quando mi offrirono un posto nel programma di dottorato, so che siete stati tristi e allo stesso tempo felici per me. Essere lontana non é stato facile, ma spero di poter ripagare con questa tesi la tenacia con la quale mi avete sostenuto nei miei giorni piú difficili. Se ho fatto tutto questo, é per rendervi orgogliosi di me e dimostrarvi che tutti gli insegnamenti che mi avete dato mi hanno reso la persona che sono oggi. Ila, sorellina, anche quando taci so che ci sei. La tua distante ma pur sempre reale presenza é stata un pilastro che mi ha sorretto e dato motivo di andare avanti. A te, principalmente questa tesi è dedicata, perché quando sono stata incerta, tu mi hai sempre detto qual era la cosa giusta da fare. E per qualche motivo avevi sempre ragione. Ti ringrazio di cuore.

Grazie a tutti. Muito obrigada para vocês. Many thanks to all.